# Effects of Alumina Nanoparticle Dispersed 3-armed Glyceryl Lactate on Biodiesel Cold Flow Properties, IC Engine Performance and Emission Characteristics

Melese Balew Belay

A Thesis Submitted to the Department of Chemical Engineering, School of Mechanical, Chemical, and Materials Engineering

Presented in Partial Fulfillment of the Requirement for the Degree of Master's in Chemical Engineering (Specialization in Process Engineering)

Office of Graduate Studies
Adama Science and Technology University

September, 2022
Adama, Ethiopia

# Effects of Alumina Nanoparticle Dispersed 3-armed Glyceryl Lactate on Biodiesel Cold Flow Properties, IC Engine Performance and Emission Characteristics

Melese Balew Belay

Advisor: Dr. Zelalem Tulmsa Tefera

Co-Advisor: Dr. Melaku Tesfaye Alemea

A Thesis Submitted to the Department of Chemical Engineering

School of Mechanical, Chemical, and Materials Engineering

Presented in Partial Fulfillment of the Requirement for the Degree of Master's in Chemical Engineering (Specialization in Process Engineering)

Office of Graduate Studies

Adama Science and Technology University

September, 2022

Adama, Ethiopia

## DECLARATION

I hereby declare that this Master's Thesis entitled "Effects of Alumina Nanoparticle Dispersed 3-armed Glyceryl Lactate on Biodiesel Cold Flow Properties, IC Engine Performance and Emission Characteristics" is my original work. That is, it has not been submitted for the award of any academic degree, diploma or certificate in any other university. All sources of materials that are used for this thesis have been duly acknowledged through citation.

| Melese Balew Belay | _____ | _____ |
|---|---|---|
| Name of student | Signature | Date |

## RECOMMENDATION

We, the advisors of this thesis, hereby certify that we have read the revised version of the thesis entitled "Effects of Alumina Nanoparticle Dispersed 3-armed Glyceryl Lactate on Biodiesel Cold Flow Properties, IC Engine Performance and Emission Characteristics" prepared under our guidance by Melese Balew Belay submitted in partial fulfillment of the requirements for the degree of Mater's of Science in Chemical Engineering. Therefore, we recommend the submission of the revised version of the thesis to the department following the applicable procedures.

| | | |
|---|---|---|
| Dr. Zelalem Tumsa | _____ | _____ |
| Major Advisor | Signature | Date |
| Dr. Melaku Tesfaye | _____ | _____ |
| Co-advisor | Signature | Date |

## APPROVAL PAGE

We, the advisors of the thesis entitled "Effects of Alumina Nanoparticle Dispersed 3-armed Glyceryl Lactate on Biodiesel Cold Flow Properties, IC Engine Performance and Emission Characteristics" and developed by Melese Balew Belay, hereby certify that the recommendation and suggestions made by the board of examiners are appropriately incorporated into the final version of the thesis.

| | | |
|---|---|---|
| Dr. Zelalem Tumsa | _____ | _____ |
| Major Advisor | Signature | Date |
| Dr. Melaku Tesfaye | _____ | _____ |
| Co-advisor | Signature | Date |

We, the undersigned members of the Board of Examiners of the thesis by Melese Balew Belay have read and evaluated the thesis entitled "Effects of Alumina Nanoparticle Dispersed 3-armed Glyceryl Lactate on Biodiesel Cold Flow Properties, IC Engine Performance and Emission Characteristics" and examined the candidate during the open defence. This is, therefore, to certify that the thesis is accepted for partial fulfillment of the requirement of the degree of Master of Science in Chemical Engineering.

| | | |
|---|---|---|
| _____ | _____ | _____ |
| Chairperson | Signature | Date |
| _____ | _____ | _____ |
| Internal examiner | Signature | Date |
| _____ | _____ | _____ |
| External examiner | Signature | Date |

Finally, approval and acceptance of the thesis is contingent upon submission of its final copy to the Office of Postgraduate Studies (OPGS) through the Department Graduate Council (DGC) and School Graduate Committee (SGC).

| | | |
|---|---|---|
| _____ | _____ | _____ |
| Department Head | Signature | Date |
| _____ | _____ | _____ |
| School Dean | Signature | Date |
| _____ | _____ | _____ |
| Office of Postgraduate Studies, Dean | Signature | Date |

# ACKNOWLEDGMENT

First of all, I would like to thank the Almighty GOD, for giving limitless blessings, wisdom, peace, protection and ability to do work. Next, I would like to express my deepest gratitude and heartful thanks to my advisor Dr. Zelalem Tumsa for his intellectual guidance, valuable advice and giving freedom of work while doing the experiments and accomplishing my thesis work. I would also like to express my deepest gratitude to my co-advisor Dr. Melaku Tesfaye for taking time to advise and assist me throughout every stage of the thesis work.

My sincere gratitude goes to my family for the numerous times they spent to help and pray for me. When times were tough, my family's effort was countless, their encouragement, financial support, and constant prayer were much welcomed and acknowledged.

And also, I would like to express my deepest appreciation for Chemical Engineering department laboratory assistants for their support during the experimental work, and thanks to my classmates for their support whenever I need them in every aspect of my thesis work, it was a pleasure to share and enjoy every situation with them. Finally, I would like to thank all the people who take part a contribution and helped me while accomplishing my thesis work.

## TABLE OF CONTENTS

ACKNOWLEDGMENT ..... iv
LIST OF TABLES ..... ix
LIST OF FIGURES ..... x
LIST OF ABBREVIATIONS ..... xi
ABSTRACT ..... xiii
CHAPTER ONE ..... 1
1. INTRODUCTION ..... 1
1.1. Background ..... 1
1.2. Statements of the Problem ..... 4
1.3. Research Questions ..... 5
1.4. Objectives of the Study ..... 5
1.4.1. General Objective ..... 5
1.4.2. Specific Objectives ..... 5
1.5. Significance of the Study ..... 6
1.6. Scope of the Study ..... 7
CHAPTER TWO ..... 8
2. LITERATURE REVIEW ..... 8
2.1. Feedstocks for Biodiesel Production ..... 8
2.1.1. Fatty Acid Profile of Different Biodiesel Feedstocks ..... 9
2.2. Biodiesel Production Technologies ..... 10
2.2.1. Catalytic Trans-esterification ..... 10
2.2.2. Supercritical Trans-esterification ..... 11
2.2.3. Ultrasound Assisted Trans-esterification ..... 12
2.2.4. Microwave Assisted Trans-esterification ..... 12
2.2.5. Biodiesel-Glycerol Separation ..... 12
2.3. Properties of Biodiesel ..... 13
2.3.1. Cold Flow Properties of Biodiesel ..... 13
2.3.2. Viscosity ..... 14
2.3.3. Flash Point and Fire Point ..... 15
2.3.4. Cetane Number (CN) ..... 15

2.3.5. Acid Value (AV) and Iodine Value (IV) ..... 15
2.3.6. Heating Value and Carbon Residue ..... 16
2.3.7. Emission Characteristics of Biodiesel ..... 16
2.4. Specification of Quality and Properties of Biodiesel ..... 16
2.5. Biodiesel Additives ..... 17
2.5.1. Cold Flow Improvers (CFIs) ..... 18
2.5.2. Oxygenated Additives ..... 21
2.5.3. Metal Oxide Based Nanoparticle Additives ..... 22
2.6. Synthesis Mechanisms of Metal Oxide Nanoparticles ..... 24
2.6.1. Top-down Approach ..... 25
2.6.2. Bottom-up Approach ..... 25
2.7. Glycerol Based Products ..... 27
CHAPTER THREE ..... 28
3. MATERIALS AND METHODS ..... 28
3.1. Materials and Reagents Used ..... 28
3.2. Methodology ..... 28
3.2.1. Characterization of Soyabean Oil ..... 28
3.2.2. Biodiesel Synthesis and Separation of Glycerol ..... 29
3.2.3. Synthesis and Purification of 3-armed Glyceryl Lactate (Gly-lac) ..... 31
3.2.4. Synthesis of Alumina Nanoparticle ($Al_2O_3$-NPs) by Sol-gel Method ..... 32
3.3. Characterizations of Biodiesel ..... 33
3.3.1. FTIR Analysis of Biodiesel ..... 33
3.3.2. NMR Analysis of Biodiesel ..... 33
3.3.3. Physico-Chemical Properties of Biodiesel ..... 33
3.4. Characterization of 3-armed Glyceryl Lactate (Gly-lac) ..... 35
3.4.1. FTIR Analysis of 3-armed Gly-lac ..... 35
3.4.2. NMR Analysis of 3-armed Gly-lac ..... 35
3.4.3. Analysis of Viscosity of 3-armed Gly-lac ..... 35
3.4.4. Acid Value Characterization for 3-armed Gly-lac ..... 36
3.5. Characterization of Alumina Nanoparticle ($Al_2O_3$-NPs) ..... 36
3.5.1. UV-Vis Spectroscopy Analysis of $Al_2O_3$-NPs ..... 36

3.5.2. FTIR Analysis of $Al_2O_3$-NPs ..... 36
3.5.3. Particle Size Analysis of $Al_2O_3$-NPs ..... 36
3.5.4. X-ray Diffraction (XRD) Analysis of $Al_2O_3$-NPs ..... 37
3.5.5. Analysis of Dispersion Stability of $Al_2O_3$-NPs with in Gly-lac ..... 37
3.6. Cold Flow Property of Analysis of Biodiesel ..... 38
3.6.1. Testing Cloud Point (CP) and Pour Point (PP) of Biodiesel ..... 38
3.6.2. The Effects of Gly:lac Molar Ratio and Loading Rate on CP and PP ..... 39
3.6.3. The Effects of $Al_2O_3$-NPs dispersed Gly-lac on CP and PP ..... 39
3.7. Analysis of IC Engine Performance and Emission Characteristics ..... 39
3.7.1. Fuel-Additive Blend Preparation ..... 39
3.7.2. The Effect of Gly-lac/$Al_2O_3$-NPs on Emission and Engine Performance of B20 ..... 40
CHAPTER FOUR ..... 44
4. RESULTS AND DISCUSSION ..... 44
4.1. Characterization of Properties of Soyabean Oil ..... 44
4.2. Characterization of Synthesized Biodiesel ..... 45
4.2.1. Functional Group Analysis of Biodiesel ..... 45
4.2.2. Analysis of Chemical Structure for Biodiesel ..... 46
4.2.3. Analysis of Biodiesel Physico-chemical Properties ..... 48
4.3. Characterization of 3-armed Gly-lac ..... 51
4.3.1. Analysis of Functional Group in 3-armed Gly-lac ..... 51
4.3.2. Analysis of Chemical Structure for 3-armed Gly-lac ..... 52
4.3.3. Viscosity of 3-armed Gly-lac for non-purified and purified ..... 56
4.3.4. Acid Value Analysis for 3-armed Gly-lac ..... 57
4.4. Characterization of $Al_2O_3$ Nanoparticle ..... 57
4.4.1. UV-vis Spectroscopy Analysis ..... 57
4.4.2. FTIR Analysis of $Al_2O_3$-NPs ..... 58
4.4.3. Particle Size Analysis (PSA) of $Al_2O_3$-NPs ..... 59
4.4.4. X-Ray Diffraction (XRD) Analysis of $Al_2O_3$-NPs ..... 60
4.4.5. Analysis Zeta Potential for Dispersion Stability of $Al_2O_3$-NPs within Gly-lac ..... 61
4.5. Cold Flow Property Analysis of Biodiesel ..... 63
4.5.1. The Effect of Gly:lac Molar Ratio on Biodiesel Cold Flow Properties ..... 63

4.5.2. The Effect of Loading Rate on Biodiesel Cold Flow Properties ..... 64
4.5.3. The Effect of 3-armed Gly-lac/$Al_2O_3$-NPs on Biodiesel Cold Flow Properties ..... 66
4.6. Analysis of IC Engine Performance and Emission Characteristics ..... 67
4.6.1. The Effect of 3-armed Gly-lac/$Al_2O_3$-NPs on Engine Performance of B20 ..... 67
4.6.2. The Effect of 3-armed Gly-lac/ $Al_2O_3$-NPs on Exhaust Gas Emission of B20 ..... 71
5. CONCLUSION AND RECOMMENDATION ..... 74
5.1. Conclusion ..... 74
5.2. Recommendations ..... 75
References ..... 76
Appendix ..... 92
Appendix A: Titration Result for Oil and Biodiesel Property Test ..... 92
Appendix B: Particle Size and Zeta Potential Analysis Result for $Al_2O_3$-NPs ..... 93
Appendix C: Cold Flow Property Analysis Results ..... 96
Appendix D: Calorific Value Test Result ..... 99
Appendix E: Analysis Results for Engine Performance and Emission Test ..... 100
Appendix F: Dept -135 for 3-armed Gly-lac (A) non-purified, (B) purified ..... 102

## LIST OF TABLES

Table 2.1: Fatty acid profile of some potential biodiesel feedstocks ..... 9
Table 2.2: Biodiesel specifications based on standard methods ..... 17
Table 2.3: Comparative summary of works related to cold flow additives of biodiesel ..... 20
Table 2.4: Summary of works related to utilization of metal oxide nano-additives ..... 23
Table 3.1: Operation parameters for trans-esterification reaction ..... 29
Table 3.2: Specification of the test diesel engine ..... 42
Table 3.3: Specification of FGA-4100 automotive gas analyzer ..... 42
Table 3.4: Experimental frame work for engine performance and emission gas test ..... 42
Table 4.1: Characterization results of soyabean oil properties ..... 44
Table 4.2: Properties of biodiesel synthesized from soyabean oil ..... 49
Table 4.3: Viscosity analysis results of 3-armed Gly-lac ..... 56
Table 4.4: Acid value of Gly-lac for purified and non-purified ..... 57
Table 4.5: Particle size analysis result of $Al_2O_3$-NPs with different dispersant ..... 59
Table 4.6: Crystalline size and d-spacing of alumina nanoparticle ..... 61
Table 4.7: Effect of Gly:lac molar ratio on biodiesel important properties ..... 65
Table 4.8: Effect of loading rate of 3-armed Gly-lac on important properties of biodiesel ..... 65
Table 4.9: Properties of the different fuel blend used in engine tests ..... 70

## LIST OF FIGURES

Figure 2.1: Different types of potential feedstocks for biodiesel production ..... 8
Figure 2.2: Reaction scheme for the catalytic trans-esterification of triglyceride ..... 10
Figure 2.3: Crystallization mechanism of biodiesel at lower temperature ..... 14
Figure 2.4: Interaction of cold flow improvers and crystal nuclei of biodiesel/diesel blend .... 18
Figure 2.5: Graphical representation of Sol-gel synthesis method for nanoparticles ..... 26
Figure 3.1: Experimental setup of biodiesel synthesis and glycerol separation ..... 30
Figure 3.2: Experimental setup for synthesis and purification of 3-armed Glyceryl lactate .... 31
Figure 3.4: Experimental setup for the synthesis of alumina nanoparticle ..... 32
Figure 3.4: Setup of cold flow property test (A) at cloud point, (B) at pour point ..... 38
Figure 3.5: Setup of (A) IC engine test, (B) FGA-4100 automotive emission gas analyzer .... 41
Figure 4.1: Fourier Transform Infrared (FTIR) spectrum of synthesized biodiesel ..... 46
Figure 4.2: $^{1}H$ NMR Chemical shift of synthesized biodiesel ..... 47
Figure 4.3: $^{13}C$ NMR Chemical Shift for Soyabean biodiesel ..... 47
Figure 4.4: Analysis result for viscosity of biodiesel ..... 50
Figure 4.5: FTIR spectrum of purified and non-purified (1:6) 3-armed Gly-lac ..... 51
Figure 4.10: Viscosity measurement for 3-armed Gly-lac ..... 57
Figure 4.11: Uv-visible Spectra of $Al_2O_3$ nanoparticle ..... 58
Figure 4.12: FTIR Spectrum of $Al_2O_3$ nanoparticle ..... 59
Figure 4.13: X-ray diffraction (XRD) patterns of alumina nanoparticle ..... 60
Figure 4.14: Physical detection for dispersion stability of $Al_2O_3$-NPs within Gly-lac ..... 62
Figure 4.15: The effects of; (A) Gly:lac molar ratio, (B) loading rate on CP and PP ..... 64
Figure 4.16: The effects of 3-armed Gly-lac/$Al_2O_3$-NPs on CP and PP ..... 67
Figure 4.17: The effect 3-armed Gly-lac/$Al_2O_3$-NPs; (A) on brake power, (B) on BTE ..... 68
Figure 4.18: The effect of 3-armed Gly-lac/$Al_2O_3$-NPs on BSFC (g/kWhr) ..... 69
Figure 4.21: The effect of 3-armed Gly-lac/$Al_2O_3$-NPs on the exhaust gas emission ..... 72

## LIST OF ABBREVIATIONS

| | |
|---|---|
| $^{13}$CNMR | Carbon Nuclear Magnetic Resonance |
| $^{1}$HNMR | Hydrogen Proton Nuclear Magnetic Resonance |
| $Al_2O_3$-NPs | Alumina Nanoparticles |
| ASTM | America Society for Testing and Materials |
| AV | Acid Value |
| B20 | 20% biodiesel + 80% diesel |
| B20A | B20 + 0.1g/l $Al_2O_3$-NPs |
| B20G | B20 + 10g/l Gly-lac |
| B20GA1% | B20G +$Al_2O_3$-NPs (1% of Gly-lac weight) |
| B20GA2% | B20G + $Al_2O_3$-NPs (2% of Gly-lac weight) |
| B20GA3% | B20G + $Al_2O_3$-NPs (3% of Gly-lac weight) |
| BP | Brake Power |
| BSFC | Brake Specific Fuel Consumption |
| CFPP | Cold Filter Plugging Point |
| CI | Compression Ignition |
| CN | Cetane Number |
| CP | Cloud Point |
| cP | Centipoise |
| EN | European Standard |
| FAAE | Fatty Acid Alkyl Ester |
| FAME | Fatty Acid Methyl Ester |
| FFA | Free Fatty Acid |
| FTIR | Fourier Transform Infrared |
| Gly:lac | Glyceryl to Lactic Acid Molar Ratio |
| Gly-lac | Glyceryl Lactate |
| HC | Hydrocarbon |
| IV | Iodine Value |
| kW | Kilowatt |
| M | Molarity |

| | |
|---|---|
| mV | Millivolt |
| N | Normality |
| NMR | Nuclear Magnetic Resonance |
| $NO_x$ | Nitrogen Oxides |
| PP | Pour Point |
| PPD | Pour Point Depressant |
| ppm | Parts Per Million |
| PSA | Particle Size Analysis |
| rpm | Revolution Per Minute |
| rps | Revolution Per Second |
| SV | Saponification Value |
| Uv-vis | Ultra-Violet Visible |
| vol% | Percentage by Volume |
| WCO | Waste Cooking Oil |
| wt% | Percentage by Weight |
| XRD | X-Ray Diffraction |

# ABSTRACT

*Biodiesel is a promising renewable energy sources to be used as an alternative for petro-diesel due to its good features such as biodegradable and non-toxic. However, biodiesel has drawbacks such as poor cold flow properties, lower engine performance. Different cold flow improvers have been explored as a better option to enhance the biodiesel cold flow properties. But, the cold flow improvers used so far are mostly petro-chemical based, and they are less efficient for biodiesel cold flow improvement. In this study a 3-armed Glyceryl lactate was used as cold flow improver and a dispersant for $Al_2O_3$-NPs in which $Al_2O_3$-NPs was used to improve engine performance and emission characteristics of biodiesel-diesel blend. The biodiesel was synthesized from soybean oil and characterized by FTIR and NMR analysis as well as physico-chemical properties were tested. Gly-lac (synthesized from glycerol and lactic acid) was purified and then characterized via FTIR, NMR, viscosity, and acid value analysis. $Al_2O_3$-NPs was synthesized by sol-gel method and characterized using UV-vis, FTIR, PSA, and XRD. In addition, Zeta potential analysis was conducted for $Al_2O_3$-NPs within Gly-lac and a value of +30.495mV was obtained. The effect of Gly:lac molar ratio and Gly-lac loading rate on biodiesel cloud point (CP) and pour point (PP) were studied, and a maximum reduction of CP by 7$^oC$ and PP by 8.14$^oC$ was achieved with the addition of Gly-lac (1:6) molar ratio at 10g/l loading rate. The Gly-lac/$Al_2O_3$-NPs (3wt% $Al_2O_3$-NPs with respect to Gly-lac) brought a maximum decline in CP by 7$^oC$ and PP by 9.44$^oC$ for biodiesel. The effect of Gly-lac/$Al_2O_3$-NPs on the engine performance and exhaust gas emission for biodiesel-diesel (B20) was also examined in which $Al_2O_3$-NPs dispersed Gly-lac brought a better result compared to $Al_2O_3$-NPs alone. The addition of Gly-lac/$Al_2O_3$-NPs (at 3wt% $Al_2O_3$-NPs) in to B20 brought a maximum increase in brake power and brake thermal efficiency by 0.843kW and* 6.837% *respectively during full load operation. Similarly, brake specific fuel consumption was reduced by 25.26%. Emissions of unburned hydrocarbon, $NO_x$, and CO were also reduced by 27.4 ppm, 98.6 ppm, and* 39.52% *respectively. Thus, $Al_2O_3$-NPs dispersed Gly-lac could be applicable to improve cold flow properties, engine performance and emission characteristics.*



**Key Words**: Biodiesel cold flow properties, Cloud point, Pour point, Engine performance, Emission characteristics, $Al_2O_3$-NPs dispersed Gly-lac.

# CHAPTER ONE

# 1. INTRODUCTION

## 1.1. Background

Presently the global energy economy is majorly reliant on fossil energy sources like petroleum diesel, coal, and natural gas (Sarkar et al., 2012). Utilization of those energy sources has brought a problems of energy security as well as high level of exhaust emissions that affect the environment (Demirbas & Fatih, 2011). Alternative fuels which are easily available, environmentally friendly, and renewable have been investigated so as to mitigate the problems posed by fossil fuels.

Among fuels with the aforementioned properties, biodiesel is the best alternative for petro-diesel. Biodiesel can be defined as a mixture of fatty acids alkyl esters (FAAE) including linoleic, lauric, palmitic, stearic, oleic. It is usually derived from catalytic trans-esterification of renewable sources (such as vegetable oils, animal fats, and algae oil), using a short-chain alcohols mostly methanol and ethanol (Ali & Mamat, 2013). Biodiesel owns a number of promising features such as better biodegradability, non-toxicity (Obedi et al., 2012), lower exhaust emissions, good lubricity, acceptable cetane number, and high flash point, as compared to that of petro-diesel (Dunn, 2001). The applicability of biodiesel is still lower due to some technical drawbacks such as poor (cold flow property, engine performance, and oxidation stability), high $NO_x$ emission, and high viscosity (Ali et al., 2015; Lawan et al., 2019; Pagliaro et al., 2007; Ryu, 2013).

Poor cold-flow properties of biodiesel such as higher (cloud point, pour point, and cold filter plugging point) is caused by crystallization of the saturated long-chain FAAEs contents as the temperature decreases below its melting point (Sierra & Guerrero, 2017). Poor cold flow behavior of biodiesel could account for the deterioration in engine performance as well as high emission of NOx, HC and particulate matter (Leng et al., 2020). There are different routes to mitigate the problems associated with the poor cold flow properties of biodiesel. Those includes; adding cold flow improvers, winterization, modifying the chemical structure of FAAE, and blending with diesel (Abdullah et al., 2007; Cornejo et al., 2017).

Utilization of various cold flow improvers has become the most feasible mechanism amongst the biodiesel cold flow property improvement methods (Lawan et al., 2019; Liu, 2015). So as

to enhance the biodiesel cold flow properties, different cold flow improvers have been investigated so far such as glycerol ketals, glycerol acetate, ethylene vinyl acetate copolymer (Cao et al., 2014), dioctyl fumarate-co-vinyl benzoate copolymers (Coussirat et al., 2019), poly (lactic acid) oligomer (Tesfaye & Katiyar, 2016), poly-alpha-olefin polymers (Xue et al., 2016). These polymers consist of either nonpolar moieties (that interact with crystal nuclei via nucleation, adsorption or co-crystallization), or polar moieties that interrupt the crystal growth, modify morphology and inhibit large crystals formation (Coussirat et al., 2019). Cold flow improvers should have the features such as; (i) similar structure and polarity with biodiesel to favor the molecular interaction, (ii) should contain chemical groups that create enough stearic hindrance on the formation of organized crystal structure, and (iii) branched molecular structure for a better efficiency in improving biodiesel cold flow property (Giraldo et al., 2013; Lawan et al., 2019).

Poor engine performance of biodiesel is another drawback that limits its wide applicability. Utilization of metal oxide nanoparticles has been studied to improve the engine performance parameters along with a reduction in exhaust gas emissions. Metal oxide nanoparticles as an additive for biodiesel/diesel has plentiful advantages such as increasing combustion enthalpies and overall energy density, lowering ignition delays, allowing a more complete combustion, decreasing the gaseous emissions (Saxena et al., 2017). Nano-sized additives are capable of enhancing the surface area to volume ratio, which tends to increase heat release rate as a result of more contact surface area for fast fuel oxidation (Sundaram et al., 2015). Alumina nanoparticle ($Al_2O_3$-NPs) has become the promising nano-additives that are employed to advance the fuel combustion of so as to improve brake power (BP) and brake thermal efficiency (BTE) as well as to reduce brake specific fuel consumption (BSFC) and exhaust gas emissions (Ağbulut et al., 2020; Hosseini et al., 2017).

Glycerol is a byproduct from the usual biodiesel production process i.e., trans-esterification reaction. At the completion of the net reaction, one mole of glycerol and three moles of alkyl esters are produced for each mole of triglycerides (TG) converted (Van Gerpen, 2005). Glycerol is a polyol molecule which is non-toxic, biodegradable, and highly stable which could be utilized for various application such as synthesis of oxygenated additives (Frusteri et al.,ll 2009), polymeric additives, pharmaceutical applications (such as moisturizer and skin care), dispersants and lubricants (Ortiz et al., 2020), synthesis of glyceryl lactate (Yuan et al., 2016).

Glyceryl lactate could be produced with different molecular structure such as in 3-armed form by varying the glycerol to lactic acid molar ratio (Tsion, 2021). 3-armed Gly-lac is a biocompatible as the raw materials (glycerol and lactic acid) are biocompatible. And 3-armed Gly-lac has both polar and non-polar moieties, and has similar molecular structure with biodiesel, which is suitable for its solubility within biodiesel when it is used as a cold flow improver. To mitigate the drawbacks of biodiesel without worsening environmental issues, the additives to be used should be biocompatible and non-toxic. However, limited investigations were done on bio-based cold flow improvers such as based on ethyl levulinate (Joshi et al., 2011) and poly(lactic acid) oligomer (Tesfaye & Katiyar, 2016). And also no work has been done on the utilization of 3-armed Gly-lac as a cold flow improver. Hence, a biocompatible 3-armed Gly-lac was utilized as a biodiesel cold flow additive to improve cloud point and pour point. The structure of this 3-armed Gly-lac is a unique feature to create a better hindrance on the formation and growth of crystals (compared to straight chain additives) to enhance cold flow properties (Lawan et al., 2019). The oxygenated nature of 3-armed Gly-lac is another suitable feature that could facilitate oxidation of fuel blends so as to reduce exhaust gas emissions (Ribeiro et al., 2007). The 3-armed Gly-lac could be used as a dispersant for $Al_2O_3$-NPs due to the existence of OH group that could hold metallic nanoparticles uniformly dispersed (Soudagar et al., 2018).

In this thesis, the main aim was to synthesize biodiesel from soyabean oil, to synthesize a biocompatible cold flow improver (3-armed Gly-lac) from lactic acid and glycerol in which both lactic acid and glycerol are biocompatible materials. $Al_2O_3$-NPs was synthesized by using sol-gel method and dispersed in 3-armed Gly-lac. The effect of $Al_2O_3$-NPs dispersed 3-armed Gly-lac on biodiesel cold flow properties (cloud point and pour point), engine performance, and exhaust gas emission was investigated. The dispersant nature of 3-armed Gly-lac was valuable for a stable dispersion of $Al_2O_3$-NPs. The dispersion stability is helpful to prevent the agglomeration tendency of nanoparticle while added in to biodiesel as well as biodiesel-diesel blend (Soudagar et al., 2020). Stable dispersion of $Al_2O_3$-NPs in 3-armed Gly-lac was a crucial to improve cold flow properties and engine performance (BTE and BSFC) in addition to exhaust gas emission reduction.

### 1.2. Statements of the Problem

Most of the modern energy demands are currently relying on petroleum energy sources. Those energy sources are non-renewable which contributes a lot for environmental pollution and have a critical issue towards energy security (Demirbas & Fatih, 2011). Biodiesel is a potential alternative renewable energy sources that could substitute the petro-diesel used in diesel engine. However, biodiesel have limitations that restrict its wide applicability. Poor cold flow properties, poor engine performance, high $NO_x$ emission are the major limitations (Ali et al., 2015; Leng et al., 2020).

Adding cold flow improvers have become the most feasible method designed to improve the cold flow properties of biodiesel (Liu, 2015). But, most of the commercially available cold flow improvers are derived from synthetic chemicals, which are non-biocompatible, expensive, and toxic. Besides, most of the additives have lower efficiency in improvement of cold flow properties of pure biodiesel because they are designed to be compatible with diesel. This problem should have to be solved by utilization of biodegradable, non-toxic, and renewable additives. Bio-based cold flow improvers such as ethyl levulinate (Joshi et al., 2011) and poly(lactic acid) oligomer (Tesfaye & Katiyar, 2016), have been studied previously. However, the efficiency of those cold flow improvers is lower due to the linear structure. Thus, utilization of a biocompatible 3-armed Gly-lac is beneficial as the 3-armed structure is a favorable feature to increase the efficiency in reducing the cloud point and pour point of biodiesel. The poor engine performance of biodiesel could also be alleviated using $Al_2O_3$-NPs along with reduction of the exhaust gas emission. But, there is a necessity of proper dispersant to enhance the dispersion stability of the nanoparticle.

Thus, in this study the 3-armed Gly-lac was utilized as a biocompatible cold flow improver, a dispersant and an oxygenated additive. The $Al_2O_3$-NPs was utilized for enhancement of engine performance and emission characteristics of biodiesel-diesel blend. Stable dispersion of $Al_2O_3$-NPs into biodiesel-diesel blend was achieved with the help of 3-armed Gly-lac.

### 1.3. Research Questions

Based on the problem statements identified above, the following research questions were raised.

- Is it possible to use 3-armed Gly-lac as a biodiesel cold flow improver, an oxygenated additive, and a dispersant for $Al_2O_3$-NPs?
- What is the effect of Gly:lac molar ratio, loading rate of 3-armed Gly-lac, and $Al_2O_3$-NPs dispersed 3-armed Gly-lac on biodiesel cold flow properties?
- What is the effect of $Al_2O_3$-NPs dispersed 3-armed Gly-lac on IC engine performance and emission characteristics of biodiesel-diesel blend?

### 1.4. Objectives of the Study

#### 1.4.1. General Objective

The general objective of this thesis was to investigate the effect of $Al_2O_3$-NPs dispersed 3-armed glyceryl lactate on the biodiesel cold flow properties as well as on IC engine performance and emission characteristics of biodiesel-diesel blends.

#### 1.4.2. Specific Objectives

The specific objectives of this thesis work were:

- Synthesize and characterize biodiesel via trans-esterification of soyabean oil.
- Synthesize, purify and characterize a 3-armed Gly-lac,
- Synthesize and characterize $Al_2O_3$-NPs through sol-gel synthesis method.
- Investigate the effect of Gly:lac molar ratio, loading rate of 3-armed Gly-lac, and $Al_2O_3$-NPs dispersed 3-armed Gly-lac on biodiesel cold flow properties.
- Investigate the effect of $Al_2O_3$-NPs dispersed 3-armed Gly-lac on IC engine performance and emission characteristics of biodiesel-diesel blend.

### 1.5. Significance of the Study

In this study, 3-armed Gly-lac (which is a biocompatible and non-toxic) that could reduce the utilization of petroleum based cold flow additives, which is advantageous regarding the environmental issue. 3-armed Gly-lac was also utilized as an oxygenated additive as well as a dispersant for the stable dispersion of $Al_2O_3$-NPs. $Al_2O_3$-NPs was a potential additive capable of reducing the exhaust gas emissions as well as fuel consumption and it is able to enhance thermal efficiency in which its efficiency was better when used with the help of dispersant (3-armed Gly-lac). The $Al_2O_3$-NPs dispersed 3-armed Gly-lac has brought an improvement in engine performance and emission characteristics. The reduction of exhaust gas emission (such as CO, HC, and $NO_x$) upon utilization of $Al_2O_3$-NPs dispersed 3-armed Gly-lac is also another environmental benefit. The increase in BTE and a reduction of BSFC upon the addition of $Al_2O_3$-NPs dispersed 3-armed Gly-lac into biodiesel-diesel blend is a valuable in economic point of view. The 3-armed Gly-lac was used as a dispersant for the $Al_2O_3$-NPs in which the utilization of one functional dispersant could be replaced by 3-armed Gly-lac having multi-function i.e. as cold flow improver, oxygenated additive, and dispersant for nano particle.

The additive used in combined form could advance the replacement of synthetic based biodiesel additives, thereby enhancing the biocompatibility of the biodiesel-additive mixture. On the other hand, glycerol is a byproduct from biodiesel production. Hence, utilization of glycerol-based additives is a crucial advantage as it could add to the economy of the biodiesel industry through utilization of biodiesel additives based on glycerol transformed product. Therefore, the extent of replacing petro-diesel with biodiesel could be increased when sustainable and biocompatible additive is used so as to reduce biodiesel drawbacks as well as the disadvantages of the synthetic based additives. This study can also induce an interest towards enhancement of critical problems of the other renewable energy sources to increase the extent of replacing petroleum-based fuels.

### 1.6. Scope of the Study

The scope of this thesis research covers:

- Characterization of important properties of soyabean oil such as acid value, %FFA, moisture content, and iodine value.
- Synthesis of biodiesel from soyabean oil and characterization of chemical structure and macro-molecular structure as well as determination of physico-chemical properties.
- Synthesis and purification of 3-armed glyceryl lactate (Gly-Lac) from glycerol (99%) and lactic acid (88%), and characterization via FTIR, NMR, acid value, and viscosity analysis.
- Synthesis of alumina nanoparticle and conducting analysis such as Uv-vis, FTIR, PSA (particle size analysis), and XRD analysis.
- Cold flow property analysis for biodiesel by adding 3-armed Gly-lac as a cold flow improver and oxygenated additive.
- Dispersion of $Al_2O_3$-NPs within Gly-lac and studying its effect on biodiesel cold flow property and on the exhaust gas emission (HC, $NO_x$, CO, $CO_2$) as well as the IC engine performance (mainly BP, BTE, and BSFC) of biodiesel-diesel blend.

# CHAPTER TWO

# 2. LITERATURE REVIEW

Biodiesel is a renewable-based liquid fuel, which is compatible with compression ignition engine as its properties such as viscosity, density, cetane number, flash point are comparable with that of petro-diesel (Obedi et al., 2012). The properties of biodiesel vary among different feedstocks as well as process technologies. This chapter focused on the description of different feedstocks and process technologies employed for the synthesis of biodiesel. Physico-chemical properties of biodiesel and additives used to improve the properties are described in this chapter.

## 2.1. Feedstocks for Biodiesel Production

Biodiesel production involves utilization of various sources such as vegetable oils, algal oils, animal fats, microbial oils and waste oils. The type of feedstocks used for biodiesel production decides the biodiesel purity as well as its fatty acid composition (Ambat et al., 2018). Lipids in the form of triglycerides (its composition varies among different feedstocks), are the main constituents of those sources of biodiesel. Various feedstocks for the production of biodiesel, which have been commonly utilized, are mainly grouped under; edible oil seed crops, non-edible oils, animal fats, algae oils, and microbial oil. The detail description is shown in Figure 2.1.

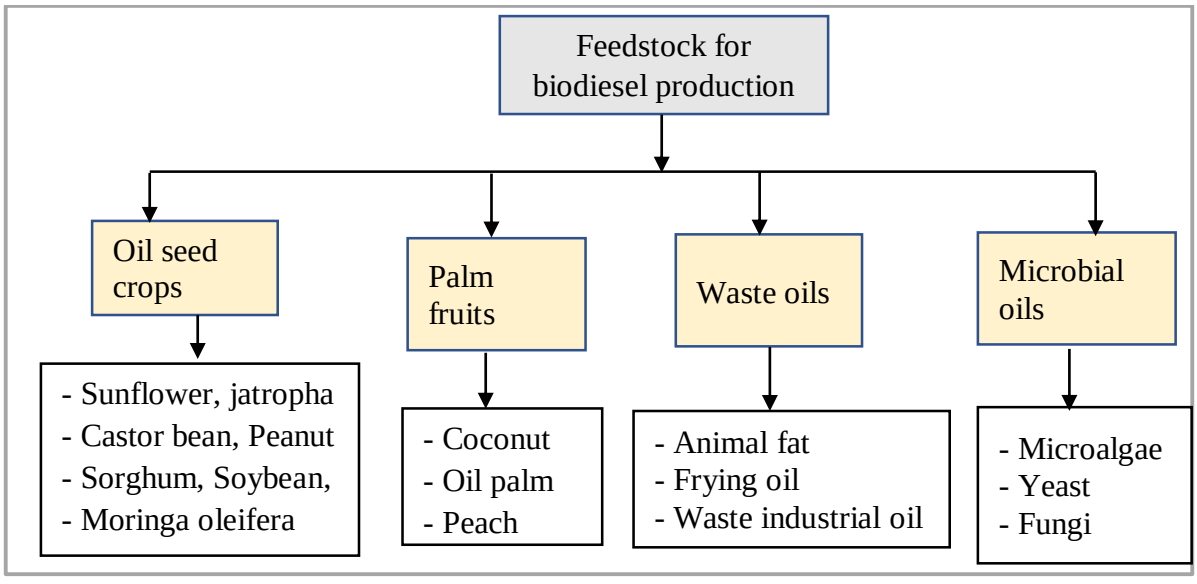


Figure 2.1: Different types of potential feedstocks for biodiesel production, adapted from (Mujeeb et al., 2016)

### 2.1.1. Fatty Acid Profile of Different Biodiesel Feedstocks

Biodiesel can be synthesized from different oil sources, and the fatty acid profile (chain length and composition) varies among different oil types, as shown in Table 2.1. The variation in fatty acid profile determines the properties of biodiesel such as cold flow properties (Yang et al., 2018), which corresponds to the variation in melting point among fatty acids with different chain length as well as number of double bond. This alters the solubility of higher melting point component (which acts as a solute) in the lower melting point component (which acts as a solvent) (Edith et al., 2012), which determines the crystallization of FAAEs to govern its cold flow properties.

Table 2.1: Fatty acid profile of some potential biodiesel feedstocks

| **Fatty Acids Composition (%)** | **Different Oil Types** | | | | | | |
|---|---|---|---|---|---|---|---|
| | Jatropha curcas | Palm kernel | Soyabean | Palm | Castor seed | Coconut | Moringa oleifera |
| Caprylic (C 8:0) | - | 3.3 | - | - | - | 7.3 | - |
| Capric (C 10:0) | - | 3.5 | - | - | - | 6.5 | - |
| Lauric (C 12:0) | - | 47.8 | - | 0.3 | - | 49.2 | - |
| Myristic (C 14:0) | 0.1 | 16.3 | - | 1.3 | 0.01 | 18.9 | 0.49 |
| Palmitic (C 16:0) | 14.2 | 8.4 | 11.0 | 43.4 | 1.64 | 8.9 | 6.54 |
| Stearic (C18:0) | 7.0 | 2.4 | 4.0 | 4.8 | 1.85 | 3.0 | 3.12 |
| Oleic (C 18:1) | 44.7 | 15.4 | 23.63 | 40 | 5.06 | 7.5 | 76.29 |
| Linoleic (C 18:2) | 32.8 | 2.4 | 54.71 | 10.5 | 6.42 | 1.8 | 9.23 |
| Linolenic (C 18:3) | 0.2 | - | 6.88 | 0.3 | 0.30 | 0.1 | 0.21 |
| Ricinoleic acid (C18:1 OH) | - | - | - | - | 82.88 | - | - |
| **Reference** | (Akbar et al., 2009) | (Akbar et al., 2009) | (Oliveira et al., 2005) | (Dayrit , 2014) | (Canoira et al., 2010) | (Dayrit, 2014) | (Aly et al., 2016) |

The fatty acid profile also influences other key biodiesel properties such as oxidation stability, exhaust gas emissions, density, viscosity (Dwivedi & Sharma, 2016; Wang et al., 2016), heating value, flash point, cetane number (Pinzi et al., 2011), acid number (Sarin et al., 2007).

## 2.2. Biodiesel Production Technologies

Biodiesel is a chemically modified alternative fuel for use in diesel engines, commonly derived from vegetable oils and animal fats. There are various biodiesel production technologies such as trans-esterification (catalytic or non-catalytic), thermal cracking (Leung et al., 2010).

### 2.2.1. Catalytic Trans-esterification

Trans-esterification is the most widely employed biodiesel production technology. It involves the reaction between oils (triglycerides) and alcohol (commonly methanol due to its low price and availability), with the help of catalyst at a desired temperature. The reaction causes restructuring the chemical structure of the oil as shown in Figure 2.2, which gives biodiesel as main product and glycerol as by product (Gerpen, 2005). This conversion reduces the high viscosity of oils and fats. For trans-esterification of triglyceride (TG) molecule, three consecutive reactions are needed in which diglycerides and monoglycerides are the intermediate products. One mole of glycerol and three moles of alkyl esters are produced (for each mole of TG converted) at the completion of the reaction (Keera et al., 2018), which then separates into three layers; glycerol at the bottom, a middle layer of soapy matter, and biodiesel on top layer (Fukuda et al., 2001).

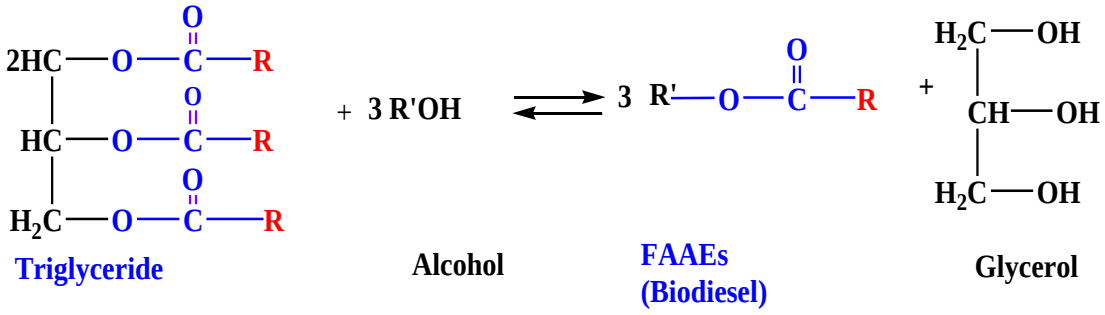


Figure 2.2: Reaction scheme for the catalytic trans-esterification of triglyceride

The catalysts for trans-esterification reaction are grouped into three categories as homogeneous, heterogeneous and enzymatic catalysts. In case of homogenous catalysts, alkali such as NaOH and KOH with loading rate of (0.4% to 2% w/w of oil) are usually preferred over other catalysts due to their ability to enhance faster reaction rate at moderate temperature and lower pressure as well as their availability at affordable price (Vicente et al., 2004). However, base catalysts have drawbacks such as highly sensitive to %FFA and moisture. For better efficiency of base catalyst, %FFA and moisture content should be less than 2% and 1.5% respectively (Chen et al., 2012). On the other hand, utilization of homogeneous acid catalysts is not affected by

%FFAs of the feedstocks. But it is not as popular as base-catalyst due to higher costs and environmental impacts. Homogenous acid catalysts are simple to use and requires less reaction time, but it becomes expensive with the requirement of product post-treatment (separation and purification) (Vicente et al., 2004). Solid acid catalyst, a class of heterogeneous catalyst, can be used in esterification and trans-esterification all together without the need for pretreatment of feedstocks having high %FFAs (Lotero et al., 2005). Thus, the production cost could be reduced by producing biodiesel from readily available feedstocks. Solid basic catalysts are also able to reduce biodiesel production cost due to lower consumption, reuse and regeneration of catalyst. Heterogeneous catalysts have limitations such as mass transfer problems that reduce the reaction rate due to; three phase formation with alcohol and oil, loss of catalyst activity in the presence of water, and product separation and purification costs. A biodiesel yield of 86.71% and 91.67% was achieved from the reaction among sunflower oil and methanol, using sodium methoxide and potassium methoxide catalysts respectively, at 1wt% catalyst loading, 6:1 alcohol to oil ratio, and a temperature of 65$^{o}$C (Vicente et al., 2004). The reaction between castor oil and methanol, at 400rpm stirrer speed, gave 95% yield at 1wt% loading rate of KOH catalyst, 9:1 alcohol to oil molar ratio, 60$^{o}$C, and 30 minute time (Keera et al., 2018).

Enzymatic trans-esterification is a possible way to solve the limitation of homogeneous catalysts such as expensive product separation, wastewater generation, and side reactions (Jegannathan et al., 2008). Immobilization of enzyme is typically done to enhance the quality of product and to increase the catalyst reuse cycle (Nielsen et al., 2008). However, there are some difficulties limiting the applicability of this process, including high cost for purchasing the enzymes, product contamination, and residual enzymatic activity.

### 2.2.2. Supercritical Trans-esterification

With the process of catalytic trans-esterification reaction, there are associated problems such as; water sensitivity, consumption and removal of catalyst, waste generation, and low purity of products (Aransiola et al., 2014). Biodiesel production at supercritical conditions could be utilized in order to alleviate those difficulties. At supercritical conditions (above the critical temperature and pressure), the reaction mixture becomes homogeneous, which favors both esterification and trans-esterification reactions. The method is suitable for any type of feedstock without pre- and post- purification steps as no catalyst is involved in the reaction. Regarding the alcohol used in the reaction, thermo-physical properties such as dielectric constant change in

supercritical state, vast solubility and diffusion associated with the two phase reaction mixture, permits a favorable condition for the reaction to complete in a short time (Leung et al., 2010). The main drawback of supercritical technologies is the necessity of high pressure, temperature, and methanol to oil ratio, which increases the production costs (Helwani et al., 2009).

### 2.2.3. Ultrasound Assisted Trans-esterification

Ultrasound assisted trans-esterification involves the stretching and compression of the reacting molecules by using sound energy at a frequency of beyond human hearing. Cavitation bubbles are formed between oil and alcohol phases due to the application of high negative pressure above the critical molecular distance, which makes efficient mixing and mass transfer rate (Baskar & Aiswarya, 2016), so that high product yield could be obtained from the trans-esterification reaction. Less energy consumption is observed in this process as compared to other processes utilizing mechanical stirring (Baskar & Aiswarya, 2016).

### 2.2.4. Microwave Assisted Trans-esterification

Microwave assisted trans-esterification involves utilization of microwave irradiation as energy stimulant. There is activation of reacting molecules with lower degree of variance by using continuously varying electrical and magnetic fields, which results interaction of quickly rotating charged ions with negligible restriction of dispersion (Azcan & Danisman, 2007). Microwave assisted trans-esterification has advantages such as fast reaction (within minutes), lower alcohol to oil ratio and small byproducts. A study by (Tesfaye & Katiyar, 2016) was done on biodiesel synthesis from soyabean oil and methanol, 6:1 alcohol to oil ratio and 1wt% KOH, using microwave assisted technique and attained 99% yield within 5 minute reaction at 60$^{o}$C.

### 2.2.5. Biodiesel-Glycerol Separation

After trans-esterification reaction, producing biodiesel (main product) and glycerol (byproduct), the separation of biodiesel and glycerol is a necessary step because of the slightly soluble nature of FAME and glycerol. The separation is usually done via formation of different phases by letting the product to settle due to density difference (Hong et al., 2014). In the presence of unreacted methanol, solubility of glycerol in ester and vice versa might rise due to the action of methanol that increases the post production costs. In addition, traces of triglycerides might form emulsion layer between the two phases. Thus, to avoid the cost and separation difficulties, it is compulsory to remove all traces of triglycerides, catalyst and solvents.

## 2.3. Properties of Biodiesel

The main goal of modifying oils via biodiesel production is to add desirable characteristics to the biodiesel such as low viscosity, better combustion, and for easy atomization inside injectors (Dwivedi & Sharma, 2014; Moser, 2009). Biodiesel is less stable than diesel in which its solidification temperature (10 to 25)$^{o}$C is exceeds that of petro-diesel (-27 to -15)$^{o}$C whereas biodiesel have higher (flash point and cetane number) and lower density compared to that of diesel (Sajjadi et al., 2016). When biodiesel is produced via trans-esterification, alkyl esters and the fatty acid composition of the oils are key parameters that affects the biodiesel properties like cold flow properties, lubricity, oxidation stability, acid number, and viscosity (Moser, 2009).

### 2.3.1. Cold Flow Properties of Biodiesel

The properties of biodiesel at low temperature are significant quality criterion because it affects the utilization of biodiesel in various climatic conditions. Cold flow properties of biodiesel are typically expressed by cloud point, pour point and cold filter plugging point (Muniz et al., 2020). Cloud point (CP) is the temperature at which visible crystal appears first upon cooling of the fuel in cold weather (Muniz et al., 2020). Pour point (PP) indicates the lowest temperature at which the amount of crystal is sufficient to gel formation so that crystal agglomerates are formed in the fuel system which causes the fuel to stop flowing thereby losing its pumping ability (Muniz et al., 2020). Cold filter plugging point (CFPP) refers to the temperature at which the test filter starts to plug due to gelling of fuel or it is the lowest temperature at which 20 ml fuel is able to pass through a 45μm filter in 1minute under vacuum pressure (Muniz et al., 2020).

Biodiesel have poor cold properties due to crystallization of saturated FAAE components via two interrelated steps i.e., nucleation and crystal growth (Dwivedi & Sharma, 2014). In nucleation stage, the formation of strong intermolecular force by liquid molecules produces enough thermodynamic force in the liquid when the temperature of biodiesel decreases below its melting point. Then crystal lattices are formed as the liquid molecules combined together. In the second stage (crystal growth), large crystals are formed on the existing crystal lattice. This crystal growth continues until the formation of an interlinking structure that results in starvation and interruption of fuel flow (Dwivedi & Sharma, 2014; Pullen & Saeed, 2014). This ultimately leads to an incomplete combustion of fuel and engine starting problems (Pullen & Saeed, 2014). The typical crystallization mechanism of FAAEs at cold temperature is illustrated figure 2.3.

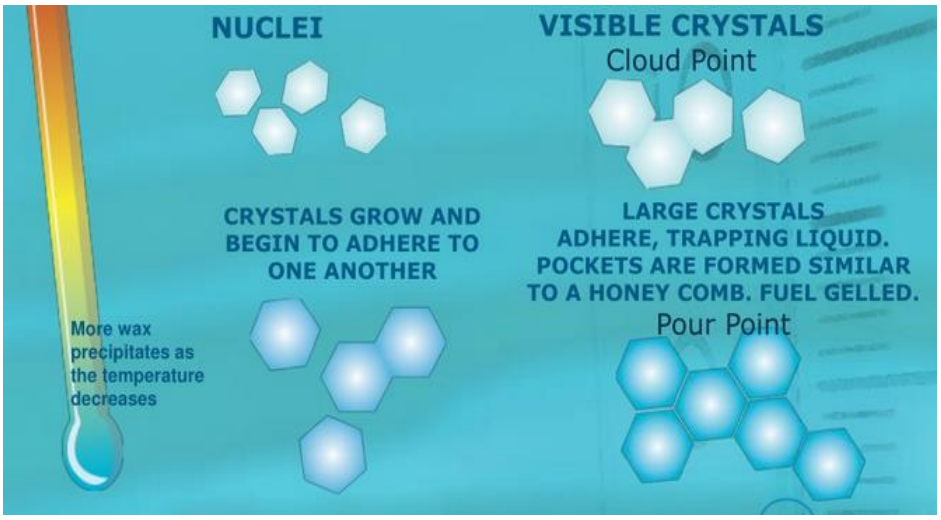


Figure 2.3: Crystallization mechanism of biodiesel at lower temperature

The fatty acid profile (saturated or unsaturated nature) in FAAEs and its chain length of the fatty acid are the dominant factors that determines its cold flow properties (Smith et al., 2010). It has been found that an increase in cloud point, pour point and cold filter plugging point of the biodiesel has been observed with higher amount of saturated FAAEs (Sierra & Guerrero, 2017). The poor cold flow behavior of saturated FAAEs is due to their uniform and straight molecular structure that makes them able to be well arranged and packed (Dwivedi & Sharma, 2016), which leads high melting and crystallization temperature (Sia et al., 2020).

### 2.3.2. Viscosity

It is known that viscosity is frictional properties of a certain fluid which measures the resistance to the normal flow of the fluid. Viscosity of biodiesel is one of the important properties that play a vital role during the combustion as a fuel. During fuel injection in the combustion chamber, the viscosity is the key property to determine spray atomization of fuel which decides the ease of combustion and thermal efficiency of the engine (Zhang et al., 2020). Lower viscosity below the standard will result unnecessary internal pump leakage and the system pressure reaches an intolerable level that will affect the injection system during the spray atomization, on the other hand higher viscosity could lead to enhanced fuel spray atomization thus improving air-fuel mixing (Xue et al., 2011), but if the viscosity is higher beyond the standard limit, it could result in poor spray atomization that causes engine operational problems such as higher emissions, lower engine performance and deposits (Lawan et al., 2019). The viscosity of biodiesel is relatively greater than that of petro-diesel but less than that of the source vegetable oils or fats

(Lawan et al., 2019). Hence, trans-esterification of high viscosity neat vegetable oils or fats to biodiesel becomes a necessary task in order to reduce the viscosity so as to minimize the engine operational problems associated with very high viscosity.

### 2.3.3. Flash Point and Fire Point

Flash point is the lowest temperature at which fuel ignition occurs when exposed to a flame. Flash point varies inversely with the fuel's volatility. At the flash point, a substance will ignite briefly, but vapor might not be produced at a rate to sustain the fire. Fire point is the lowest temperature at which the vapor of a fuel will initiate and sustain the combustion reaction for at least five seconds after ignition by an open flame of standard dimension (ASTM, 2015). Biodiesel have higher flash point and fire point as compared to that of petro-diesel fuel which make it safe for transportation, handling, and storage (Xue et al., 2011).

### 2.3.4. Cetane Number (CN)

Cetane number is an important factor which determines the combustion quality of a fuel throughout compression ignition. Cetane number is a measure of the fuel ignition delay, which indicates the time that passes between the fuel injection into the cylinder and its ignition. The shorter the ignition delay means higher CN, which is associated with lower $NO_x$ emissions. The cetane number of biodiesel (45 - 70) is higher than that of typical petro-diesel (40 - 52) (Smith et al., 2010). Fatty acid distribution in original oils determines the cetane number of biodiesels. Higher cetane number is associated with longer and more saturated fatty acids in the source oils.

### 2.3.5. Acid Value (AV) and Iodine Value (IV)

AV is a measure amount of free fatty acids (FFAs) that exist in biodiesel which is usually expressed as mg of KOH required to neutralize 1g of biodiesel. FFAs are saturated or unsaturated monocarboxylic acids that exist naturally in oils or fats, but not attached to glycerol backbones. Free fatty acids depend on the chain length of carbon as well as the saturated and unsaturated nature of carbons bonds in the fatty acid. Iodine value (IV) is a measure of total unsaturation of fatty acids measured in grams of iodine per 100g of biodiesel sample, when formally adding iodine to the double bonds. The iodine value (IV) in biodiesel affects its oxidation stability in which higher IV leads to easy oxidation in contact with air. The structure and composition of FAs in the biodiesel feedstock determines the IV of biodiesel.

### 2.3.6. Heating Value and Carbon Residue

Heating value is a vital property of fuels that have a significant influence on power generation during fuel combustion. It is a measure of the extent of releasing heat energy by the combustion of a unit value of fuels for doing the target work in the engine. Biodiesel have relatively lower heating value which results in a reduction in power generation (Xue et al., 2011). One of the most important parameters that determine the heating value of biodiesel is moisture content of the oil. Carbon residue is an indicator of the tendencies of the fuel to deposit carbon after combustion. Carbon residue for biodiesel is more important than that of conventional diesel fuel because it highly shows the presence of free fatty acids, unsaturated fatty acids, glycerides, and soaps (Atabani et al., 2012).

### 2.3.7. Emission Characteristics of Biodiesel

Emission characteristics of biodiesel and/or diesel could be expressed in terms of different gases emitted from the combustion process such as CO, $CO_2$, $NO_x$, HC, or particulate matters (Rashed et al., 2016; Wang et al., 2016). Biodiesel has become advantageous fuel because of its important features such as high oxygen content, free from aromatic hydrocarbons and harmful deposits, biodegradable, non-toxic, non-explosive, and easy to handle (Noor et al., 2018; Muniz et al., 2019). However, biodiesel has inferior thermal efficiency, high $NO_x$ emissions, limiting its application (Tomar & Kumar, 2020). Commonly, thermal and prompt mechanisms are responsible for $NO_x$ formation during the combustion of biodiesel (Varatharajan et al., 2011). In case of thermal mechanism, oxidation of excess hydrocarbon could lead to high local temperature which allows the formation of $NO_x$, whereas in prompt mechanism, the formation free radical in the front flame initiates the $NO_x$ formation. There is a poor spray and atomization of biodiesel while utilization of neat biodiesel due to its high viscosity and density as well as its poor cold flow behavior, which could result in clogging of fuel lines and filters (Pullen & Saeed, 2014). This might result an incomplete combustion of biodiesel, consequently there might be an increase in emission of CO, unburned hydrocarbons, and particulate matters (Mirhashemi & Sadrnia, 2019).

## 2.4. Specification of Quality and Properties of Biodiesel

There are different standards for testing different important characteristics of biodiesel. America society for testing and materials international (ASTM, ASTM D 675-02) is one of the major specification standards for testing biodiesel. Besides, the European standard (EN 14214) is also

accepted by all member states of the European committee for standardization of biodiesel. These test standards measures that the fuel performs same as supposed in compression ignition (CI) engine. The standards are also tests to assure that the manufacturers are producing a high quality biodiesel. Table 2.2 shows the specification of biodiesel properties and test methods.

Table 2.2: Biodiesel specifications based on standard methods (Atabani et al., 2012)

| **Properties of biodiesel** | **Units** | **ASTM D-6751** | | **EN 14214** | |
|---|---|---|---|---|---|
| | | **Limits** | **Test Methods** | **Limits** | **Test Methods** |
| Kinematic viscosity (40°C) | $mm^2/s$ | 1.9 - 6.0 | D445 | 3.5 - 5.0 | EN ISO 3104 |
| Density (15°C) | $kg/m^3$ | --- | --- | 860 - 900 | EN ISO 3675 |
| Cetane number | --- | ≥ 47 | D613 | ≥ 51 | EN ISO 5165 |
| Flash point | °C | ≥ 130 | D93 | ≥ 120 | ISO/CD 3679 |
| Acid number | mg KOH/g | ≤ 0.80 | ≤ 0.80 | ≤ 0.5 | EN 14104 |
| Iodine number | g $I_2$/100g | --- | --- | ≤ 120 | EN 14111 |
| Free glycerol | Mass% | ≤ 0.020 | D6584 | ≤ 0.02 | EN 14105 |
| Total glycerol | Mass% | ≤ 0.240 | D6584 | ≤ 0.25 | EN 14105 |

"---" undetermined

### 2.5. Biodiesel Additives

Additives are substances of organic-based or metal-based that is easily soluble in fuel. The main purpose of the additives could be to improve the fuel's cold flow properties (cloud point, pour point, cold filter plugging point), heating value, engine performance, emission characteristics (Lawan et al., 2019; Xue et al., 2011), and others. Fuel additives began to be commercialized in 1923 to provide the octane rating desired to allow automobile designers to attain adequate efficiency and performance of engine by increasing compression ratios (ATC Document 113, 2013). In the 1930s, antioxidant additives were introduced to solve the oxidation problems and formation of gums from broken components in gasoline refineries (ATC Document 113, 2013). The introduction of the wax crystal modifiers (cold flow improvers) in the 1970s was significant advance for maintaining the performance of diesel engines specially in the cold climate (ATC Document 113, 2013). Various additives for the improvement of the fuel properties have been

commercialized in different eras. The most widely used additives includes cold flow improvers, oxygenated additives, cetane number improvers, nano-additives (Kannan et al., 2011).

### 2.5.1. Cold Flow Improvers (CFIs)

Cold flow improvers (CFIs) are additives that are supposed to have low molecular weight, branched nature, and non-aromatic (Abe et al., 2016). While using biodiesel in cold climate, growth of crystal size might occur and adhere each other as temperature drops, which leads to blocking fuel filters and feed lines by large crystals, that may possibly lead to eventual power loss and engine stoppage (Rashedul et al., 2014). Cold flow improvers helps in modifying the shape, size, growth rate, and agglomeration of crystal nuclei, thereby hindering the formation of large crystal by favoring the formation of a small needle-shaped (10 - 100) nm crystals (Cao et al., 2014; Giraldo et al., 2013). An important class of cold flow improvers is the so called "tailor-made" additives, in which they uniquely contain special chemical groups (moieties) so as to modify the solute molecules and readily adsorbed at growth sites on the surface of crystal nuclei. The typical interaction between the crystal molecules and the cold flow additives is described in figure 2.4.

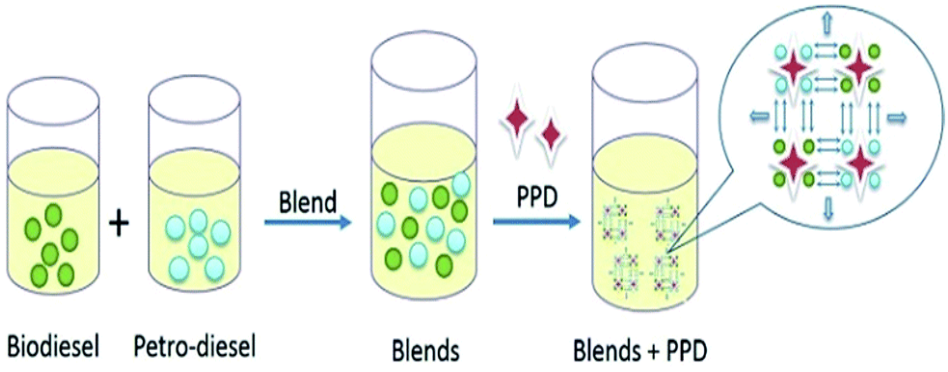


Figure 2.4: Interaction of cold flow improvers and crystal nuclei of biodiesel/diesel blend

Different studies have been conducted towards the synthesis and utilization of cold flow improvers for biodiesel so as to assure its wide applicability. Giraldo et al., (2013) investigates that a reduction in CP, PP and crystal size was observed with the addition of glycerol ketals, glycerol acetates and 2-Butyl esters (due to their similar structure with biodiesel), in which the effect was improved as the amount of each additive increases. The branched nature of 2-Butyl ester was responsible for its superior efficiency. Cao et al., (2014) investigate the effect of ethylene vinyl acetate copolymer (EVAC) on cold flow properties of waste cooking oil

biodiesel-diesel blend. A significant reduction in CP, PP, and CFPP by 8$^{o}$C, 11$^{o}$C, and 10$^{o}$C respectively. However, kinematic viscosity significantly increased at high concentration of EVAC. And it was observed a lower effect of the additives on CP, PP, and CFPP at high biodiesel content.

Yang et al., (2021) studies the effect of polar groups in polymethacrylate polymers on cold flow properties of diesel, by mixing using ultrasonicate for 30 minute at 30$^{o}$C. Polymethacrylate polymers improved the fluidity of diesel significantly. This is because alkyl groups of the polymeric additive co-crystallize with the n-alkanes in diesel through van der Waals force to hinder regular arrangement of crystals. Besides, the polar groups of the additive interrupt the growth of crystal, modify its morphology and inhibit large crystal formation via adsorption on growth sites. However, the benzene functional groups might be a source soot emissions (Abe et al., 2016).

Coussirat et al., (2019) evaluates the efficiency of dioctyl fumarate-co-vinyl benzoate copolymers (CP3, CP5 and CP7) as a cold flow improver by applying into waxy crude oil. CP5 and CP7 copolymers were found to have better interaction with the paraffin fraction of the crude oil as compared to CP3, which shows that the molecular weight of polymers is an important structural parameter for cold flow improvers. However, vinyl benzoate (VB) rich higher molecular weight copolymers have no noticeable effect on cold flow behavior of waxy crude oil, which might be attributed to the structure of additives, which contains branches of 8 C atoms in which their chain length is not enough to induce noticeable spatial intervention on wax crystal molecules. The vinyl benzoate group could result in high level of harmful emissions during the combustion, which might pose another limitation in environmental point of view.

A comparative study was done on the effect of tripropionin, glycerol formal, acetol, solketal on the cloud point (CP) of biodiesel (Senra et al., 2019). Addition of 5wt% and 15wt% solketal, glycerol formal, tripropionin to biodiesel reduced its CP by 1.2°C and 3.2°C; 1.8°C and 2.3°C; 1.4°C and 2.5°C respectively. The glycerol formal and tripropionin have better impact than that of solketal with 5wt%, whereas their effect was smaller with 15wt%. This could be due to the self-association of these additives (i.e., glycerol formal and tripropionin) at lower percentage as compared to that of solketal. On the other hand, it was difficult with acetol (because of its less bulkiness than the other additives investigated), to interfere with the nuclei formed by C14:0 and C16:0. But it was possible for acetol to integrate and disrupt the formation of nuclei from

longer FAMEs (such as C18:0). Thus, we can understand that various cold flow additives can interact in different manner with biodiesel obtained from different feedstocks.

The solid point (SP) and CFPP of WCO biodiesel-diesel blend was evaluated with the addition of meth-cyclohexyl methacrylate-methacrylate copolymers (MCHMA-R1MC, R1 = C12, C14, C16, C18) (Yuan et al., 2022). The best reduction of SP and CFPP by 25°C and 18°C was attained with the addition of 2000 ppm MCHMA-C14MC into B20. MCHMA-C16MC and MCHMA-C18MC have a lower impact on SP and CFPP, within (5 - 10)°C and (0 - 7)°C, respectively, whereas MCHMA-C12MC has the least effect on ΔSP of B20. Thus, the efficiency of cold flow improvers is dependent on their chain length, in which additives have superior effect when their n-alkyl chain length is closer to average carbon number of the biodiesel.

Table 2.3: Comparative summary of works related to cold flow additives of biodiesel

| Additives | Biodiesel Used | Additive loading | Findings |
|---|---|---|---|
| Poly-methacrylic acid and poly-acrylic acid (Muniz et al., 2019) | Palm oil biodiesel/ diesel blend | (25, 50, 100, 500, and 1000) ppm | ✓ Addition of 1000 ppm $A_{12}M_{14}$ copolymer results in reduction of pour point by 26°C and 7°C for B5 and B20 respectively. |
| Polyglycerol esters (PGE) & ethylene-vinyl acetate (EVA) (Hamada et al., 2010) | Palm oil biodiesel | (1 - 2) wt% | ✓ Reduction of CFPP by 3°C, 5°C, 6 °C with 2wt% EVA, 2wt% PGE, and 1wt% PGE + 1wt% EVA respectively.<br>✓ Decline in solid fat content by 26% and 31% at 1.2wt% PGE and 1wt% PGE + 1wt% EVA respectively. |
| Poly-alpha-olefin (Xue et al., 2016) | WCO biodiesel/ diesel blend | 200, 400, 600, 800 ppm | ✓ Addition of 400 ppm to B20 results optimum reduction of CP, CFPP and PP by 8°C, 9 °C and 7°C respectively.<br>✓ Addition 400 ppm to B40 results optimum reduction of CP, CFPP and PP by 4°C, 4°C and 4°C respectively. |
| Glycerol ketals, glycerol acetates and 2-Butyl esters (Giraldo et al., 2013) | Palm oil biodiesel | (1, 3, 5, and 10) vol% | ✓ Reduction of CP and PP by 5°C with 5% glycerol ketals/acetates<br>✓ Reduction of CP and PP by 6°C with 5% 2-Butyl esters. |

| | | | |
|---|---|---|---|
| Poly (lactic acid) oligomer (Tesfaye & Katiyar, 2016) | Soyabean biodiesel-diesel blend | (3, 5, 10, 15, and 25) g/l | ✓ CP and PP decreased by 4$^{o}$C and 2$^{o}$C respectively with 3g/l, 5g/l, 10g/l<br>✓ Emission of CO & HC shows a reduction in B20. |
| Ethyl levulinate (Joshi et al., 2011) | Cotton seed oil biodiesel | (2.5, 5, 10 and 20) vol% | ✓ A reduction in CP, PP, and CFPP by (4 - 5)$^{o}$C, (3 - 4)$^{o}$C, and 3$^{o}$C respectively with 20vol% of additive.<br>✓ Oxidative stability was also improved |
| Alkyl acrylate-vinyl acetate-maleic anhydride terpolymer (Feng et al., 2014) | Diesel | (0.05, 0.1, 0.15, 0.2, 0.25) wt% | ✓ A decrease in PP by 16$^{o}$C with 0.25% AVM-$_{14}$<br>✓ A decrease in CFPP by 5$^{o}$C with 0.25% AVM-$_{16}$ (AVM-$_{14}$ & $_{16}$ are chain lengths of the terpolymer). |

The cold flow improvers utilized so far are mostly synthesized from toxic and non-biocompatible chemicals (Coussirat et al., 2019; Giraldo et al., 2013; Feng et al., 2014; Muniz et al., 2019; Yang et al., 2021). And also the majority of the additives are designed for diesel cold flow improvement so that their efficiency is less in pure biodiesel (Cao et al., 2014; Coussirat et al., 2019; Xue et al., 2016). Thus, the development of biodegradable cold flow improver has become an interest for researchers in recent years. For example, a study was done on the utilization of bio-compatible additives such as poly (lactic acid) oligomer (Tesfaye & Katiyar, 2016), ethyl levulinate (Joshi et al., 2011), for improving the cold flow properties of biodiesel. Thus, the advancement of bio-compatible cold flow improvers could be a valuable to improve the cold flow properties as well as to mitigate the limitations of non-biocompatible and toxic cold flow improvers.

### 2.5.2. Oxygenated Additives

Oxygenated additives are those that contain sufficient oxygen content to reduce the fuel ignition temperature. Oxygenated additives permit efficient inflame of fuels that allows more complete fuel combustion, which results lower exhaust gas emissions (Rashedul et al., 2014). The reduction of emissions by oxygenated additives depends on oxygen content and molecular structure of the fuels.

Yasin et al., (2014) evaluates the effect of methanol on engine performance and exhaust gas emissions by comparing with the biodiesel-diesel blends. The result revealed that, addition of methanol brought a reduction in density and viscosity of the fuel blend, which tends to improve the fuel spray atomization that enhances the combustion. Methanol-B20 blend and B20 were found to have comparable BTE, both higher than that of pure diesel. However, an increase in $NO_x$ emission (due to extended ignition delay causing more fuel injection in the premixed combustion), a lower BP (due to lower heating value), and high BSFC was observed in the methanol-B20.

Another study by Imdadul et al., (2016) revealed that the addition of 2-ethylhexyl nitrate (EHN) at (1000 and 2000 ppm) into diesel-biodiesel-pentanol blend results an improved cetane number and reduction of; ignition delay, $NO_x$ emission, and BSFC. The increase in cetane number could be due to disruption of nitrate molecules in EHN to form free radicals resulting in higher decomposition. However, carbon monoxide (CO) and hydrocarbon (HC) emissions were high, which attributes to a reduction of oxidative free-radical formation and the reducing capability for CO oxidation.

### 2.5.3. Metal Oxide Based Nanoparticle Additives

Various kinds of metal oxide additives based on such as; aluminum (Al), cerium (Ce), magnesium (Mg), copper (Cu), iron (Fe), that are formed as nano particles could be used as a fuel additive in the diesel engine. The metal oxide nanoparticles are able to achieve more complete fuel ignition to minimize exhaust gas emissions and to enhance energy release rate due to more surface contact for fast fuel oxidation (Sundaram et al., 2015). The nano-additives are capable to increase brake power and brake thermal efficiency (BTE) as well as to reduce brake specific fuel consumption (BSFC) (Kannan et al., 2011). Principally, the action of metal oxide nano-additives is either it reacts (as a catalyst) with carbon atom and release oxidation temperature, or it reacts with water vapor to generate hydroxyl radicals in which the radicals are power full oxidizing agent and have a great impact to reduce exhaust emissions (Rashedul et al., 2014). Metal oxide nano-particles donates oxygen atom from their lattice structure so as to catalyze the combustion reaction (Prabakaran & Vijayabalan, 2018). Those additives are capable of increasing combustion enthalpy and energy density, shortening ignition delay, and reducing toxic emissions (Saxena et al., 2017).

Numerous studies have been conducted regarding the effect of metal oxide nano-additives on the combustion efficiency of biodiesel and diesel blends. Ağbulut et al., (2020) studied the comparison among $Al_2O_3$, $TiO_2$, $SiO_2$ nano-additives by adding into WCO biodiesel-diesel blend (B10) at 100 ppm. Utilization of $Al_2O_3$ brought the higher impact on BTE, BSFC and CO due to highest heating value of B10$Al_2O_3$ and its high oxygen content, compared to the others. Whereas the maximum decrease in $NO_x$ emission was achieved with the addition of $TiO_2$ due to its least heat capacity.

Table 2.4: Summary of works related to utilization of metal oxide nano-additives

| **Biodiesel source** | **Additive Used** | **Additive loading** | **Findings** | **Reference** |
|---|---|---|---|---|
| Algae oil biodiesel-diesel (B20) | $CeO_2$-NPs | (25, 50, 75, and 100) ppm | ✓ (2 - 5)% improvement of BTE<br>✓ Up to 0.25% reduction in BSFC | (Kalaimurugan et al., 2020) |
| WCO biodiesel-diesel blends | $Al_2O_3$-NPs | (40, 80, 120 and 160) ppm | ✓ Reduction of BSFC up to 10.41%,<br>✓ A reduction in emission of CO and HC up to 39.47% and 11 ppm respectively. | (Ghanbari et al., 2021) |
| Poultry litter biodiesel-diesel (B20) | $Al_2O_3$-NPs | 30 mg/l | ✓ Up to 1% improvement in BTE.<br>✓ A reduction in emission of CO and HC by (14.3 - 30.7)% and (4 - 8) ppm respectively. | (Ramesh et al., 2018) |
| Honge oil biodiesel-diesel blend (B20) | $Al_2O_3$-NPs with sodium dodecyl sulfate (surfactant) | (20, 40, 60) ppm, 1:4 mass ratio of surfactant to $Al_2O_3$ | ✓ BTE enhanced by 10.57%<br>✓ BSFC reduced by 11.65%<br>✓ HC, CO, and smoke emissions were decreased by 26.72%, 48.43%, and 22.84% respectively. | (Soudagar et al., 2020) |
| Calophyllum inophyllum biodiesel-diesel blend (B20) | $Al_2O_3$-NPs + exhaust gas recirculation (EGR) | 40 ppm | ✓ 5.04% and 7.71% increase in BTE for B20 and B20 + 20% EGR respectively.<br>✓ 11.5% and 13.33% reduction in BSFC for B20 and B20 + 20% EGR respectively. | (Anchupog., 2018) |

| | | | | |
|---|---|---|---|---|
| | | | ✓ A reduction in CO, NOx, and HC 6.09%, 12.83%; 7.76%, 23.2%; 12.24%, 9.25%, for B20 and B20 + 20% EGR respectively. | |
| Jatropha oil methyl ester (JOME) | $Al_2O_3$-NPs | 50 and 150 mg/l | ✓ 9.1% and 12.2% reduction in BSFC of JOME with respective addition of (50 and 150) mg/l.<br>✓ BTE increased by 2.4% and 6.2% with respective addition of (50 and 150) mg/l into JOME.<br>✓ At 50 and 150 mg/l, reduction in emission of HC, CO, and $NO_x$ by 5.7% and 13.7%; 8.4% and 16.7%; 1.8% and 4.7% respectively. | (Shrivastava et al., 2018) |

Graphene oxide nanoplatelets (GNP) combined with dimethyl carbonate (DMC) was added in to B30 and brought a 22.80% improvement of BTE, and reduction of BSFC, CO, HC, and NOx by 5.05%, 4.41%, 25%, and 3.65% respectively (Razzaq et al., 2021). This could be due to high thermal conductive nature of GNP and high oxygen content of DMC. Addition of ZnO and $TiO_2$ nanoparticles in to calophyllum-inophyllum biodiesel improved BTE by (5 - 17)% (Nanthagopal et al., 2017) in which $TiO_2$ was better than ZnO to enhance BTE, which indicates that $TiO_2$ has better oxidizing capacity compared to ZnO, due to its high oxygen content in its lattice structure. The metal oxide nano-additives have better efficacy when they are used with the help of dispersants to prevent the agglomeration of particles (Soudagar et al., 2020). Thus, it is required to use suitable dispersant with environmentally friendly and better compatibility with fuels.

### 2.6. Synthesis Mechanisms of Metal Oxide Nanoparticles

Nano-sized materials having a particle size of (1 to 100) nm (Govindrao et al., 2019), have become very attractive in various application areas including biofuels, catalysis, magnetic, electronic industry (optoelectronics and sensors), pharmaceuticals, agricultural, environmental remediation, and cosmetics (Oskam, 2006; Sekoai et al., 2019) due to the magnificent characteristics. Metal oxide nanoparticles (MONPs) exhibit unique physical, chemical, optical

and electrical properties as compared to their bulk form. This is because of the quantum confinement and availability of more surface atoms to participate in various reactions, and also MONPs have enhanced reactivity and selectivity compared to the interior atoms (Parashar et al., 2020; Sekoai et al., 2019). The successful application of MONPs is achieved through a controlled synthesis mechanisms in order to attain a narrow particle size distribution (Oskam, 2006). The general methods for the synthesis of MONPs can be divided into two groups (i) top-down approach, and (ii) bottom-up approach.

### 2.6.1. Top-down Approach

The top-down synthesis method is based on a systematic break down of large piece of materials into smaller entities in order to produce fine nanoparticles (Nikam et al., 2018). Such methods include ball milling, sputtering, laser ablation, electro-spraying, and electron beam evaporation (Parashar et al., 2020). The top-down synthesis approach has drawbacks such as (i) the requirement of complex, expensive and energy intensive process, (ii) the nanoparticles produced using this method have surface defects and non-uniform shapes, which hinders its applicability.

### 2.6.2. Bottom-up Approach

The bottom-up strategy is performed on the basis of integration of atoms or molecules which leads to distribution of different sizes of nanoparticles (NPs) (Parashar et al., 2020). This approach is mainly based on chemical synthesis or biological method.

**Biological method**: This method involves utilization of biological materials that are rich in metabolites such as plant extracts, biopolymers, bacteria, fungus, algae, and yeast for the preparation of metal and metal oxide nanoparticles (Aisida et al., 2019). Those metabolites such as flavonoid, alkaloid, tannin, saponin and phenolic acid are used for reducing metal ions by the redox reaction in the formation metallic or metal oxide nanoparticles (Aisida et al., 2019). The biocompatibility of the biological materials is the major advantage of this synthesis method as compared to the others (Ahmadi et al., 2020). However, biological methods have limitation such as variable size ranges for nanoparticles, which might cause a problem while predicting its application (Pantidos, 2014), and it needs purification step for the biogenic reducing agent which adds extra task in the synthesis method.

**Chemical method**: It is relatively simple, scalable and have better control over nanostructure (Nikam et al., 2018). This method involves the action of different chemical reducing agents like Sodium citrate, Ascorbate, Sodium borohydride ($NaBH_4$), tollens reagent elemental hydrogen,

and metal-complex forming agents like citric acid and urea. And also it involves surfactants (Amines, alcohols and acids) to control the agglomeration of particles. The main advantage of the chemical methods is that it allows to have the nano-particles with a defined size, dimension, and structure, which could be useful for various applications such as catalysis, sensing and in electronic devices (Nikam et al., 2018; Parashar et al., 2020). Chemical synthesis method includes such as sol-gel method, polyol method, hydrothermal method, co-precipitation method, micro-emulsion technique. The synthesis of nanoparticles through chemical methods particularly sol-gel method requires low processing temperature and less energy and also it provides a large degree of control over the synthesis products, which makes this method more economical (Parashar et al., 2020). Sol-gel method is an effective method for the synthesis of high-quality metal oxide nanoparticles as well as mixed oxide composites, which has excellent control over the texture and surface properties of the materials (Parashar et al., 2020).

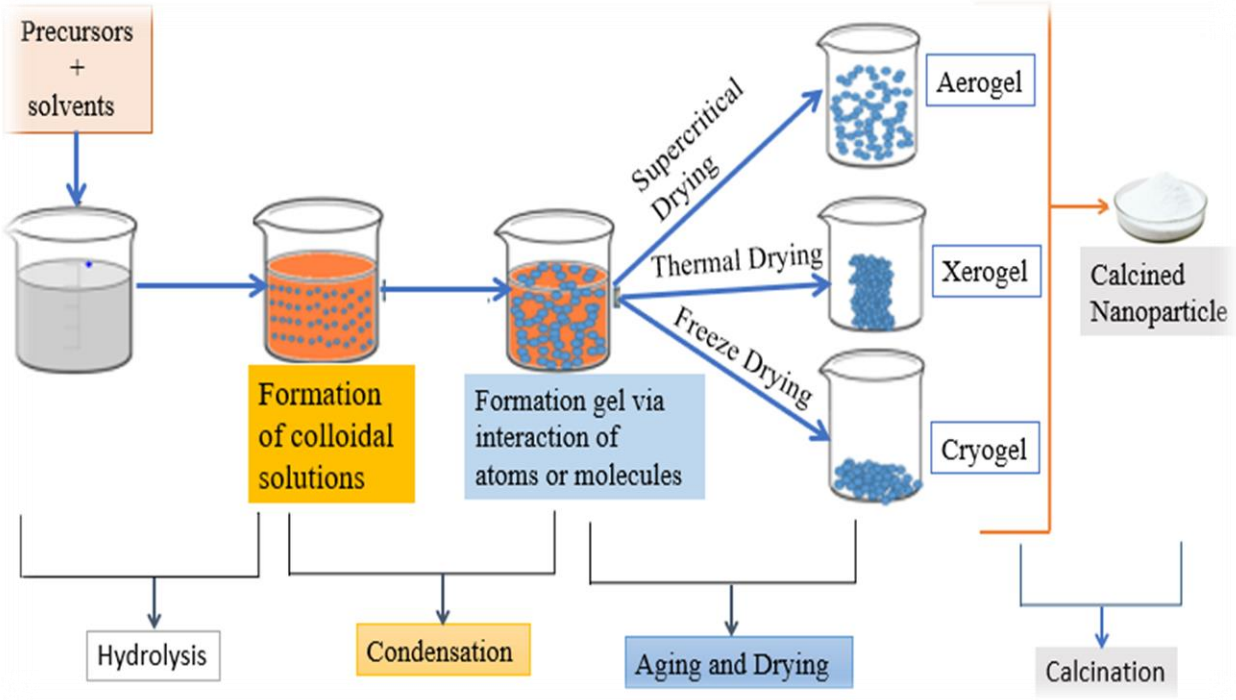


Figure 2.5: Graphical representation of Sol-gel synthesis method for nanoparticles

The sol-gel synthesis method is based on the conversion of raw materials or precursors into colloidal solutions (sol) in which the prepared sols are going to be converted to nanoparticles after a series of steps such as hydrolysis, polycondensation, aging, drying, and calcination (thermal decomposition), Figure 2.5 shows those steps graphically (Parashar et al., 2020). Utilization of some toxic chemicals, for reducing agents as well as for controlling

agglomeration, could be the main disadvantage of the chemical method. But, it is possible to use less toxic chemical agents like citric acid (which is organic based), and the toxic chemical could be removed by heat treatment via calcination.

### 2.7. Glycerol Based Products

Previously, production of glycerol had been mainly based on petrochemicals for several years, but recently, due to a huge increase in biodiesel production from renewable sources, leads to surplus production of glycerol in average 10 wt% of the trans-esterification product (Pagliaro et al., 2007), which reduce synthetic based glycerol production plants. Finding an appropriate value chain to convert the surplus glycerol into valuable products should be focused to improve the economy of biodiesel production process. Glycerol (1,2,3-propanetriol) is a highly functional molecule which consists of three hydroxyl groups. Glycerol could be transformed into various value-added products via different conversion routes such as selective oxidation of glycerol into 1,3-dihy-droxyacetone and glyceric acid (Katryniok et al., 2011), hydrogenolysis into propylene glycol and ethylene glycol (Nakagawa et al., 2014), pyrolysis into synthesis gas (Fernández et al., 2009), Utilization of glycerol to produce cold flow additives for biodiesel such as glycerol alkyl ethers, glycerol ketals, glycerol acetate (Giraldo et al., 2013) have become another vital valorization pathways. This could be beneficial for biodiesel plants to enhance properties of biodiesel (such as cold flow properties and emissions characteristics) by converting the surplus byproduct (glycerol) in to biodiesel additives. Recently, glycerol was utilized to synthesize glyceryl lactate (Gly-lac) via esterification reaction among lactic acid and utilized for polymer plasticizer (Yuan et al., 2016). Glyceryl lactate could be synthesized in three-armed structure by allowing lactic acid to grow on three core oxygen molecule of glycerol (Tsion, 2021). An optimum temperature of 190$^{o}$C, reaction time of 8 hour, and different glycerol to lactic acid molar ratio (1:3, 1:6, 1:9, and 1:12) were used to produce 3-armed Gly-lac with different chain length. The 3-armed Gly-lac could be used for various applications such as dispersant for nanoparticles, cold flow improver for biodiesel, oxygenated additive, and others.

# CHAPTER THREE

# 3. MATERIALS AND METHODS

## 3.1. Materials and Reagents Used

**Chemicals and Reagents**: Different chemicals and reagents (analytical grade) were used for the synthesis of biodiesel, synthesis and purification of glyceryl lactate (Gly-lac), synthesis of alumina nanoparticle, and for conducting different titrations. The chemicals and reagents include; methanol (99%, Sisco Research Laboratories Pvt Ltd. India), sodium hydroxide (99.8%, LABKEMICAL India), soyabean oil, sulfuric acid (98%), distilled water, sodium thiosulphate (99.55%, Trust Chemical Laboratories), ethanol (96%, KILITCHESTRO BIOTECH PLC, Ethiopia), iodine solution, starch (99%, Ranchem China), potassium hydroxide (99.8%, Central Drug House (P) Ltd., India), phenolphthalein indicator (Dallul Pharmaceuticals PLC), glycerol (99.7%, Ranchem Industry &Trading India), lactic acid (88%, Loba Chemie Pvt. Ltd. India), chloroform (99.99%, Fisher chemicals the scientific UK), sodium chloride (99%), ethyl acetate (99.5%, Central Drug House (P) Ltd. India), citric acid, and aluminum nitrate nonahydrate (98%, Alpha Chemika India).

**Materials or Equipment's:** The materials that were used while accomplishing this thesis work includes; measuring cylinder, beakers (different capacity), hot plate with magnetic stirrer, conical flask, separatory funnel, temperature-controlled oven, Petri dish, round bottom flask, condenser (reflux and horizontal), vacuum pump, chiller, heating mantle, Ultrasonicate, Erlenmeyer flask, pepete, stand with clamp, spatula, thermometer, weight balance, hydrometer.

## 3.2. Methodology

In this section, the different methods followed for the synthesis biodiesel, Gly-lac, and alumina nanoparticles are discussed. In addition, the different characterizations techniques (both analytical as well as instrumental) utilized are also discussed in detail in this section.

### 3.2.1. Characterization of Soyabean Oil

Physicochemical properties of soyabean oil such as iodine value, acid value, free fatty acid (%FFA), and moisture content were examined to assure its suitability for the biodiesel synthesis.

**Acid value and % FFA:** Determination of acid value and %FFA was conducted via titration using 0.1N aqueous solution of NaOH. A known mass of oil was taken into a conical flask and dissolved with ethanol (neutralized with 0.1N NaOH solution) and boiled under continuous

stirring. Then, the dissolved sample was titrated using 0.1NaOH solution until pink colour was observed in which phenolphthalein was used as an indicator for the endpoint of titration. Acid value and %FFA were calculated by using equations (3.1) and (3.2) (Ved & Padam, 2013).

$$\text{Acid Value} = \frac{Mw_{NaOH} \text{x N x} V_T}{W_S} \qquad \text{Eq (3.1)}$$

$$\%FFA = \frac{\text{Acid Value}}{2} \qquad \text{Eq (3.2)}$$

Where; '$Mw_{NaOH}$' is molecular weight of NaOH, 'N' is normality of NaOH, '$V_T$' is titrant volume used, and '$W_S$' is weight of sample oil.

**Moisture Content**: The moisture content of the soyabean oil was determined by oven drying method. A 10 g of soyabean oil was taken in petri dish and dried in a temperature-controlled oven at 105 $^oC$ with timely weighing the mass until we got a constant mass.

$$\text{Moisture content (\%)} = \frac{(\text{initial mass} - \text{final mass})}{\text{initial mass}} \text{ x } 100 \qquad \text{Eq (3.3)}$$

**Iodine Value (IV):** Iodine value was determined using green potentiometric method (Tubino & Aricetti, 2013). Sample soyabean oil was dissolved in 96% ethanol and mixed with 0.1M ethanolic iodine solution. After 5 minute agitation of the mixture with magnetic stirrer, distilled water was added and vigorously stirred again for 5 minute. The titration was done using 0.1N sodium thiosulfate solution and 1% starch solution (as indicator), until a milky white color was observed. The iodine value was calculated using equation (3.4) (Ved & Padam, 2013).

$$\text{Iodine Value (IV)} = \frac{12.69\,(B-S)N}{W_S} \qquad \text{Eq (3.4)}$$

Where; 'B' and 'S' are titrant volume used for blank and sample solution respectively, '$W_S$' is weight of sample, and N is normality of sodium thiosulfate solution.

### 3.2.2. Biodiesel Synthesis and Separation of Glycerol

**Biodiesel Synthesis:** The biodiesel synthesis was done via catalytic trans-esterification reaction between soyabean oil and methanol using homogenous base catalyst (sodium hydroxide). The parameters for trans-esterification reaction are shown in Table 3.1, defined based on the previous works (Keera et al., 2018; Tesfaye & Katiyar, 2016; Vicente et al., 2004).

Table 3.1: Operation parameters for trans-esterification reaction

| Alcohol to oil Molar ratio | Reaction temperature ($^oC$) | Reaction time (hour) | Catalyst load (wt% of oil) |
|---|---|---|---|
| **6:1** | 60 | 1 | 1 |

During the biodiesel synthesis, 150 g of soyabean oil was poured into a round-bottom flask and heated until the reaction temperature reaches 60°C. 1.5 g of NaOH pellet was dissolved in 31.335 g of methanol. Then, methanol-NaOH mixture was added into the flask, containing the preheated soyabean oil. The reaction was conducted in oil bath for 1 hour at 60°C with continuous agitation at 8 rps under reflux condition. Figure 3.1 illustrates the experimental setup of biodiesel synthesis and glycerol separation.

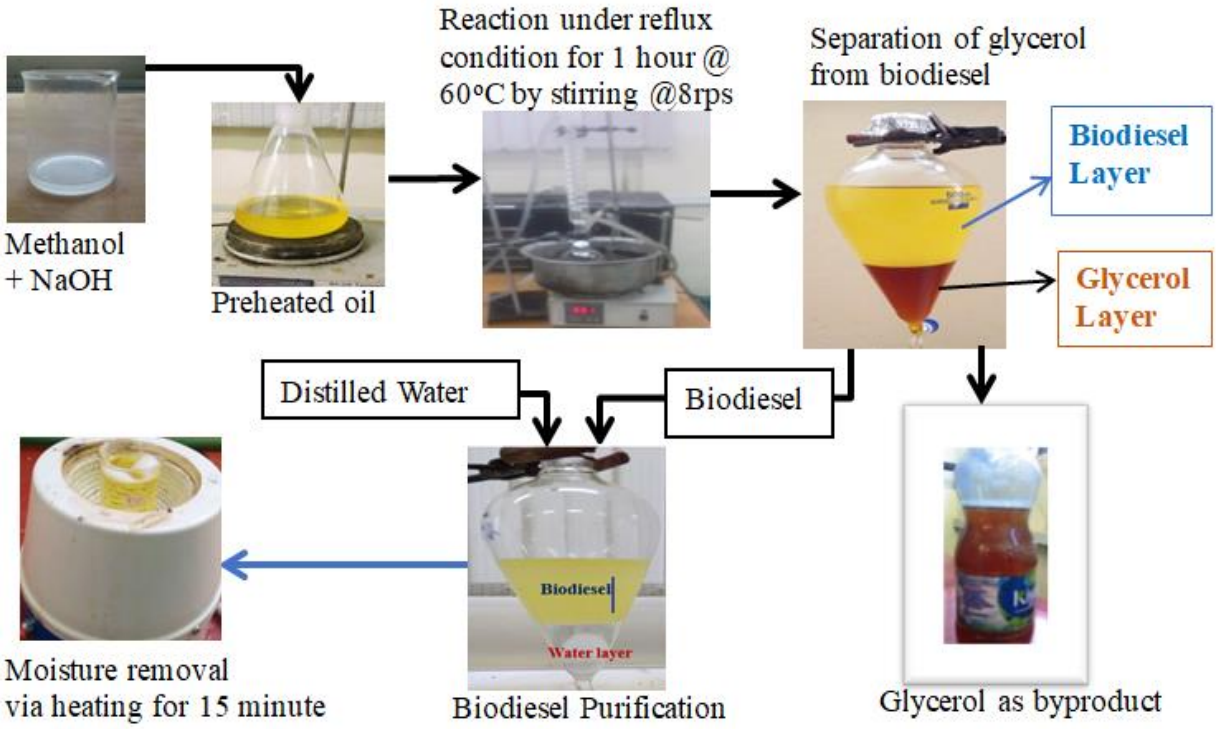


Figure 3.1: Experimental setup of biodiesel synthesis and glycerol separation

**Glycerol Separation and Purification of Biodiesel:** After the completion of the reaction, the reaction mixture was poured into separatory funnel and kept on for 12 hour (Meher et al., 2006) so as to separate biodiesel and glycerol. The glycerol layer was removed at the bottom of separatory funnel and the biodiesel layer was subjected for washing with aqueous solution of $H_2SO_4$ (1:1) (Meher et al., 2006) to neutralize the mixture of esters. Following the neutralization, successive washing was carried out with distilled water to remove traces of catalyst and alcohol until the water layer remains completely translucent (Hong et al., 2014). Finally, biodiesel was boiled at 70°C for 15 minute to remove suspended moisture (Sahoo & Das, 2009).

### 3.2.3. Synthesis and Purification of 3-armed Glyceryl Lactate (Gly-lac)

The synthesis of 3-armed Gly-lac was done via esterification of glycerol and lactic acid by means of condensation reaction. The reaction conditions were selected based the study by (Tsion, 2021). The reactants (glycerol and lactic acid), with different molar ratios (1:3, 1:6, 1:9, 1:12), were loaded into a round bottom flask and well mixed by hand shake. The mixture in a round bottom flask was placed inside a temperature-controlled oven at 190$^{o}$C for 8 hour reaction time. Figure 3.2 shows the experimental setup of synthesis and purification of 3-armed Gly-lac.

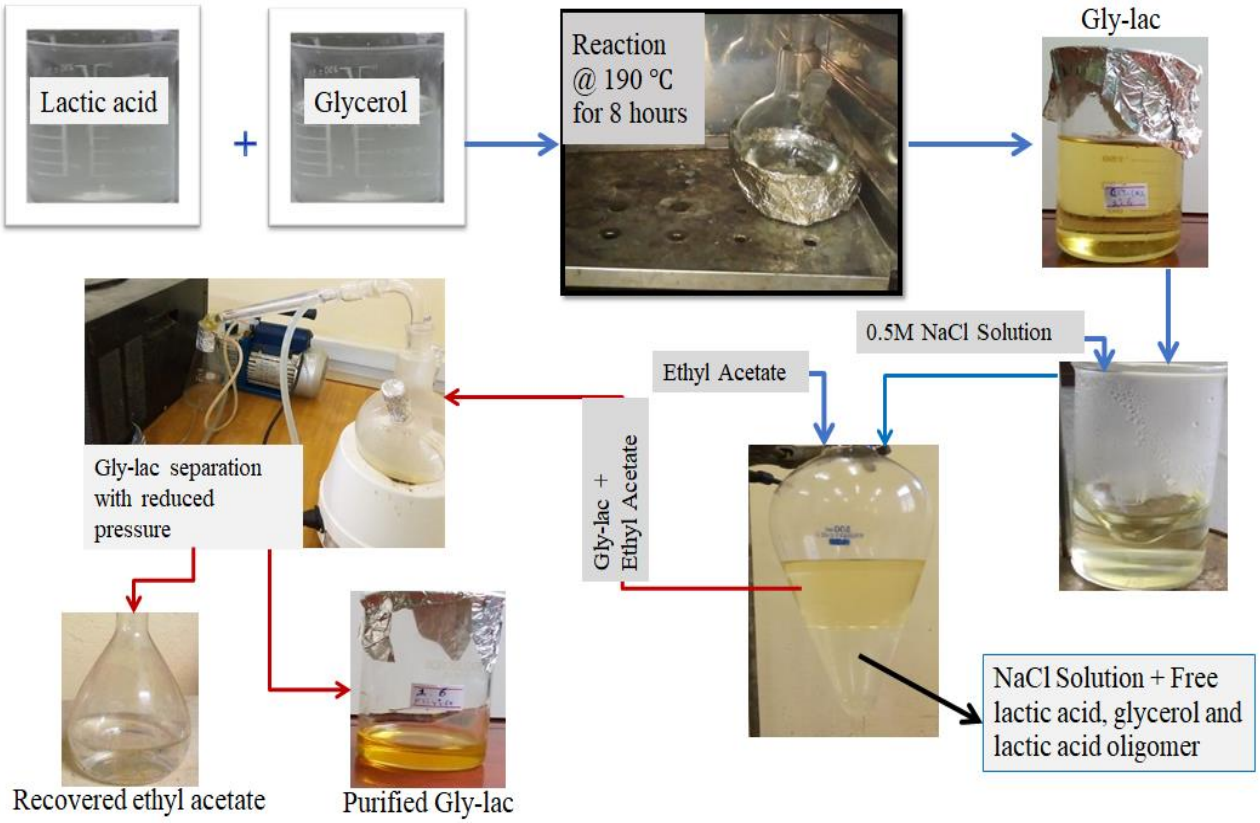


Figure 3.2: Experimental setup for the synthesis and purification of 3-armed Glyceryl lactate

Purification of 3-armed Gly-lac was conducted based on the solubility difference for lactic acid and glycerol among ethyl acetate and aqueous solution of sodium chloride (Yuan et al., 2016). The synthesized 3-armed Gly-lac was first dissolved in 0.5M aqueous solution of sodium chloride and delivered into separatory funnel. Then, ethyl acetate was added into the separatory funnel and mixing was performed by hand shake. The mixture was kept on for 20 minute to allow phase separation. The bottom layer containing NaCl solution with dissolved lactic acid, glycerol, and lactic acid oligomer was removed. The layer containing ethyl acetate and 3-armed

Gly-lac was poured in to a round bottom flask connected to horizontal condenser, and separation of 3-armed Gly-lac from ethyl acetate was done by heating under vacuum pump pressure.

### 3.2.4. Synthesis of Alumina Nanoparticle ($Al_2O_3$-NPs) by Sol-gel Method

Alumina nanoparticle ($Al_2O_3$-NPs) was synthesized via sol-gel method using aluminum nitrate nonahydrate ($Al(NO_3)_3.9H_2O$) as a precursor and citric acid ($C_6H_8O_7.H_2O$) as a metal complex forming agent. Figure 3.3 describes experimental setup for the synthesis of $Al_2O_3$-NPs.

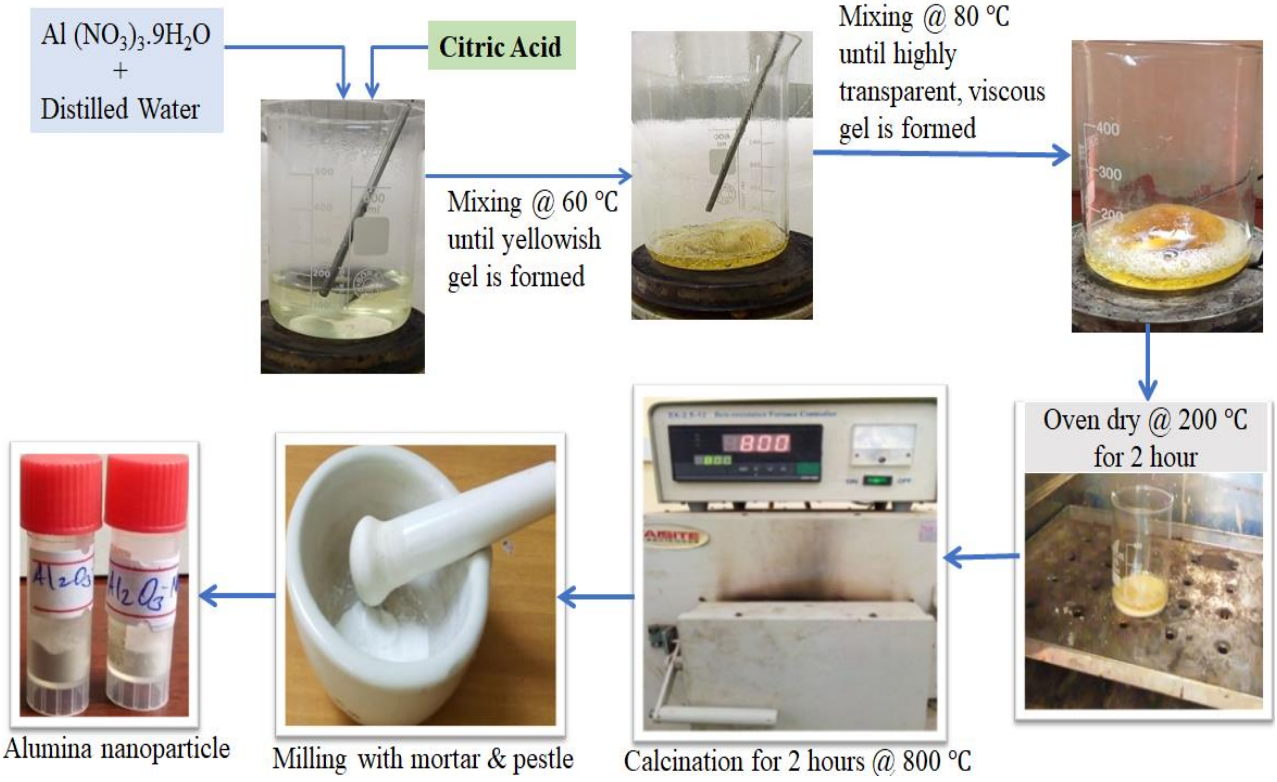


Figure 3.4: Experimental setup for the synthesis of alumina nanoparticle

The synthesis of $Al_2O_3$-NPs was conducted by following the previous study by (Li et al., 2006; Suhasinee Behera et al., 2017). A 0.5M solution of $Al(NO_3)_3.9H_2O$ was prepared using 100 ml of distilled water. And then citric acid was added into the solution with 1:1.5 molar ratio of $Al(NO_3)_3.9H_2O$ to citric acid. The solution was stirred at 60$^o$C until the appearance of yellowish colour. Then, the temperature was raised to 80$^o$C and the mixing was continued until the formation of transparent and highly viscous gel. The gel was subjected for oven drying for 2 hour at 200$^o$C followed by calcination using a muffle furnace at 800$^o$C for 2 hour. Finally, size reduction using mortar and pestle was carried out for the $Al_2O_3$-NPs.

### 3.3. Characterizations of Biodiesel

#### 3.3.1. FTIR Analysis of Biodiesel

Fourier Transform Infrared (FTIR) spectroscopy analysis was conducted in order to detect the functional groups in the synthesized biodiesel. The FTIR spectrum for the biodiesel was measured using FTIR spectrometer with a model number (FT/IR-6600 type A), at 2 mm/sec scanning speed within the wave number range of (400 - 4000) $cm^{-1}$ at 4 $cm^{-1}$ resolution. During the FTIR analysis, the biodiesel sample was first diluted at 1:20 with KBr and a background of pure KBr was acquired before scanning the sample.

#### 3.3.2. NMR Analysis of Biodiesel

Nuclear Magnetic Resonance (NMR) analysis ($^{1}$H NMR and $^{13}$C NMR) was conducted to investigate the chemical structure of FAMEs (biodiesel) synthesized from soyabean oil and methanol. Prior to the NMR analysis, the biodiesel sample was completely dissolved in deuterated chloroform ($CDCl_3$) and filtered using a 0.25µm filter. Then, the sample was transferred to a 5 mm diameter NMR tube. For the analysis of $^{1}$HNMR, the chemical shift at 7.26 ppm (a standard chemical shift of deuterated chloroform in $^{1}$H NMR) and for $^{13}$C NMR analysis (77.16 ppm) were used as reference line. The conversion during biodiesel synthesis was determined from the result of $^{1}$H NMR analysis, using equation (3.5), adapted from (Tariq et al., 2011).

$$\text{Conversion (\%)} = 100 \times \frac{2A_{ME}}{3A_{CH2}} \qquad \text{Eq (3.5)}$$

Where; '$A_{ME}$' is integral area of $OCH_3$ group, and '$A_{CH2}$' is integral area of the $\alpha$-$CH_2$ group.

#### 3.3.3. Physico-Chemical Properties of Biodiesel

**Viscosity:** Viscosity is a measure of the resistance to flow. Viscosity of biodiesel was measured at room temperature using VK-2000 viscometer based on the method adapted from (Akanksha et al., 2009). The biodiesel sample was first poured into clean and dry Borosilicate beaker (250 ml). The analysis was done using spindle number 5, which rotates at 25 rpm with 100% torque.

**Density**: Density of biodiesel is a vital physical property that determines its characteristics (such as fuel atomization, energy density) when used in diesel engine. The density of biodiesel was determined based on the hydrometer method defined in ASTM D 1298-85 (ASTM, 1999). A glass hydrometer with specific gravity range of (0.7 - 1.0) was used for measuring the specific gravity. Then, the specific gravity was correlated with density by using the equation (3.6**)**.

$\rho_S = \rho_W$ x SG Eq (3.6)

Where; '$\rho_S$' is density of substance '$\rho_w$' is density of water, and 'SG' is specific gravity.

**Calorific Value (CV)**: CV is the energy released in the form of heat when a fuel undergoes complete decomposition with oxygen at standard conditions. The calorific value of biodiesel was determined based on the adiabatic calorimeter analysis method using oxygen Bomb calorimeter (Awulu et al., 2018). During the test, 1gram of biodiesel sample was transferred into clean and dry crucible fixed with the electrode placed inside the bomb. The bomb head was carefully and tightly closed and connected to the oxygen cylinder. Then, the bomb was transferred into the calorimeter bucket filled with distilled water. The calorimeter is helpful to automatically determine the calorific value from the heat release during combustion. The calorific value test was conducted at Geo-chemical laboratory, Geological Survey of Ethiopia.

**Iodine Value (IV):** IV was determined using green potentiometric method (Tubino & Aricetti, 2013), via titration of sample and blank solution with 0.1N sodium thiosulfate solution using 1% starch solution as an indicator. Sample biodiesel was dissolved in 96% ethanol and mixed with 0.1M ethanolic iodine solution. The titration was done after adding 1% starch solution (as indicator), until the appearance of a milky white color. IV was determined using equation (3.4).

**Saponification Value (SV):** The SV of biodiesel was detrmined via titration of the sample solution and blank solution with 1.5N HCl and using phenolphthalein indicator. A sample solution was prepared by dissolving biodiesel in 0.5N ethanolic KOH solution (Sahar et al., 2018) via heating at 40°C. The solution was refluxed using reflux condenser until the formation of clear solution (end of reaction). The blank (0.5N ethanolic KOH) solution was also heated and refluxed. The titration was done until the disappearance of pink color. SV was calculated using eq (3.7).

$$SV = \frac{(B-S) \text{ x } N \text{ x } 56.1}{W} \quad \text{Eq (3.7)}$$

Where; 'B' and 'S' are the titrant volumes required for titration of blank and sample respectively, 'N' is normality of HCl, and 'W' is weight of sample.

**Cetane Number (CN):** CN is an important property which determines the ignition probability of fuels. Fatty acid distribution in is original oils decides the cetane number of biodiesels. Cetane number of the biodiesel was calculated using the correlation with the saponification value and iodine value, adapted from (BOSE, 2009; Sahar et al., 2018), as shown in equation (3.8).

$$\text{Cetane Number} = 46.3 + \frac{5458}{SV} - 0.225 \times IV \qquad \text{Eq (3.8)}$$

Where; 'SV' and 'IV' represents the saponification value and iodine value respectively.

**Flash Point and Fire Point:** Flash point and fire point are important biodiesel properties that determine the ease of handling and storage. Flash point and fire determination was carried out based on standard flash point test method (ASTM, 2015; Kaisan et al., 2020). The biodiesel sample was subjected for continuous heating using heating mantle with temperature detection using thermometer and passing a light source (flame) over the surface of sample. The flash point temperature was detected at which a flame was created in the biodiesel sample. At the fire point temperature, the flame was formed at the surface of biodiesel sample and sustained for 5 second.

### 3.4. Characterization of 3-armed Glyceryl Lactate (Gly-lac)

#### 3.4.1. FTIR Analysis of 3-armed Gly-lac

The molecular group formed by the reaction among lactic acid and glycerol during the synthesis of 3-armed Gly-lac was characterized by using FTIR analysis. The FTIR spectrum of the 3-armed Gly-lac was measured using FTIR spectrometer with model number (FT/IR-6600 type A), at 2 mm/sec scanning speed. The spectrum was recorded in the wave number range of (400 - 4000) $cm^{-1}$ at 4 $cm^{-1}$ resolution. During the analysis, the Gly-lac sample was first diluted at 1:20 with KBr, and a background pure KBr was acquired prior to scanning the sample.

#### 3.4.2. NMR Analysis of 3-armed Gly-lac

The chemical structure of 3-armed Gly-lac as well as the existence of free and oligomer lactic acid was identified using Nuclear Magnetic Resonance ($^{1}$H NMR and $^{13}$C NMR) analysis. During the analysis, 3-armed Gly-lac (both non-purified and purified) was first dissolved in deuterated chloroform ($CDCl_3$) and filtered using 0.25μm filter, and transferred to 5 mm diameter NMR tube. During the NMR analysis, standard chemical shift of deuterated chloroform (7.26 ppm for $^{1}$H NMR) and (77.16 ppm for $^{13}$C NMR) were used as the reference line (Francis, 2012).

#### 3.4.3. Analysis of Viscosity of 3-armed Gly-lac

Determination of viscosity for non-purified and purified 3-armed Gly-lac was conducted at room temperature using VK-2000 viscometer, based on the method adapted from (Akanksha et al., 2009). The Gly-lac sample was first transferred into clean and dry Borosilicate beaker, and the analysis was done using spindle number 5, which rotates at 25 rpm with 100% torque.

### 3.4.4. Acid Value Characterization for 3-armed Gly-lac

The acid value of 3-armed Gly-lac (non-purified and purified) was characterized to compare the extent of unreacted lactic acid among different chain 3-armed Gly-lac, and for examining the extent of purification by comparing the acid value of non-purified and purified 3-armed Gly-lac. The acid value for of 3-armed Gly-lac was determined by titration of the sample dissolved in chloroform and blank solution with 0.1N KOH solution using 1 ml phenolphthalein indicator, following the ASTM D974-12 standard method (Knothe, 2006). 1g of 3-armed Gly-lac was dissolved in 20 ml of chloroform, and titrated using 0.1N aqueous solution of KOH until the appearance of pink colour (end point of titration).

$$AV = \frac{(B-S) \text{ x } N \text{ x } 56.1}{W_s} x \ 100 \ \% \qquad \text{Eq (3.9)}$$

Where; 'AV' is acid value (in mg KOH/g), 'B' and 'S' are titrant volumes used for blank and sample solution respectively, 'N' is normality of KOH solution, and '$W_S$' is weight of sample.

## 3.5. Characterization of Alumina Nanoparticle ($Al_2O_3$-NPs)

### 3.5.1. UV-Vis Spectroscopy Analysis of $Al_2O_3$-NPs

UV-vis spectroscopic analysis was conducted for $Al_2O_3$-NPs in order to analyze its specific absorption band and to compare with its standard wave length at which absorption of UV-visible light by $Al_2O_3$-NPs is occurred. Before the analysis, $Al_2O_3$-NPs were dispersed in distilled water. Then, the Uv-vis absorbance of the dispersed sample was recorded in the wave length range of (200 - 800) nm using UV-vis instrument (UV-Vis NIR CLB, V-770) at 1000 nm/min scanning rate using (Deuterium/Tungsten) light sources.

### 3.5.2. FTIR Analysis of $Al_2O_3$-NPs

FTIR analysis of $Al_2O_3$-NPs was performed to understand its macromolecular structure so as to confirm the existence of expected function groups within the nanoparticle. The FTIR spectrum of the as prepared $Al_2O_3$-NPs was measured using FTIR spectrometer with a model number (FT/IR-6600 type A). The sample was first diluted at 1:20 with KBr prior to the analysis, and a background of pure KBr was acquired before scanning the sample.

### 3.5.3. Particle Size Analysis of $Al_2O_3$-NPs

The analysis of particle size for the $Al_2O_3$-NPs was performed using Particle Size Analyzer (PSA)/Zetasizer-Nano, model number ZEN 3600 (Malvern Instrument Ltd. Worcestershire,

UK). The size measurement of PSA was based on dynamic light scattering (DLS), which measures the particle size with a measurement range of (0.3 nm to 10 µm). Before the analysis, the sample was dispersed two types of dispersants (distilled water and propan-2-ol) for 40 minute. The sample dispersed in both dispersant solvents was analyzed to understand the effect of dispersant on the particle size of the nanoparticle. The result of PSA was reported by percent intensity to determine the average particle size of the nanoparticle.

### 3.5.4. X-ray Diffraction (XRD) Analysis of $Al_2O_3$-NPs

The XRD analysis of the as prepared $Al_2O_3$-NPs was conducted using (XRD-700 XRAY diffractometer, shimadzu Corporation, Japan) with continuous scanning at a speed of $3^o$/min within ($10^o$ - $80^o$) diffraction angles. During the XRD analysis, the sample was placed into the center of the instrument and illuminated with a beam of X-rays, and the XRD patterns from the sample was recorded via measurements of the diffraction angles of X-ray beams altered by the interference of atomic structure of the sample.

**Scherrer equation**:

$$D = \frac{K\lambda}{\beta\cos\theta} \qquad \text{Eq (3.10)}$$

Where; 'D' is Crystallite size, 'K' is shape factor (Scherrer constant = 0.9), '$\lambda$' is wave length of X-ray ($\lambda$ = 0.15406 nm), '$\beta$' is Full width half maxima (FWHM), '$\theta$' is diffraction angle.

**Bragg's equation**:

$$d = \frac{n\lambda}{2\sin\theta} \qquad \text{Eq (3.11)}$$

Where; 'd' is d-spacing, 'n' is order of diffraction (n = 1), '$\theta$' is diffraction angle, and '$\lambda$' is wave length of incident X-ray ($\lambda$ = 0.15406 nm).

### 3.5.5. Analysis of Dispersion Stability of $Al_2O_3$-NPs with in Gly-lac

The dispersion stability of $Al_2O_3$-NPs within purified Gly-lac was analyzed by physical detection and as well as using Zeta potential analysis. In the physical detection, the $Al_2O_3$-NPs was first dispersed in purified Gly-lac at different loading rate of $Al_2O_3$-NPs (1wt%, 2wt%, 3wt%, and 4wt%). The dispersion was agitated by ultrasonicating for 45 minute to reduce particle aggregation and to enhance its dispersion (Anchupogu, 2018; Soudagar et al., 2018). Then, the sample was kept on for 72 hours and noticed if a visible separate phase was created or not in the dispersion.

The analysis of zeta potential was conducted after obtaining the maximum loading rate at which stable dispersion was possible during the physical detection. Zeta potential analysis was conducted at 3wt% $Al_2O_3$-NPs loading rate with in Gly-lac. Zeta potential was measured using Zetasizer Nano instrument (Nano ZS (Red badge)) with model number ZEN 3600 (Malvern Instrument Ltd. Worcestershire, UK). The size range for Zetasizer to measure zeta potential was (3.8 nm - 100 µm). A 4mW He-Ne laser (with 632.8 nm wavelength) light source was used to provide an incident and a reference beam. The minimum required concentration was (0.1-1)%w/v to obtain sufficient scattering from the solution to perform effective zeta potential measurement.

### 3.6. Cold Flow Property of Analysis of Biodiesel

Biodiesel cold flow properties (cloud point and pour point) tests were conducted in the laboratory of Nazteck Petroleum group (LUBTAM Company), located in Gelan city.

#### 3.6.1. Testing Cloud Point (CP) and Pour Point (PP) of Biodiesel

The measurement of CP and PP was performed by using automatic cloud point and pour testing machine (Koehler model) based on the ASTM standard methods, ASTM D2500-ISO3015 for cloud point and ASTM D97-ISO3016 for pour point. The setup for cloud point and pour point test machine is shown in Figure 3.4.

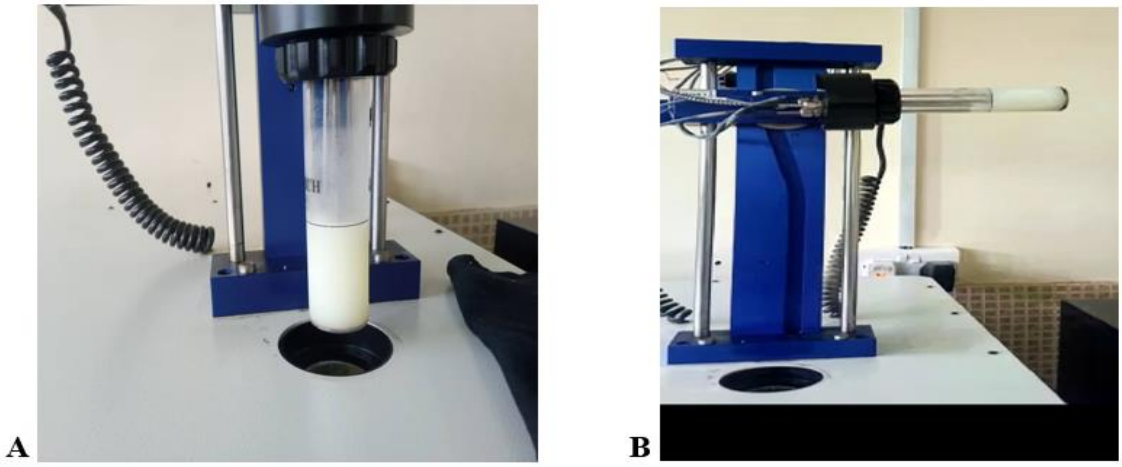


Figure 3.4: Setup of cold flow property test (A) at cloud point, (B) at pour point

During the analysis, the biodiesel sample was poured into the cylindrical sample holder fitted with thermometer. Then the sample holder was placed inside the cooling bath. For the cloud point test, the detection was done for every 1$^{o}$C drop in the sample temperature until the formation of a haze at the bottom of the sample holder as shown in Figure 3.4A. For pour point

test, the detection was done for every 3$^{o}$C drop in sample temperature until the sample ceases to flow when the sample holder is held horizontally for 5 second as shown in Figure 3.4B.

### 3.6.2. The Effects of Gly:lac Molar Ratio and Loading Rate on CP and PP

The purified 3-armed Gly-lac with different Gly:lac molar ratio (1:3, 1:6, 1:9, and 1:12) was used as cold flow improver for biodiesel. Biodiesel-(3-armed Gly-lac) mixture was prepared by dissolving the purified Gly-lac within biodiesel by heating at 60$^{o}$C using hot plate and agitating at 200 rpm for 10 minute, and subsequent ultra-sonication at 30$^{o}$C for 30 minute to allow further mixing (Yang et al., 2021). Here, the effect of Gly:lac molar ratio on CP and PP was studied by loading each Gly:lac molar ratios (1:3, 1:6, 1:9, and 1:12) into biodiesel at constant loading rate of 10 g/l based on previous works (Hamada et al., 2010; Tesfaye & Katiyar, 2016; Yang et al., 2021). Then, the effect of loading rate of 3-armed Gly-lac on CP and PP was investigated using the selected Gly:lac molar ratio (1:6). The CP and PP of biodiesel were tested by loading the 3-armed Gly-lac in to biodiesel at a rate of (5 g/l, 10 g/l, and 15 g/l).

### 3.6.3. The Effects of $Al_2O_3$-NPs dispersed Gly-lac on CP and PP

The effect of $Al_2O_3$-NPs dispersed Gly-lac on CP and PP was studied with the selected Gly:lac molar ratio and Gly-lac loading rate. The $Al_2O_3$-NPs (1wt%, 2wt%, and 3wt%) was dispersed in Gly-lac (1:6) and labeled as GAl1%, GAl2, GAl3% respectively. The Gly-lac loading rate with respect to biodiesel was 10 g/l selected from the study of loading rate effect on CP and PP. The ultrasonic method was used to disperse the $Al_2O_3$-NPs within Gly-lac to enhance its dispersion (Soudagar et al., 2018). Then, the Gly-lac/$Al_2O_3$-NPs blend was dissolved in biodiesel with the help of ultrasonicate at 30$^{o}$C for 30 minute (Yang et al., 2021). The CP and PP tests were conducted with the addition of GAl1%, GAl2, and GAl3% into biodiesel.

## 3.7. Analysis of IC Engine Performance and Emission Characteristics

### 3.7.1. Fuel-Additive Blend Preparation

- **Biodiesel-Diesel Blend (B20)**: It was prepared by mixing the synthesized soyabean-based biodiesel and diesel with a B20 proportion (i.e., 20% biodiesel and 80% diesel). The B20 blend was mixed by hand shake for 5 minute to allow homogenous mixture.
- **B20-(3-armed Gly-lac) Blend (B20G)**: In order to prepare B20-(3-armed Gly-lac) blend, first 10 g of 3-armed Gly-lac was dissolved in 200 ml of B20 via heating using hot plate at 60$^{o}$C for 10 minute. Then, additional B20 was added to make one 1liter of B20-**(**3-armed

Gly-lac) blend. B20-(3-armed Gly-lac) blend was further mixed with the help of ultrasonicate at 30°C for 20 minute (Yang et al., 2021).

- **B20-(3-armed Gly-lac)-$Al_2O_3$-NPs Blends**: In this case, first the $Al_2O_3$-NPs were dispersed in 3-armed Gly-lac at different loading rate of $Al_2O_3$-NPs (1wt%, 2wt%, and 3wt% with respect to 3-armed Gly-lac). Then, the 3-armed Gly-lac/$Al_2O_3$-NPs blend was mixed with B20 using ultrasonicate at 30°C for 20 minute (Yang et al., 2021). The B20-(3-armed Gly-lac)-$Al_2O_3$-NPs blends (at 10g/l of 3-armed Gly-lac/$Al_2O_3$-NPs) were labeled as B20GA1%, B20GA2%, B20GA3% for respective $Al_2O_3$-NPs loading rate of 1wt%, 2wt%, and 3wt%.
- **B20-$Al_2O_3$-NPs Blend (B20A)**: In this case, the $Al_2O_3$-NPs (0.1 g/l with respect to B20 which is in equal amount with 1wt% in case of B20-(3-armed Gly-lac)-$Al_2O_3$-NPs) were dispersed in B20 by using ultrasonicate at 30°C for 45 minute (Anchupogu, 2018).

### 3.7.2. The Effect of Gly-lac/$Al_2O_3$-NPs on Emission and Engine Performance of B20

The experiments for engine performance and exhaust gas emission tests were conducted at Defense University Engineering College in Automotive workshop. Four strokes, single cylinder, water cooled diesel engine (Model-R180) was used for IC engine performance test. The experimental setup of IC engine test is shown in Figure 3.5A. In parallel with IC engine test, a probe, which is a component of automotive emission gas analyzer (FGA-4100) shown in Figure 3.5B, was connected with the exhaust gas line in order to measure the concentration of exhaust gases. During the engine performance and emission gas analysis, biodiesel-diesel blend (B20) was used as a reference so as to investigate the effect of $Al_2O_3$-NPs dispersed 3-armed Gly-lac on performance parameters (brake power, brake thermal efficiency, and brake specific fuel consumption) as well as on the exhaust gas emission (HC, CO, $CO_2$, and $NO_x$).

The IC engine performance and emission test experiments were done at various engine loads (%) at constant engine speed of 1500 rpm. During the test, measurement of torque was performed with the help of hydraulic dynamometer, and the volumetric flow rate of fuel sample consumed by the combustion process was determined with the help of fuel flow meter.

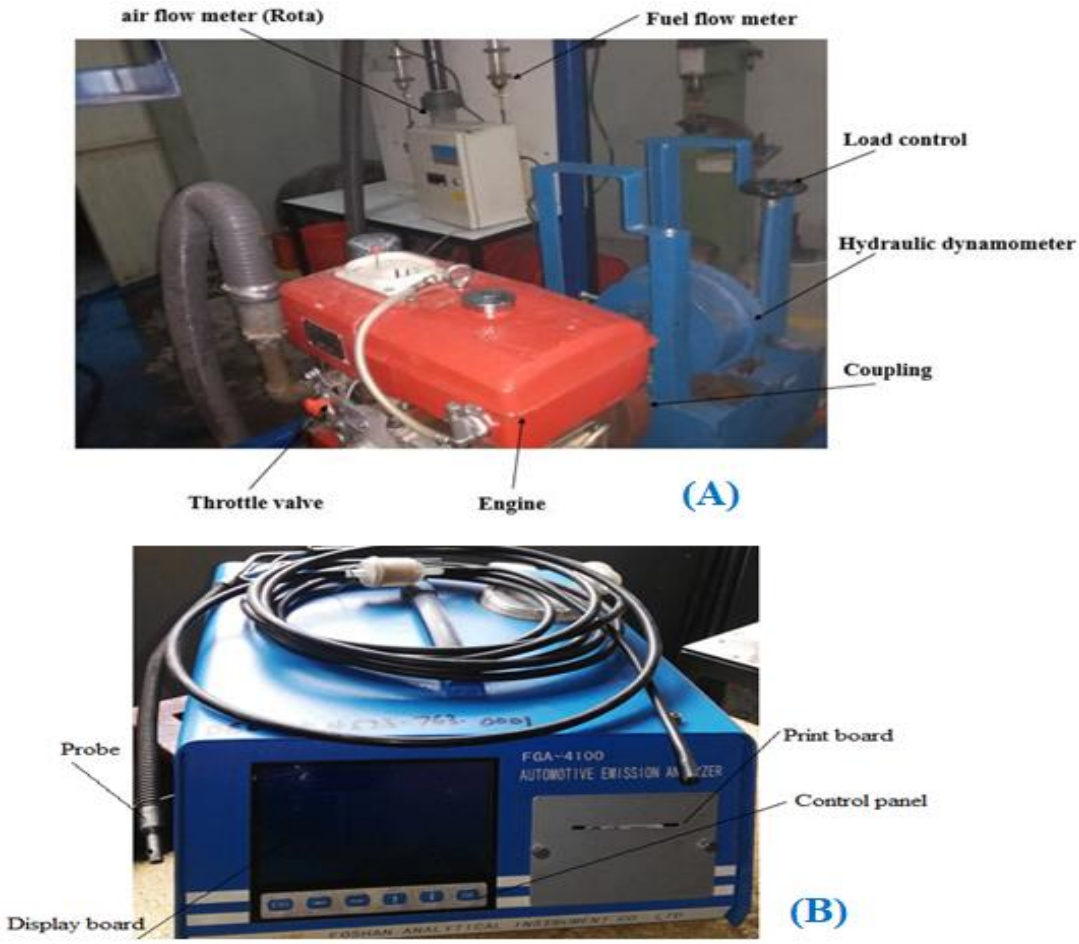


Figure 3.5: Setup of (A) IC engine test, (B) FGA-4100 automotive emission gas analyzer

The specifications of the IC diesel engine and that of the FGA-4100 automotive gas analyzer are described in Table 3.2 and 3.3 respectively. The experimental frame work followed during the analysis of IC engine performance and exhaust gas emission for biodiesel-diesel-additive blends is illustrated in Table 3.4.

Table 3.2: Specification of the test diesel engine

| Name | Details | Name | Details |
|---|---|---|---|
| Model | R180 | Injection timing | $23^0$ bTDC |
| Engine type | 4-stroke, single cylinder, water cooled DI diesel engine | Displacement volume | 402 cc |
| Loading device | Hydro-dynamometer | Maximum torque | >=23.4 |
| Rated power | 5.67 kW at 2600 rpm | Nozzle opening pressure | 20MPa |
| Cylinder bore and stroke | 80 mm x 80mm | Nozzle type, hole diameter | Pintle, 0.84 mm |
| Compression ratio | 21:1 | Net weight(kg) | 72 |

Table 3.3: Specification of FGA-4100 automotive gas analyzer

| Gas | Measurement Range | Resolution |
|---|---|---|
| CO | 0-10 %vol | 0.01% |
| $CO_2$ | 0-20% vol | 0.1% |
| HC | 0-2000 ppm | 1ppm |
| Nox | 0-5000 ppm | 1ppm |

Table 3.4: Experimental frame work for engine performance and emission gas test

| Controlled variables | | Fuel-additive blend samples | Performance parameters evaluated | Emission gases measured |
|---|---|---|---|---|
| Engine speed | Load (%) | | | |
| Constant at 1500 rpm | ✓ 20%<br>✓ 40%<br>✓ 60%<br>✓ 80%<br>✓ 100% | B20<br>B20G (B20 + Gly-lac)<br>B20A (B20 + $Al_2O_3$)<br>B20GA1% (B20 + Gly-lac + 1wt%$Al_2O_3$)<br>B20GA2% (B20 + Gly-lac + 2wt%$Al_2O_3$)<br>B20GA3% (B20 + Gly-lac + 3wt%$Al_2O_3$) | ✓ Brake power (BP) in kW.<br>✓ Brake thermal efficiency (BTE) in %<br>✓ Brake specific fuel consumption (BSFC) in kg/kWh. | ✓ HC (ppm)<br>✓ CO (%vol)<br>✓ $CO_2$ (%vol)<br>✓ NOx (ppm) |

- **Brake Power (BP)**: The power available at the engine crank shaft (drive shaft) is referred as brake power or shaft power or delivery power. BP was calculated by using equation (3.12).

$$BP = \frac{2\pi x N x T}{60{,}000} \qquad \text{Eq (3.12)}$$

Where; 'BP' is brake power in kW, 'N' is engine speed in (rpm), and 'T' is Torque in (N.m).

- **Brake specific fuel consumption (BSFC):** Describes the amount of fuel consumed for the generation of unit brake power. It is expressed as the ratio of mass flow rate of fuel (kg/s) to brake power (kW) generated from the combustion of the fuel in the engine.

$$BSFC = \frac{\dot{m}_f x 3600}{BP} \qquad \text{Eq (3.13)}$$

Where; 'BSFC' is brake specific fuel consumption in (kg/kWhr), '$\dot{m}_f$' is mass flow rate of fuel in kg/s, and 'BP' is brake power in kW.

- **Brake thermal efficiency (BTE)**: It is the critical engine performance parameters for a certain fuel which describes its ignition capability, or it shows how well the fuel's energy is transformed into useful work (Ağbulut et al., 2020). BTE was calculated using eq (3.14).

$$BTE\ (\%) = \frac{BP}{\dot{m}_f x CV} \text{ x } 100\% \qquad \text{Eq (3.14)}$$

Where; 'BTE' is brake thermal efficiency in (%), '$\dot{m}_f$' is mass flow rate of fuel in kg/s, 'CV' is calorific value of the fuel sample, and 'BP' is brake power in kW.

# CHAPTER FOUR

# 4. RESULTS AND DISCUSSION

In this chapter, the different results obtained are discussed in detail starting from the results of soyabean oil characterization. The results from different characterizations of biodiesel (synthesized from soyabean), synthesized and purified Gly-lac, and for the synthesized alumina nanoparticle are also discussed in this chapter. The results from the analysis of cold flow properties of biodiesel were also discussed in this chapter with an emphasis on the effects of Gly:lac molar ratio, Gly-lac loading rate, and $Al_2O_3$-NPs dispersed Gly-lac on biodiesel cold flow properties (mainly cloud point and pour point). Later in this chapter, the results from the analysis engine performance and exhaust gas emission for biodiesel-diesel were understood in detail. In this case the effects of $Al_2O_3$-NPs dispersed Gly-lac on brake power, brake thermal efficiency, and the emission of unburned hydrocarbon (HC), NOx, and CO were discussed using B20 as a baseline reference.

## 4.1. Characterization of Properties of Soyabean Oil

**Acid Value and %FFA**: Acid value for any type of oil describes the extent by which the free fatty acid is present in oil, which is defined as the weight in mg of KOH required to neutralize the free fatty acid in 1 g of oil (Seneviratne & Jayathilaka, 2020). The acid value and %FFA were determined by titration using 0.1N NaOH solution until the appearance of pink colour. The parameters used to determine acid value and %FFA were mass of soyabean oil used, the titrant volume used, molecular weight of NaOH, and normality of NaOH solution. The acid value and %FFA of soyabean oil were found to be 0.99 mg KOH/g and 0.495% respectively as shown in Table 4.1. The titration results and calculations are shown in **Appendix A (**Table A1).

Table 4.1: Characterization results of soyabean oil properties

| Acid value | %FFA | Moisture content | Iodine value |
|---|---|---|---|
| 0.99 mg KOH/g | 0.495% | 1.43% | 126.054 g $I_2$/100 g oil |

**Moisture Content of Oil**: The soyabean oil moisture content was found to be 1.43% as shown in Table 4.1. See **Appendix A (**Table A2) for detail results of the moisture content test.

Free fatty acids (FFA) are formed via hydrolysis of triglycerides by the action of enzymes such as lipase (Seneviratne & Jayathilaka, 2020). A certain oil to be used in homogenous base trans-esterification reaction, its %FFA and moisture content should be less than 2% and 1.5%

respectively (Chen et al., 2012), otherwise the reaction between base catalyst and excess free fatty acid could be favored to form soap. The value of %FFA (0.45%) and moisture content (1.43%) for the soyabean oil were suitable for the biodiesel synthesis through base catalyzed trans-esterification reaction, which was performed with appropriate reaction conditions.

**Iodine Value (IV)**: IV of soyabean oil was found 126.054 g $I_2$/100 g as shown in Table 4.1. Iodine value measures the unsaturation degree of fatty acids, which is expressed as the number of grams of iodine required to saturate 100 g of oil. The higher iodine value indicates high unsaturation degree, as $I_2$ reacts with the double bonded fatty acid contents of the given oil (Seneviratne & Jayathilaka, 2020). The standard for soyabean oil IV is (120 - 143) g $I_2$/100 g (Seneviratne & Jayathilaka, 2020). Here, the soyabean oil IV was in agreement with its standard value which was good to use the soyabean oil for biodiesel synthesis. The titration results for iodine value determination are shown in **Appendix A (**Table A3). The IV soyabean oil is in agreement with a study by (Soares & Rocha, 2018), in which IV of refined soyabean oil was 133 g $I_2$/100 g.

### 4.2. Characterization of Synthesized Biodiesel

The biodiesel was synthesized from soyabean oil, separated from glycerol and purified by washing with distilled water. During the glycerol separation a clear phase separation was detected in which the top layer was biodiesel whereas glycerol was in bottom layer due to the higher density of glycerol relative to biodiesel. The different characterizations of soyabean-based biodiesel are discussed in this section.

#### 4.2.1. Functional Group Analysis of Biodiesel

The FTIR spectrum of the synthesized soyabean-based biodiesel is shown in Figure 4.1, in which different transmittance peaks were observed associated with the stretching and bending vibration of different functional groups while being exposed to infrared radiation. A strong peak was observed at 1744 $cm^{-1}$, which is attributed to the stretching vibration of the carbonyl (C=O) group in the methyl ester (Rabelo et al., 2015). The spectra at 1170 $cm^{-1}$, 1196 $cm^{-1}$, and 1026 $cm^{-1}$ indicate the stretching vibration of $O–CH_3$ (Rabelo et al., 2015). The transmittance peaks at 2921 $cm^{-1}$ and 2858 $cm^{-1}$ denote the C–H stretching (Nabi et al., 2009; Rabelo et al., 2015). The other spectra was observed at 1440 $cm^{-1}$ and 1461 $cm^{-1}$, which illustrate the asymmetric stretching of $CH_3$ and the C–H bending, respectively (Nabi et al., 2009; Rabelo et al., 2015).

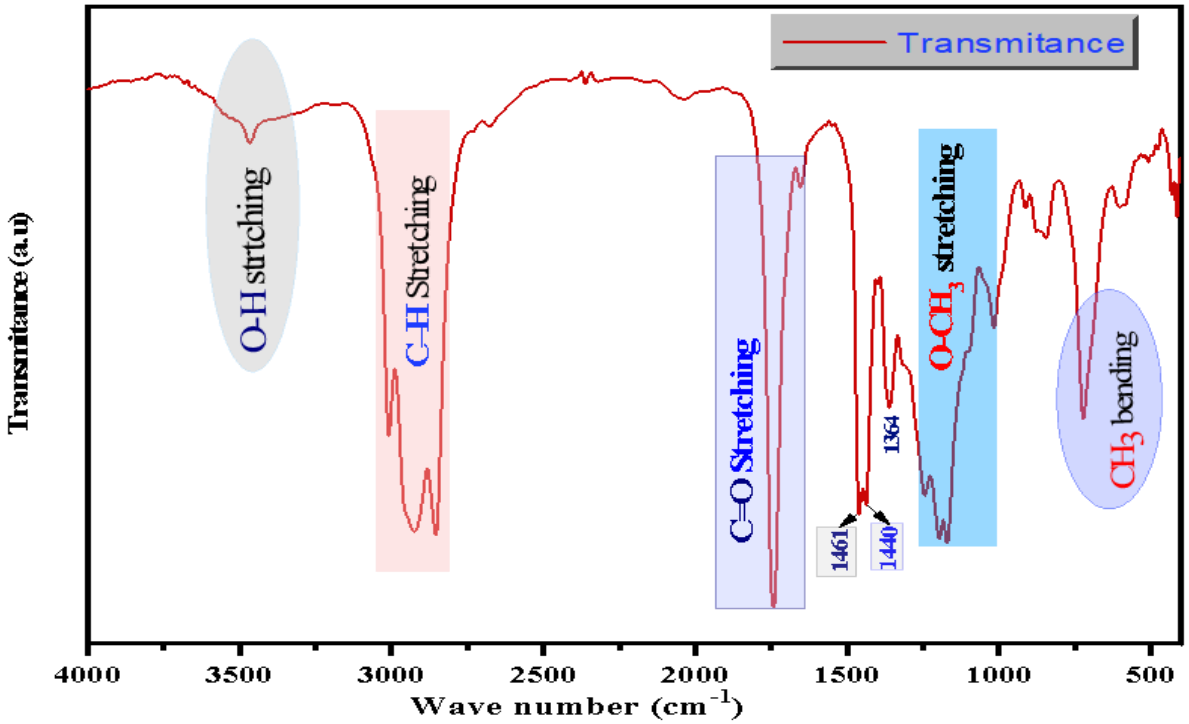


Figure 4.1: Fourier Transform Infrared (FTIR) spectrum of synthesized biodiesel

The characteristics peaks at 725 $cm^{-1}$ and 1364 $cm^{-1}$ are attributed to bending vibration of $CH_3$ and $(CH_2)$ n respectively (Nabi et al., 2009). The other peak at 3472 $cm^{-1}$ describes the OH stretching that could be suspended from residual glycerol. In general, the existence of the function groups in biodiesel was confirmed by their characteristic's peaks in the FTIR spectrum.

### 4.2.2. Analysis of Chemical Structure for Biodiesel

**$^1$H NMR analysis:** A $^1$H NMR spectrum of the as synthesized soyabean-based biodiesel is shown in Figure 4.2. The chemical shift for the unsaturated protons (CH=CH) and the outer hydrogen in the conjugated double bonds (-CH=CH–CH=CH-) were detected at (5.21 - 5.21) ppm, which are expected in the range of (5.06 - 5.65) ppm (Doudin, 2021; Sarpal et al., 2015). Those groups require high shifting energy due to de-shielded nature because of the strong attraction force among the double bonded carbons. The triplet peaks at (1.91 - 1.94) ppm and (2.63 - 2.66) ppm are attributed to methylene group in allylic ($CH_2$-CH=CH) and bisallylic (CH=CH-$CH_2$-CH=CH) groups, respectively (Sarpal et al., 2015). The allylic and unsaturated groups indicate the existence of unsaturated FAME, whereas the presence of bisallylic methylene group validates the existence of the di-unsaturated FAME.

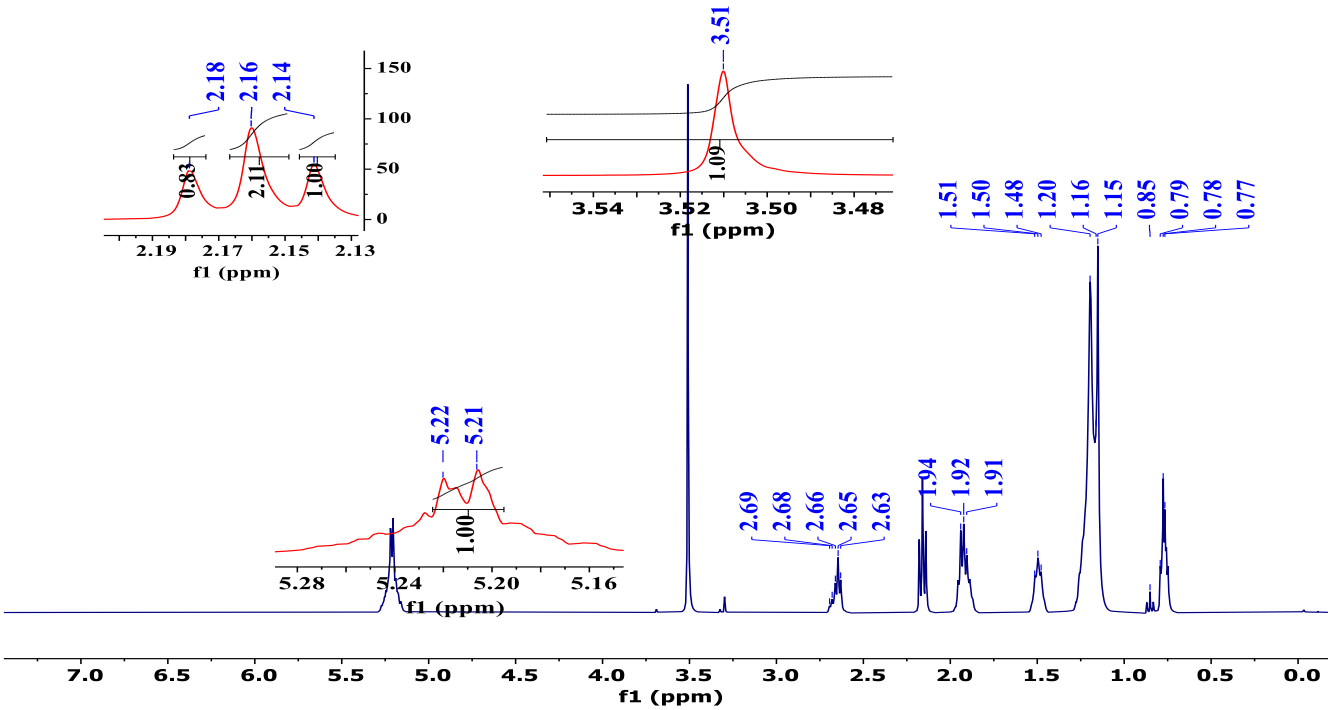


Figure 4.2: [1]H NMR Chemical shift of synthesized biodiesel

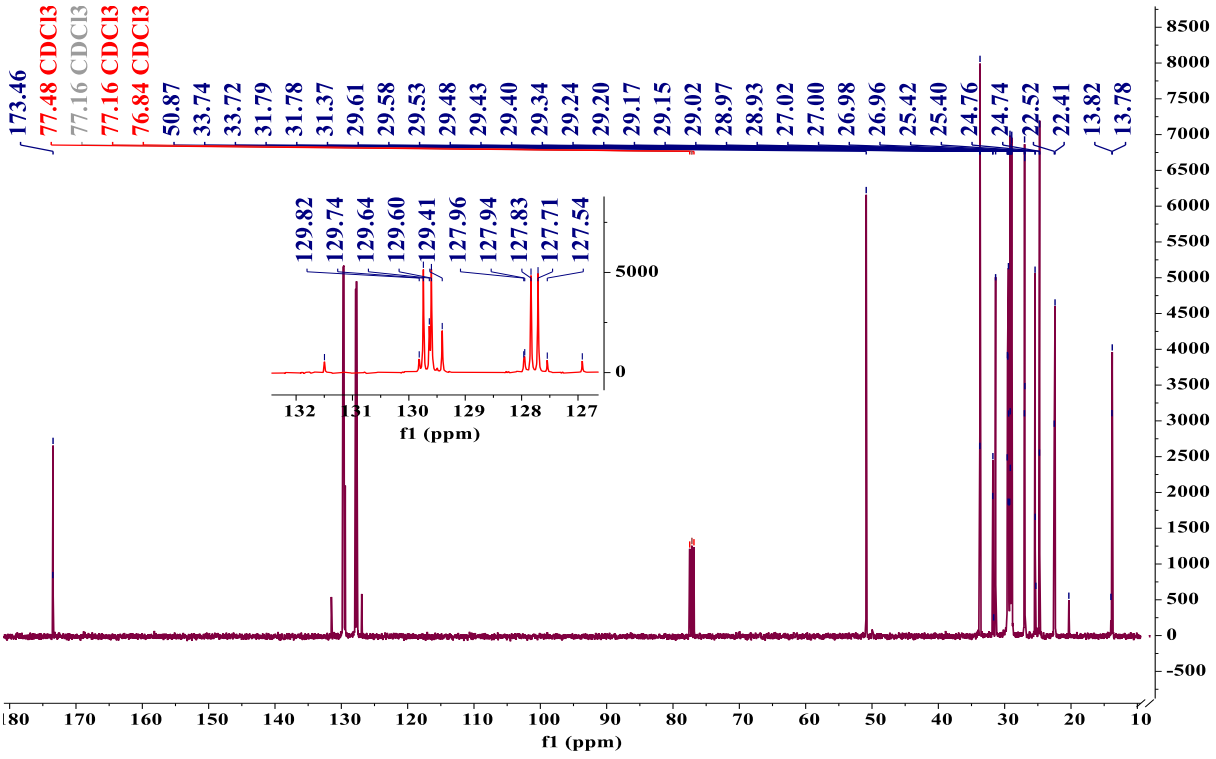


Figure 4.3: [13]C NMR Chemical Shift for Soyabean biodiesel

The chemical shifts at 2.68 ppm and 2.69 ppm represent the methylene group between two double bonds of linoleic (C18:2) and linolenic (C18:3) groups (Morgenstern et al., 2006; Sarpal et al., 2015), which are the key components of soyabean-based biodiesel. The other chemical shifts at 3.51 ppm, 2.18 ppm, and (1.48 - 1.51) ppm are attributed to the methoxy group (O-$CH_3$), $\alpha$-$CH_2$ group (adjacent to carbonyl group, $CH_2$-C=O), and $\beta$-$CH_2$ ($CH_2$-$CH_2$C=O) respectively (Sarpal et al., 2015; Tariq et al., 2011). Those peaks are evidence for the existence of methyl esters in the as synthesized biodiesel. The doublet at (1.15 - 1.20) ppm describes the long alkyl chain ($CH_2$) n. The chemical shift at (0.77 - 0.85) ppm is attributed to the terminal -$CH_3$ group (Tariq et al., 2011).

$^1$H NMR is also helpful to determine the conversion of oil into FAME by using integral areas of $OCH_3$ and $\alpha$-$CH_2$ groups (Tariq et al., 2011). Conversion was calculated using equation (3.5).

$$\text{Conversion (\%)} = 100 \text{ x } \frac{2A_{ME}}{3A_{CH2}} = 100 \text{ x } \frac{2x1.09}{3x0.83} = 87.55\%$$

Where; '$A_{ME}$' is integral area of $OCH_3$ = 1.09, and '$A_{CH2}$' is integral area of $\alpha$-$CH_2$ = 0.83.

**$^{13}$C NMR Analysis**: The $^{13}$C NMR chemical shifting of biodiesel is shown in Figure 4.3, in which the chemical shifting at different frequency corresponds to carbon atom involved in various chemical groups. The chemical shift value at (173.46 - 173.49) ppm describes the carbonyl group (C=O) group, and the other carbonyl (C–O) group was indicated by the chemical shift at 50.87 ppm (Tariq et al., 2011). The chemical shift was observed at (129.41 - 129.82) ppm, which denotes the unsaturated carbons (-CH = CH-) and the outer carbons of the non-conjugated group (-CH = CH - $CH_2$ - CH = CH-), whereas the inner carbons of the non-conjugated group (-CH = **C**H - $CH_2$ - **C**H = CH-) are represented by the chemical shift at (127.54 - 127.96) ppm (Doudin, 2021). The existence of chemical shift at (13.78 - 13.98) ppm, (22.41 - 31.79) ppm, and 33.74 ppm represent the carbon in the terminal methyl group, long carbon chain ($CH_2$) n, and the methylene -$CH_2$- group adjacent to the carbonyl group, respectively (Doudin, 2021; Tariq et al., 2011).

### 4.2.3. Analysis of Biodiesel Physico-chemical Properties

**Iodine value (IV)**: IV of the synthesized biodiesel was found to be 73.602 g $I_2$/100g as shown in Table 4.2, which is in agreement with the biodiesel standard (IV≤120). IV is the measure of amount in gram of iodine absorbed by 100 g of biodiesel, which defines the unsaturation nature of biodiesel that helps to examine its oxidation stability. High unsaturation degree leads to the

occurrence of oxidation reaction caused by addition of oxygen in double bonds which deteriorate the oxidation stability of the biodiesel (Lawan et al., 2019; Sahar et al., 2018). The IV result is in agreement with previous works by (Sahar et al., 2018) in which IV was found 63.5 g I2/100 g.

**Saponification Value (SV)**: SV is defined as the mg of KOH required to neutralize 1 gram biodiesel. High SV indicates the existence of high fraction of free fatty acid and vice versa. The biodiesel standard for SV is (<320 mg KOH/g) (Sahar et al., 2018). In this study, the biodiesel SV was found to be 148.104 mg KOH/g as shown in Table 4.2, which is in agreement with its standard, describing that it has acceptable quality.

**Cetane Number (CN):** The CN of biodiesel was fond to be 66.59. As per the standards, biodiesel have a cetane number (45 - 70), therefore the synthesized biodiesel has acceptable cetane number. Fuel with high cetane number has good ignition feature, which indicates short ignition delay period between the start of fuel injection and the start of auto ignition. The cetane number of the soyabean-based biodiesel was relatively higher, which shows a good ignition probability.

Table 4.2: Properties of biodiesel synthesized from soyabean oil

| Properties | Unit | Synthesized Biodiesel | Biodiesel Standards | Reference |
|---|---|---|---|---|
| Iodine value (IV) | g $I_2$/100g | 73.602 | ≤ 120 | (Sahar et al., 2018) |
| Saponification value (SV) | mg of KOH/g | 148.104 | < 320 | |
| Cetane number | --- | 66.59 | (45 - 70) | (Smith et al., 2010) |
| Flash point | ℃ | 153 | ≥ 130 | (Astm D, 2012; ASTM D6751-02, 2002) |
| Fire point | ℃ | 165 | --- | |
| Kinematic Viscosity @ 25ºC | $mm^2/s$ | 4.24 | 1.9 - 6.0 | |
| Density | $g/cm^3$ | 0.885 | 0.86 - 0.9 | EN ISO 3675 |
| Calorific Value | kJ/kg | 38970.75 | --- | --- |

**Viscosity:** Viscosity of biodiesel is a crucial property that influences its flow ability within the engine pipe line. As shown in Table 4.2, the biodiesel viscosity standard is (1.9 - 6) $mm^2/s$. Viscosity below the lower limit could result in unnecessary internal pump leakage which ultimately leads to the formation of black smoke. On the other hand, viscosity above the standard

limit might result in poor spray atomization that causes engine operational problems such as higher emissions, lower engine performance and deposits (Lawan et al., 2019). As shown in Figure 4.4, the viscosity analysis result was 3.75 cP that is equivalent to 4.24 $mm^2/s$, which is in agreement with its standard as per the ASTM D-6751. The viscosity result is also in agreement with the previous work done by (Tesfaye & Katiyar, 2016), in which viscosity was found to be 4.17 $mm^2/s$.

Figure 4.4: Analysis result for viscosity of biodiesel

Flash point and fire point are also important properties of biodiesel that determines the ease of handling and storage (Agarwal et al., 2010). A high flash point and fire point of biodiesel indicates that the biodiesel is safe for handling and storage (Agarwal et al., 2010). On the other hand, the flash point should not exceed 176$^oC$, as too high flash point could affect its vaporization, which have negative impact when it is used in diesel engine (Kaisan et al., 2020). As shown in Table 4.2, flash point and fire point of biodiesel were found to be 150$^oC$ and 163$^oC$ respectively which is in agreement with its standards, indicating that the biodiesel is safe for handling and storage.

Density of biodiesel is another key property which determines its consumption in which a certain fuel should have to be less dense that favors a lower fuel consumption. Density of biodiesel was obtained 0.885 $g/cm^3$ which is in agreement with the standard limit (0.86 - 0.9) $g/cm^3$ as per the EN ISO 3675 standard. The density result of biodiesel is comparable with study by (Tesfaye & Katiyar, 2016), in which density of 0.891 $g/cm^3$ for soyabean-based biodiesel was obtained.

### 4.3. Characterization of 3-armed Gly-lac

3-armed Gly-lac was synthesized from the reaction among glycerol and lactic acid. Purification was done due to the possibility for the existence of free lactic acid and lactic acid oligomer. The characterizations for synthesis and purification of 3-armed Gly-lac are discussed in this section.

#### 4.3.1. Analysis of Functional Group in 3-armed Gly-lac

The FTIR spectrum of the synthesized 3-armed Gly-lac (non-purified and purified) is shown in Figure 4.5. A strong transmittance peak at 1748 $cm^{-1}$ indicates the stretching vibration of carbonyl group (C=O) (Slivniak & Domb, 2005). This peak is very intense in case of the purified 3-armed Gly-lac compared to the non-purified, which might be due to removal of unreacted and oligomer lactic acid. The transmittance peaks at 945 $cm^{-1}$ and 1039 $cm^{-1}$ are due to stretching vibrations of C–O in primary and secondary hydroxyl group from glycerol respectively (Gómez-Siurana et al., 2013). The transmittance peaks around 2930 $cm^{-1}$ denotes CH stretching in $CH_3$ and $CH_2$ groups.

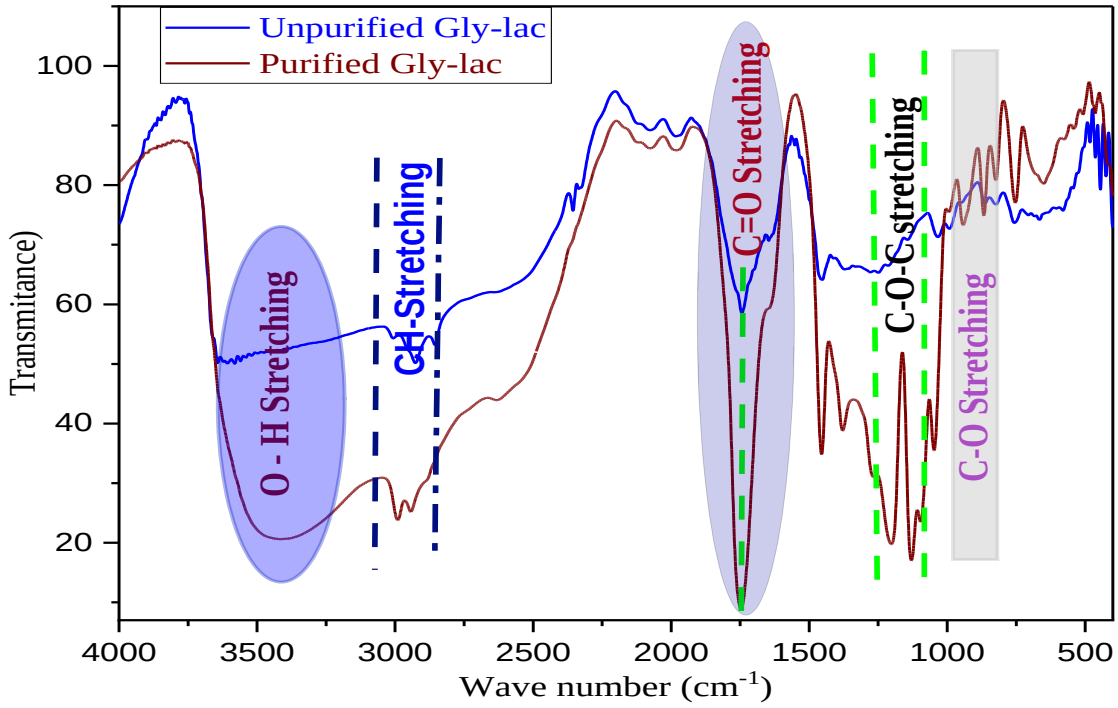


Figure 4.5: FTIR spectrum of purified and non-purified (1:6) 3-armed Gly-lac

A transmittance peak at 1645 $cm^{-1}$ in non-purified 3-armed Gly-lac is attributed to the stretching vibration of (C=O) group in the free lactic acid (Tang et al., 2019), however, this peak is not available in the purified one that validates the removal of free lactic acid via purification. The

transmittance peak at (1300 - 1000) $cm^{-1}$ indicates the C-O-C stretching vibration. A broad peak at (3260 - 3650) $cm^{-1}$ was observed in non-purified 3-armed Gly-lac that indicates O-H stretching, which attributes to both 3-armed Gly-lac and lactic acid in broad range. In the case of purified 3-armed Gly-lac, the OH peak is sharp and intense, which converges into a narrow range (3330 - 3500) $cm^{-1}$. This is a validation for the removal of free and oligomer lactic acid.

### 4.3.2. Analysis of Chemical Structure for 3-armed Gly-lac

**$^1$H NMR Analysis**: $^1$H NMR spectrum is used to determine the chemical shift for the H proton which involves in different functional groups. In this case, the $^1$H NMR spectrum is used to analyze the H proton in the chemical structure of the 3-armed Gly-lac synthesized from lactic acid and glycerol. It is also helpful to determine the presence and absence of free lactic acid and oligomer, before and after purification of 3-armed Gly-lac. Figures 4.6 and 4.7 illustrate the $^1$H NMR spectrum of both non-purified and purified 3-armed Gly-lac respectively, typically for (1:6) molar ratio with the inclusion of its possible structure.

The reaction among glycerol and lactic acid could be confirmed by the methylene group from esterified glycerol at the core of 3-armed Gly-lac chain, which is indicated at (4.25 - 4.29) ppm, and that of methine group from lactic acid at 4.09 ppm (Li et al., 2014) as shown in Figure 4.6 for the non-purified 3-armed Gly-lac. Whereas for the purified one (shown in Figure 4.7), the chemical shift for the core methylene group was shifted into (4.13 - 4.15) ppm and that of methine group was shifted into 3.98 ppm. The existence of chemical shift at (3.54 - 3.63) ppm is responsible for the terminal OH group in the 3-armed Gly-lac end chain, in which its value was shifted to (3.40 - 3.51) ppm in case of purified 3-armed Gly-lac. The decrease in chemical shifting value in case of the purified 3-armed Gly-lac could be due to the shielding effect by electrons which would have been de-shielded due to the van der Waals attraction with the approaching free and oligomer lactic acid. As shown in Figure 4.6, three doublet peaks were detected at a chemical shift value of (1.33 - 1.35) ppm, (1.39 - 1.41) ppm, and (1.44 - 1.46) ppm that corresponds to the esterified methyl ($CH_3$) group (Gross et al., 2018). Those peaks indicate the existence of six methyl group with small variation in chemical shift value. This variation could be the effect of the van der Waals attraction force by free and oligomer lactic acid. On the other hand, in case of purified 3-armed Gly-lac, the methyl group was denoted by a singlet peak at 1.33 ppm. This describes that all the methyl group become in similar energy level due to

diminishing of the van der Waals attraction upon the removal of free and oligomer lactic acid via purification.

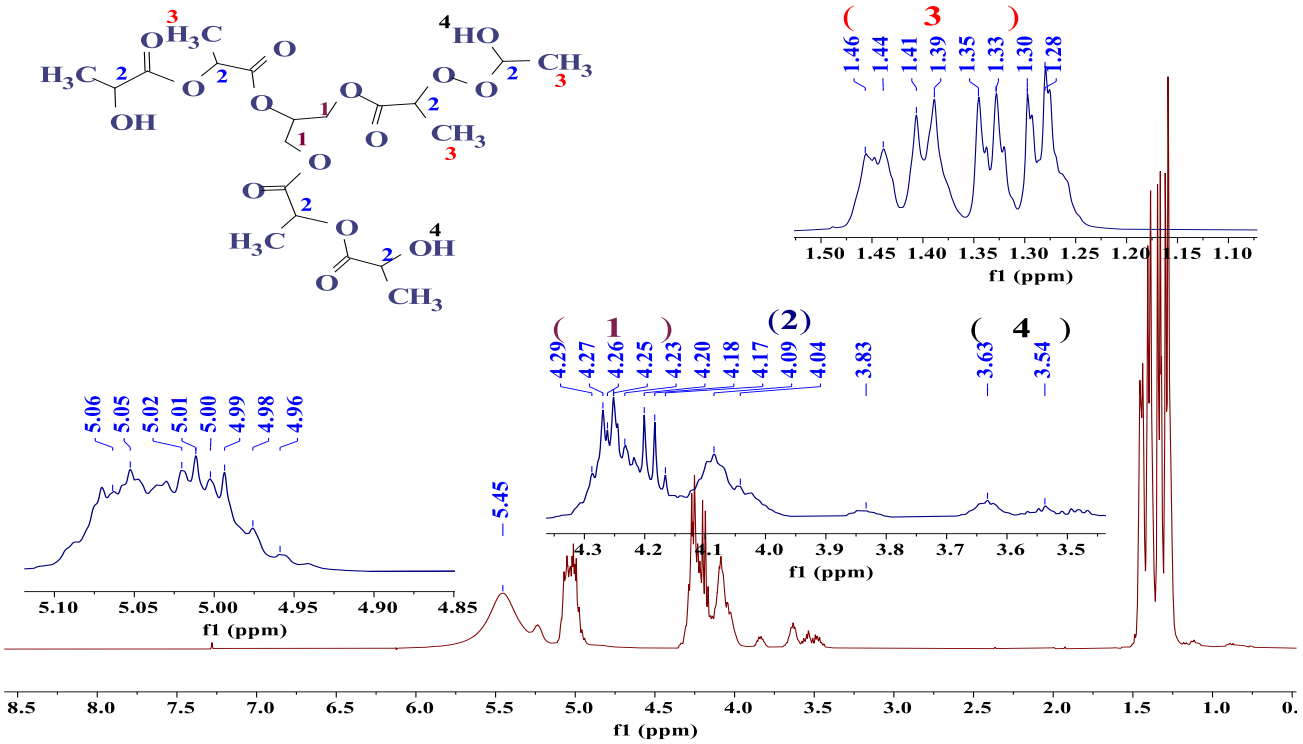


Figure 4.6: [1]H NMR spectrum of non-purified 3-armed Gly-lac for (1:6) molar ratio

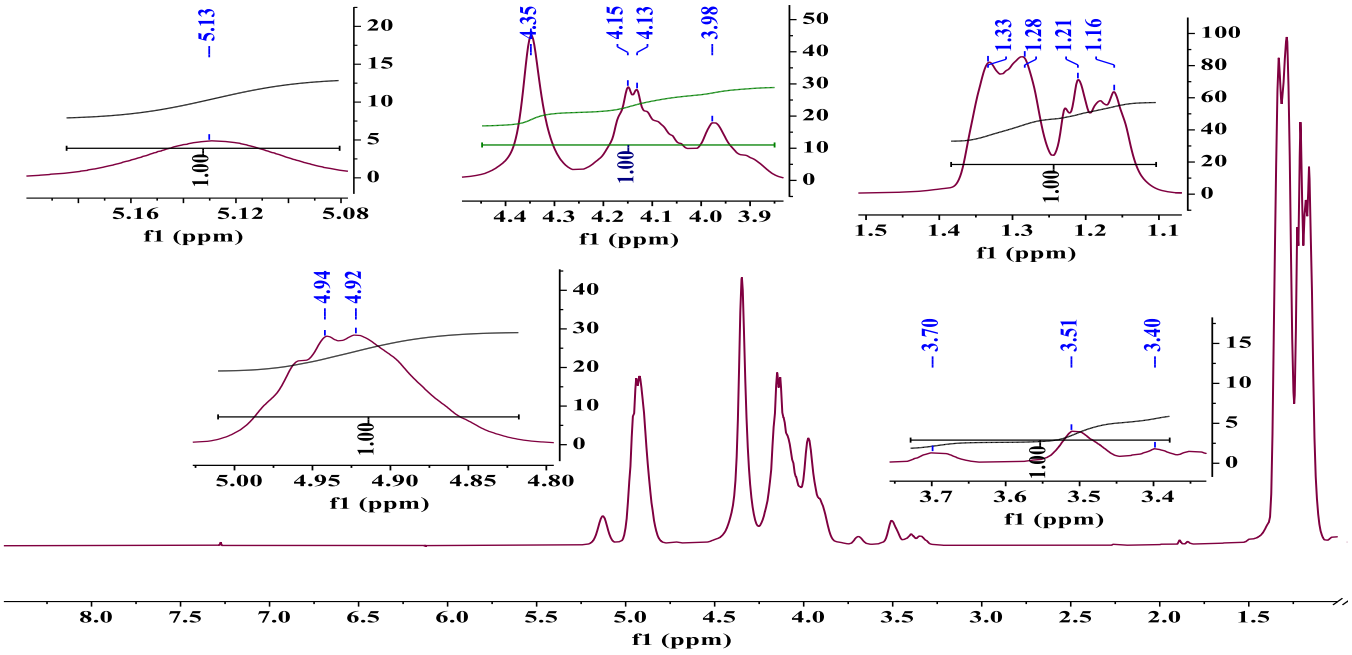


Figure 4.7: [1]H NMR spectrum of purified 3-armed Gly-lac for (1:6) molar ratio

As shown in Figure 4.6, the peak (1.27 - 1.30) ppm in non-purified 3-armed Gly-lac denotes the $CH_3$ group in unreacted and oligomer lactic acid (Rashkov et al., 1996), on the other hand, only a small peak with a minimal integral area exist at 1.28 ppm in the purified 3-armed Gly-lac as shown in Figure 4.7. In addition, the intensity of this peak was decreased and comparatively the intensity of OH and methine groups was increased. This illustrates the removal of free and oligomer lactic acid that have been approaching to the OH and methine groups. The chemical shift at (4.17 - 4.23) ppm and (4.96 - 5.06) ppm in non-purified 3-armed Gly-lac indicates the methine (CH) group in dimer and trimmer lactic acid (Espartero et al., 1996), but those peaks were absent in the purified 3-armed Gly-lac shown in figure 4.7, which is evidence for the removal of lactic acid oligomer via purification. In the purified 3-armed Gly-lac there exist a new peak at (1.16 - 1.21) ppm as shown in Figure 4.7, which might be attributed to the hydrogen in methyl and methylene groups of ethyl acetate that could be left over after purification (Sharma et al., 2007). The chemical shift at 4.04 ppm is attributed to the methine group in the free lactic acid monomer (Espartero et al., 1996), whereas this chemical shifts doesn't exist in the purified 3-armed Gly-lac, which validates the removal of unreacted lactic acid through purification.

**$^{13}$C NMR Analysis**: The $^{13}$C NMR analysis was used to determine the carbonyl bonds within the CO, CH, $CH_2$, and $CH_3$ in the structure of 3-armed Gly-lac, which is shown in Figures 4.8 & 4.9 for the non-purified and the purified respectively. The carbon associated with ester group ((C=O)-O), which was observed at (172.28 - 172.64) ppm is an indication for the occurrence of a reaction among lactic acid and glycerol. A resonance at (169.46 - 169.91) ppm is attributed to the carbonyl adjacent to (-O-$CH_2$) group, this peak also occurred in purified 3-armed Gly-lac at (168.97 - 169.59) ppm with a small decrease in chemical shift value, which could be attributed to more shielding by electron due to reduction of van der Waals force upon the removal of unreacted and oligomer lactic acid. In both the non-purified and purified 3-armed Gly-lac, the chemical shift at (66.10 - 69.67) ppm indicates the methine (-CH-) group. The end chain carbonyl group adjacent to the $\alpha$-methine was denoted by the chemical shift at (174.54 - 174.95) ppm, whereas the methyl ($CH_3$**)** group in the end chain was identified at a chemical shift value of (16.34 - 19.84) ppm. The existence of two methylene ($CH_2$-CH-$CH_2$) groups was verified by DEPT-135 analysis shown in **Appendix F**, in which two downward peaks were observed at (62.80 – 62.86) ppm and (65.21 - 65.38) ppm. These peaks are attributed to the esterified

methylene group (Rashkov et al., 1996), which is another evidence for the occurrence of a reaction among glycerol and lactic acid.

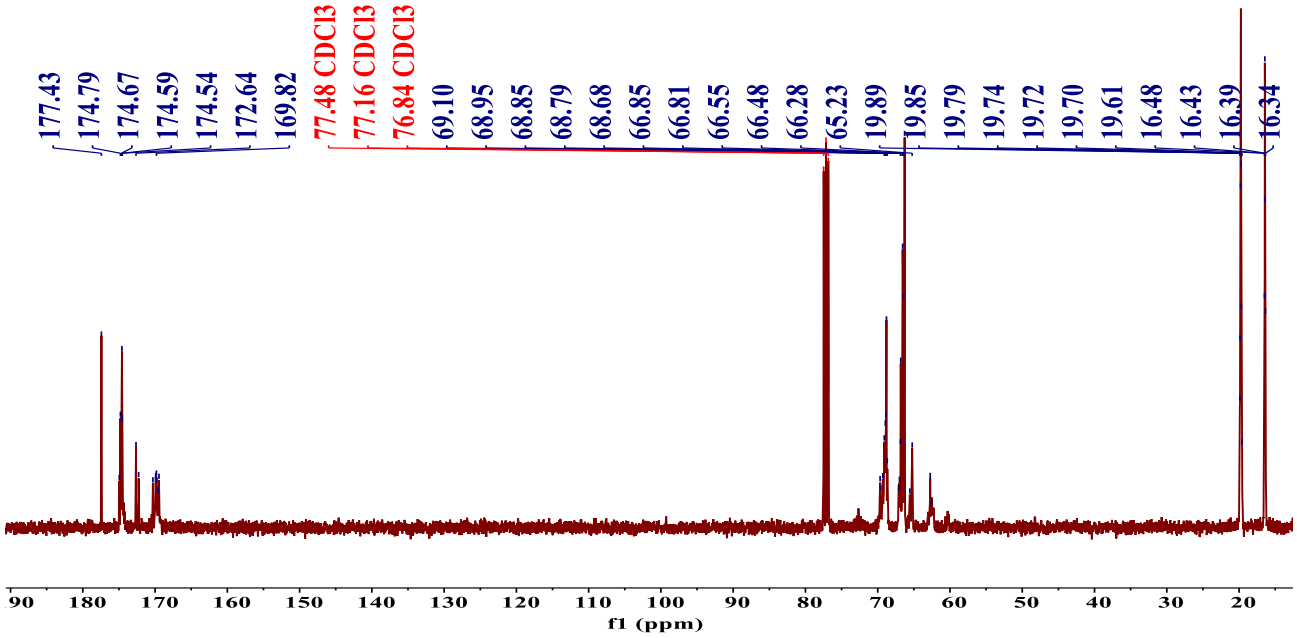


Figure 4.8: $^{13}$C NMR spectrum of non-purified 3-armed Gly-lac for (1:6) molar ratio

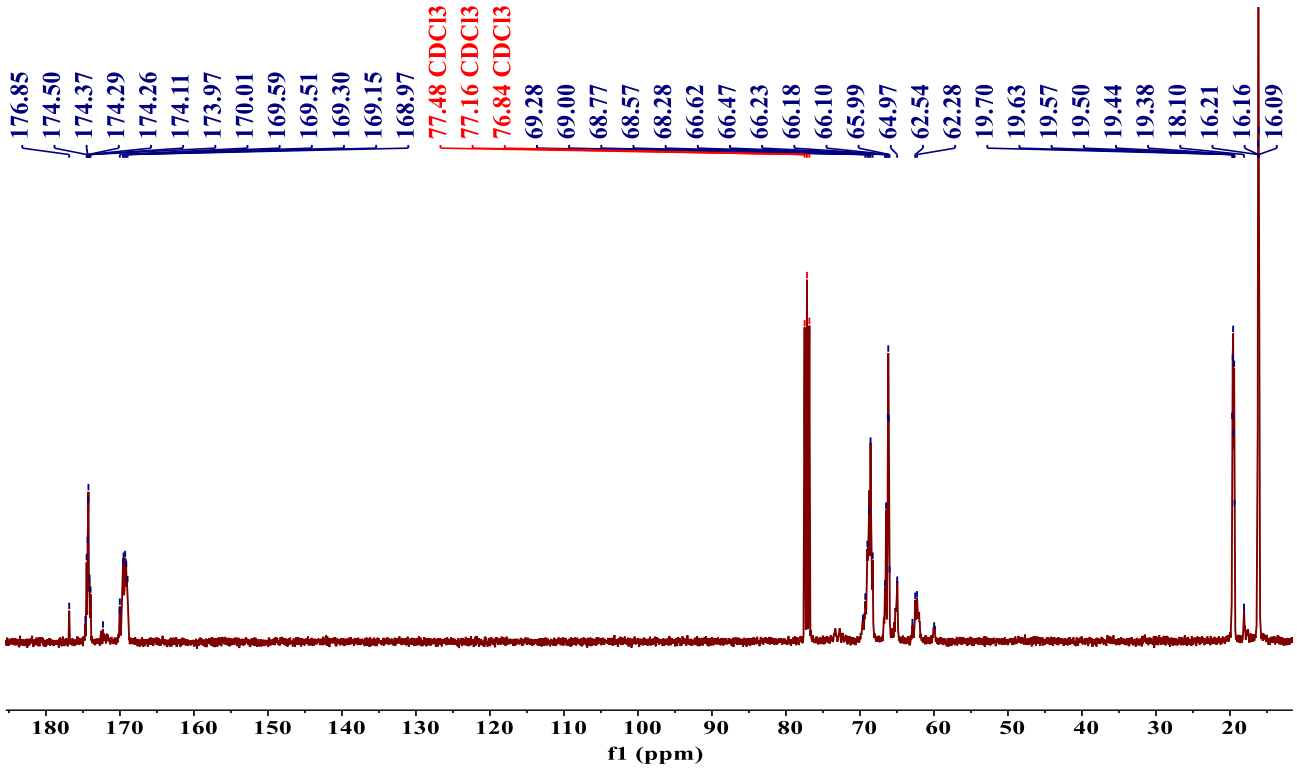


Figure 4.9: $^{13}$C NMR spectrum of purified 3-armed Gly-lac for (1:6) molar ratio

As shown in Figure 4.8, the carbonyl group from the lactic acid monomer could be observed at 177.43 ppm (Espartero et al., 1996) in non-purified 3-armed Gly-lac. This peak have higher intensity than that of $\alpha$-methine group in non-purified 3-armed Gly-lac, but this peak was found at (176.85 ppm) with lower intensity than that of $\alpha$-methine group in purified 3-armed Gly-lac as shown in figure 4.9. This is evidence for the removal of unreacted lactic acid via purification. For the non-purified 3-armed Gly-lac shown in Figure 4.8, an intense peak was observed at 170.31 ppm that denotes the carbonyl group in the trimmer lactic acid (Espartero et al., 1996). The intensity of this peak was higher that of the carbonyl adjacent to (-O-$CH_2$) group in the non-purified 3-armed Gly-lac as shown in Figure 4.8, whereas the reverse is true for the purified one as shown in Figure 4.9, which is evidence for the removal of oligomer lactic acid via purification. The other carbon signals were observed at (76.84 - 77.48) ppm which represents the carbons from solvent Deuterated chloroform ($CDCl_3$) used for dissolving the sample in the analysis (Borowicz et al., 2019).

### 4.3.3. Viscosity of 3-armed Gly-lac for non-purified and purified

The viscosity of the synthesized 3-armed Gly-lac (both purified and non-purified) was determined for the different molar ratios. The viscosity result was used as a confirmation for the synthesis of 3-armed Gly-lac with different chain length as well as validating its purification. The chain length of a given material determines its molecular weight that affects its viscosity (Pinzi et al., 2011).

Table 4.3: Viscosity analysis results of 3-armed Gly-lac

| **Viscosity (cP)** | **Molar ratio** | | | |
|---|---|---|---|---|
| | 1:3 | 1:6 | 1:9 | 1:12 |
| Non-purified | 348 | 385 | 427 | 462 |
| Purified | $>$ 5270 cP | $>$ 5270 cP | $>$ 5270 cP | $>$ 5270 cP |

As shown in Table 4.3, the viscosity of the 3-armed Gly-lac was increased with increasing Gly:lac molar ratio, this is because the chain length of the 3-armed Gly-lac is enlarged when high amount of lactic acid (with high Gly:lac molar ratio) is supplied into the reaction thereby the molecular weight is intended to become higher, which results a high viscosity (Akbar et al., 2009). The viscosity of the purified 3-armed Gly-lac was increased for all Gly:lac molar ratios as shown in Table 4.3. The viscometer used for viscosity analysis can only measure viscosity up to 5270 cP. As a result, the viscometer was unable to display a measurement for the viscosity

of purified 3-armed Gly-lac as shown in Figure 4.10, indicating that the viscosity is higher than 5270 cP. The increase in viscosity might be due to removal of unreacted and oligomer lactic acid through purification.

Figure 4.10: Viscosity measurement for (1:12) 3-armed Gly-lac (A) non-purified, (B) purified

### 4.3.4. Acid Value Analysis for 3-armed Gly-lac

The acid value is helpful for understanding the existence of free lactic acid in 3-armed Gly-lac as well as it could be used for analyzing the extent of purification.

Table 4.4: Acid value of Gly-lac for purified and non-purified

| **Acid Value** (mg KOH/g) | **Gly:lac Molar ratio** | | | |
|---|---|---|---|---|
| | 1:3 | 1:6 | 1:9 | 1:12 |
| Non-purified | 73.85 | 131.463 | 151.27 | 159.382 |
| Purified | 32.326 | 84.045 | 90.724 | 108.106 |

As shown in Table 4.4, the acid value was increased with increasing Gly:lac molar ratio, which might be attributed to the increase in unreacted lactic acid and lactic acid oligomer. This could be due to the fact that as the amount of input lactic acid increased keeping the reaction time and temperature constant, there is high tendency for the increase in unreacted lactic acid and for the formation of lactic acid oligomer. On the other hand, the acid value was decreased for all Gly:lac molar after the purification, which might be due to the removal of unreacted and oligomer lactic acid during purification, which results a decrease in acid value.

## 4.4. Characterization of $Al_2O_3$ Nanoparticle

### 4.4.1. UV-vis Spectroscopy Analysis

The Uv-vis absorption of the as prepared $Al_2O_3$-NPs was observed at 223 nm wave length as shown in Figure 4.11. The Uv-vis spectroscopy analysis was based on the absorption of Uv-vis

light radiation by a chemical compounds that results a distinct spectrum at a specific wave length of absorption, which depends on its size and morphology (Nduni et al., 2021).

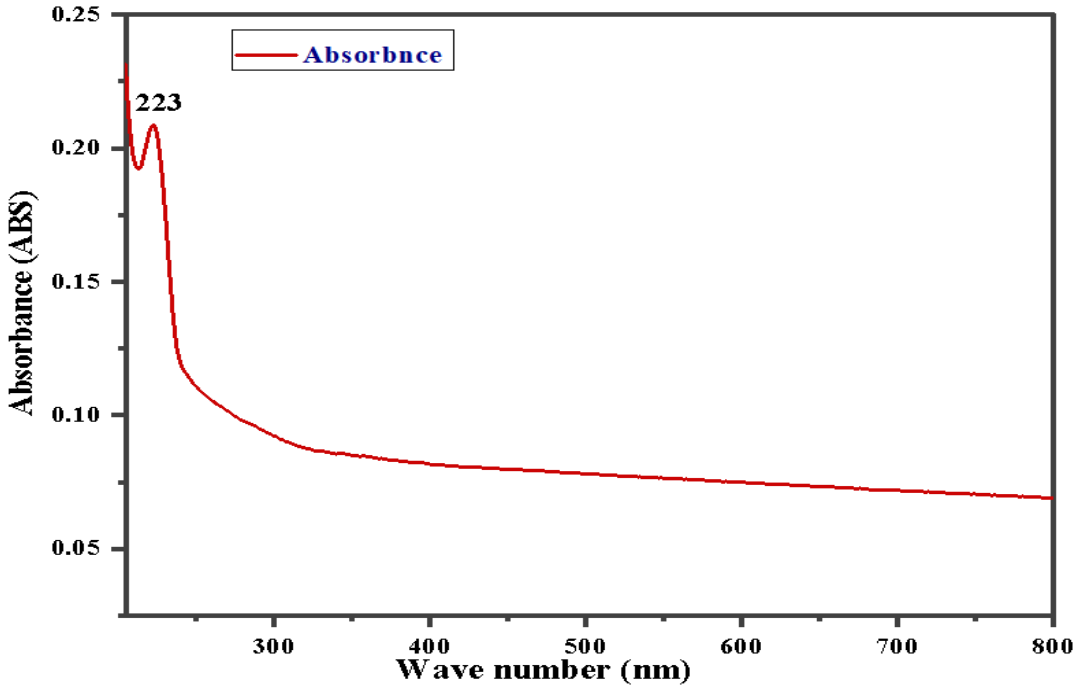


Figure 4.11: Uv-visible Spectra of $Al_2O_3$ nanoparticle

A specific chemical species has a specific wave length at which absorption of Uv-visible light occurs. The Uv-vis absorption of $Al_2O_3$-NPs has been characterized so far and it could be detected within (200 - 300) nm wave length range (Nduni et al., 2021; Vijaya et al., 2018; Yuan. et al., 2015) and the as prepared $Al_2O_3$-NPs has absorption band at 223 nm which is in agreement with these previous works, which confirms that the $Al_2O_3$-NPs was perfectly synthesized.

### 4.4.2. FTIR Analysis of $Al_2O_3$-NPs

The FTIR analysis for the as prepared $Al_2O_3$-NPs is described in Figure 4.12, which describes the transmittance peaks attributed to stretching and bending vibration of the associated functional groups existing in the $Al_2O_3$-NPs. The FTIR spectrum of the $Al_2O_3$-NPs was analyzed and compared with its standard spectra. A characteristics peak was observed at 3460 $cm^{-1}$ that indicates the O-H stretching of α-$Al_2O_3$-NPs, similar result was obtained previously (Nduni et al., 2021). Transmittance peaks were observed at 421 $cm^{-1}$, 438 $cm^{-1}$, 459 $cm^{-1}$, 486 $cm^{-1}$, 516 $cm^{-1}$, 570 $cm^{-1}$, 615 $cm^{-1}$, and 664 $cm^{-1}$ which are attributed to the stretching vibration of the (O-Al-O) groups (Nduni et al., 2021; Vijaya et al., 2018). Those peaks are characteristics peaks of α-$Al_2O_3$-NPs.

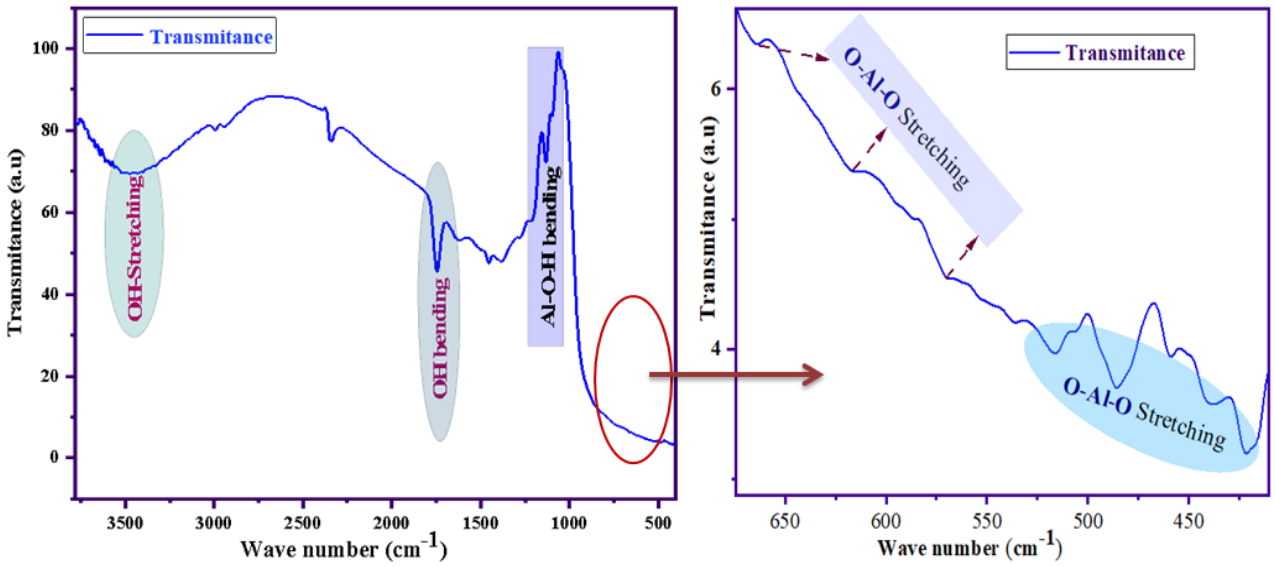


Figure 4.12: FTIR Spectrum of $Al_2O_3$ nanoparticle

The other transmittance peak was detected around 1078 $cm^{-1}$, which is attributed to the (Al–O–H) symmetric bending (Djebaili et al., 2013; Nduni et al., 2021), whereas the peak around 1605 $cm^{-1}$ denotes the OH bending vibration (Vijaya et al., 2018). Thus, the characteristics transmittance peaks detected in the FTIR spectrum are evidence for the synthesis of $Al_2O_3$-NPs.

### 4.4.3. Particle Size Analysis (PSA) of $Al_2O_3$-NPs

The particle size of the as prepared $Al_2O_3$-NPs was determined using particle size analyzer (PSA), which measures the size distribution of the nanoparticle based on intensity. The analysis was performed with two different dispersants at similar dispersion time to investigate the effect of dispersant on the size distribution of the nanoparticle. As shown in Table 4.5, the particle size of $Al_2O_3$-NPs was obtained within the nano-size level (i.e. below 100 nm). The raw data of particle size analysis is shown in **Appendix B (**Figure B1 and B2**)**.

Table 4.5: Particle size analysis result of $Al_2O_3$-NPs with different dispersant

| Dispersant | Dispersion time (minute) | % Intensity | Size (d. nm) |
|---|---|---|---|
| Propan-2-ol | 40 | 100 | 91.28 |
| Water | 40 | 100 | 71.24 |

When we compare between the dispersants, the size of $Al_2O_3$-NPs is lower when the dispersion was performed using water as compared to that of propan-2-ol which elaborates that water has better dispersion ability for the $Al_2O_3$-NPs. The variation in dispersion ability between water

and propan-2-ol could be due to the difference in stearic interaction with the surface of $Al_2O_3$-NPs, which is brought on by the variation in polarity among water and propan-2-ol.

### 4.4.4. X-Ray Diffraction (XRD) Analysis of $Al_2O_3$-NPs

XRD analysis was used to identify the crystalline structure of $Al_2O_3$-NPs as well as the crystalline phase of the nanoparticle. The XRD pattern of the as prepared $Al_2O_3$-NPs is shown in Figure 4.13, in which different peaks were observed with respect to angle of diffraction. The XRD patterns are described by specific lattice plane direction of $Al_2O_3$-NPs corresponding to the peak position.

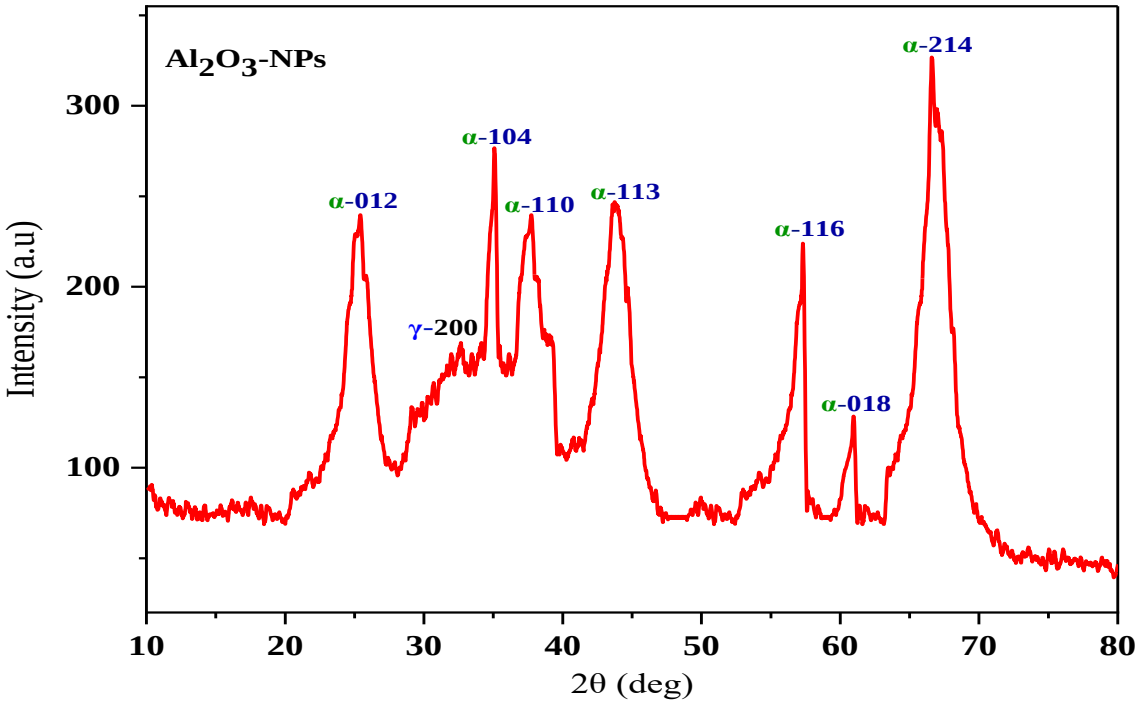


Figure 4.13: X-ray diffraction (XRD) patterns of alumina nanoparticle

The diffraction peaks have been appeared at lattice plane directions of (012), (104), (110), (113), (116), (018), (214), which corresponds to a diffraction angle (2θ) value of 25.43°, 35.08°, 37.82°, 43.76°, 57.35°, 61.04°, and 66.58° respectively. Those lattice planes designate the specific plane orientations of the typical hexagonal and rhombohedral structure of the $\alpha$-$Al_2O_3$-NPs (Farahmandjou & Golabiyan, 2016; Mohammed et al., 2020). Another small peak was observed at a diffraction angle of 32.56° (200), which indicates the cubic structure $\gamma$-alumina nanoparticle (Patra et al., 2012). The XRD analysis result for the $Al_2O_3$-NPs corresponds to the Joint Committee on Powder Diffraction Standards (JCPDS card no. 029-0063 Fd-3m). The XRD

analysis result revealed that the as prepared $Al_2O_3$-NPs has an $\alpha$-crystalline phase with a small portion of $\gamma$-phase that is superimposed over the $\alpha$-$Al_2O_3$-NPs as shown in Figure 4.13.

The crystalline size and d-spacing for the $Al_2O_3$-NPs were determined by using equation (3.8) and (3.9) respectively. As shown in Table 4.6, the average crystal size (D) of $Al_2O_3$-NPs and that of the average d-spacing were found to be 4.7025 nm and 0.2146 nm respectively.

Table 4.6: Crystalline size and d-spacing of alumina nanoparticle

| **Peak position ($2\theta$)** | **FWHM** | **Crystal size D (nm)** | **D-Average (nm)** | **d-spacing (nm)** | **Average d-spacing (nm)** |
|---|---|---|---|---|---|
| 25.43396 | 2.37151 | 3.434127757 | 4.702554982 | 0.34992116 | 0.214661601 |
| 35.08498 | 10.10895 | 0.824197256 | | 0.255562979 | |
| 37.78167 | 1.5333 | 5.476130632 | | 0.237918686 | |
| 43.7629 | 2.43242 | 3.519562119 | | 0.206687982 | |
| 57.35224 | 1.59141 | 5.68986464 | | 0.160526698 | |
| 61.04296 | 0.89793 | 10.27041782 | | 0.151675256 | |
| 66.58143 | 2.56614 | 3.703584646 | | 0.140338446 | |

The crystalline size of the nanoparticles has a great impact on their application such as on catalysis. The crystal size of the nanoparticle determines its physical properties such as surface area and surface energy. A small crystallite size of the nanoparticle permits high surface area (Wang et al., 2014), which could enhance its catalytic performance. The lower crystallite size could also have lower particle agglomeration (Suhasinee et al., 2017) when it is used as nano-fluid such as for fuel additive. In this study, a small crystal size of $Al_2O_3$-NPs (4.7025 nm) was obtained, which is in agreement with previous study (Velu & Gangwal, 2006). The small crystal size might be advantageous as it could enhance its catalytic efficiency while used for biodiesel-diesel additive to enhance engine performance and to reduce emission gas.

### 4.4.5. Analysis Zeta Potential for Dispersion Stability of $Al_2O_3$-NPs within Gly-lac

The zeta potential analysis was conducted so as to investigate the dispersion stability of $Al_2O_3$-NPs within Gly-lac. Zeta potential refers to the electric potential (electrostatic repulsive forces) in the interfacial double layer at the position of the slipping plane, which is associated with a point in the considerable volume of fluid away from the interface (Soudagar et al., 2018). Before

conducting zeta potential analysis, the maximum possible loading rate of $Al_2O_3$-NPs in Gly-lac was identified by physical detection of the dispersion. As shown in Figure 4.14, at loading rate of 4wt% of the $Al_2O_3$-NPs within Gly-lac, there was noticeable particle agglomeration. To prevent the particle agglomeration, the dispersion of $Al_2O_3$-NPs in Gly-lac should be lower than 4wt%. Thus, the Zeta potential analysis was conducted at 3wt% loading rate to further validate the dispersion stability.

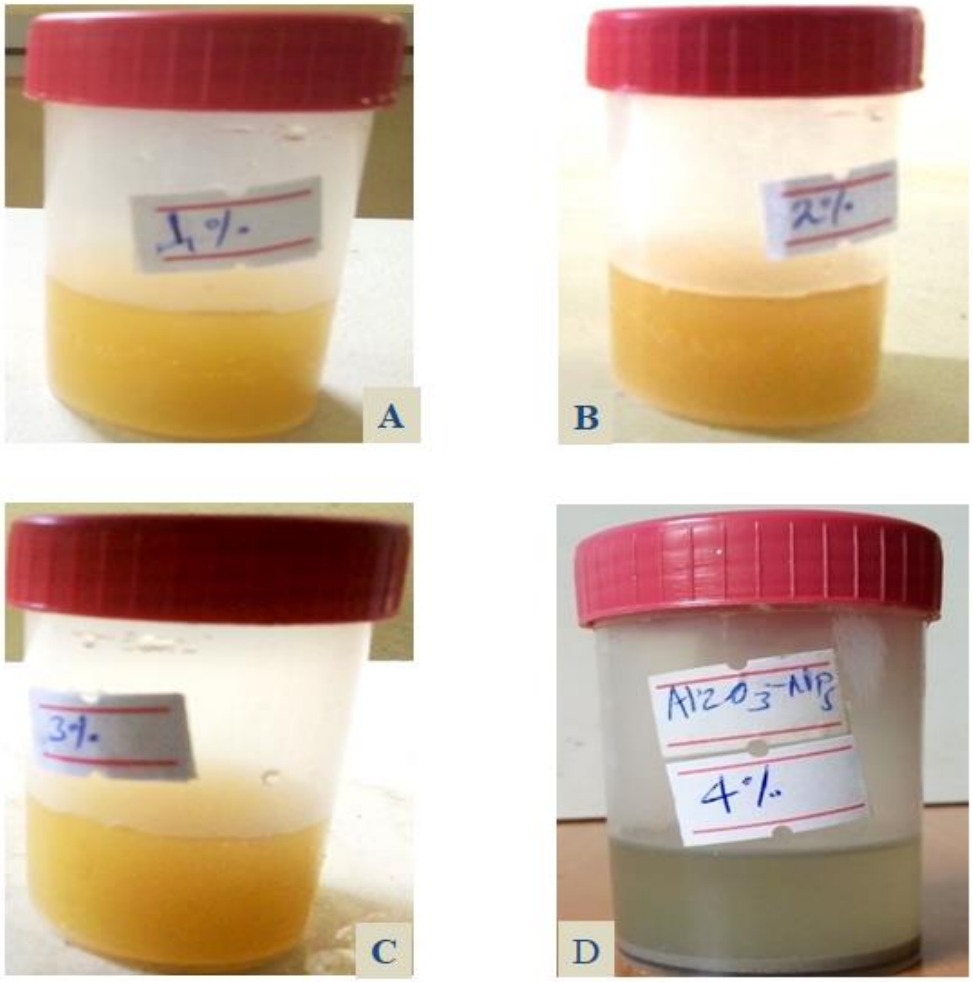


Figure 4.14: Physical detection for dispersion stability of $Al_2O_3$-NPs within Gly-lac at loading rate of (A) 1wt%, (B) 2wt%, (C), 3wt% and (D) 4wt%

The dispersion stability of nanoparticle is influenced by zeta potential or their surface charge. It is altered by the sum of van der Waals attraction forces and electrostatic repulsive forces among the nanoparticles in the dispersion, in which the stability is attained when the electrostatic repulsive forces exceed the van der Waals attraction forces (Babita et al., 2016). An absolute

zeta potential more than 60 mV shows excellent dispersion stability, and that of above 30 mV shows a good stable dispersion, whereas zeta potential below 5 mV permits a noticeable particle agglomeration (Soudagar et al., 2018). The zeta potential for the as prepared $Al_2O_3$-NPs when it is dispersed in Gly-lac was found +30.495 mV, as shown in **Appendix B** (Figure B3), which indicates the better stable dispersion of $Al_2O_3$-NPs within Gly-lac. And the positive sign in the zeta potential result shows that the $Al_2O_3$-NPs have a positive surface charge. The zeta potential result is in agreement with (Lee et al., 2008) in which zeta potential was obtained 34 mV for $Al_2O_3$-water nano-fluid and concluded that the nano-fluid has better dispersion stability.

### 4.5. Cold Flow Property Analysis of Biodiesel

The effect of 3-armed Gly-lac on the cold flow properties of biodiesel was investigated through evaluation of cloud point (CP) and pour point (PP) of biodiesel before and after the addition of purified 3-armed Gly-lac synthesized with four glycerol to lactic acid (Gly:lac) molar ratios (1:3, 1:6, 1:9, and 1:12). The raw data of cold flow property analysis results are shown in **Appendix C**. The addition of different Gly:lac molar ratio and loading rate of 3-armed Gly-lac into biodiesel have brought a decrease in both CP and PP of biodiesel as shown in Figures 4.15 and 4.16. The reduction effect of 3-armed Gly-lac on CP and PP might be as a result of co-crystallization of non-polar groups of 3-armed Gly-lac with crystal molecules and simultaneous hindrance of crystal growth by the 3-armed Gly-lac polar groups, or it could be due to the adsorption of polar groups of 3-armed Gly-lac on the surface of crystal nuclei, thereby modifying the shape and size of the crystal nuclei (Boshui et al., 2010; Feng et al., 2014). The 3-armed structure of Gly-lac might be also able to provide a barrier for agglomeration of crystal lattices so that it could enhance the flow-ability of biodiesel at low temperature. The effect of Gly:lac molar ratio and loading rate of 3-armed on CP and PP was investigated by varying one parameter at a time. Here, first the effect of Gly:lac molar ratio was investigated at loading rate of 10 g/l. Then, a selected Gly:lac molar ratio was used to study the effect of loading rate.

#### 4.5.1. The Effect of Gly:lac Molar Ratio on Biodiesel Cold Flow Properties

The effect of Gly:lac molar ratio on cloud point (CP) and pour point (PP) of biodiesel is shown in Figure 4.15, in which the efficiency of 3-armed Gly-lac, to reduce the CP and PP of biodiesel, changes with variation in Gly:lac molar ratio. Amongst the four Gly:lac molar ratio, a maximum reduction of CP by 7$^o$C and PP by 8.14$^o$C was achieved by the addition of a (1:6) Gly:lac molar ratio. And the least reduction of CP by 4$^o$C and PP by 5.02$^o$C was obtained with the

incorporation of (1:12) Gly:lac molar ratio in to biodiesel. The difference in efficiency among the different Gly:lac molar ratios might be due to the fact that the cold flow improvers have superior efficiency when their alkyl chain length is more closer to the carbon chain length of the target biodiesel (Yuan et al., 2022). In this case, the carbon chain length of soyabean-based biodiesel is closer to (1:6) as compared to those of (1:3, 1:19, 1:12) molar ratio, which resulted that the 3-armed Gly-lac (1:6) has greater efficiency in reducing the CP and PP of biodiesel. The closeness of alkyl chain length of 3-armed Gly-lac (1:6) to the biodiesel carbon chain length might be able to satisfy the necessity of the balance among the 3-armed Gly-lac alkyl groups and the biodiesel methyl ester groups. Consequently, the interaction between the 3-armed Gly-lac molecule with the methyl ester group might be able to create steric hindrance on the formation and growth of crystal so as to enhance the flow-ability of biodiesel (Phan et al., 2021). On the other hand, when higher alkyl groups exist in the cold flow improver (3-armed Gly-lac) beyond the optimal level, the interaction among 3-armed Gly-lac molecule and crystal nuclei might be interrupted and cause a decline in efficiency to trap longer alkyl chains of biodiesel, which could favor self-crystallization (Phan et al., 2021) in which self-crystallization reduces the biodiesel flow-ability at lower temperature.

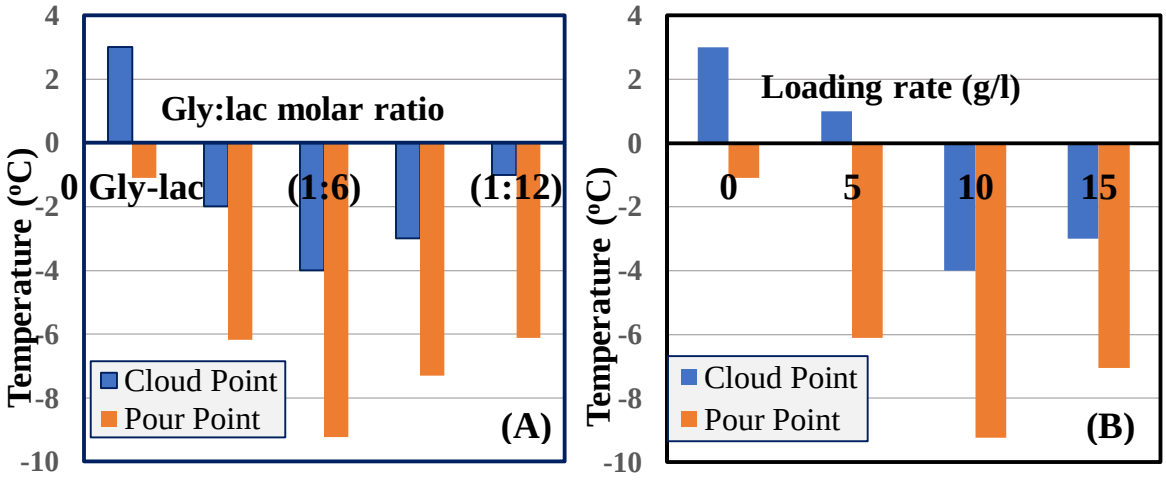


Figure 4.15: The effects of; (A) Gly:lac molar ratio, (B) loading rate on CP and PP of biodiesel

### 4.5.2. The Effect of Loading Rate of 3-armed Gly-lac on Biodiesel Cold Flow Properties

The effect of loading rate of 3-armed Gly-lac on cloud point (CP) and pour point (PP) of biodiesel is shown in Figure 4.15B, which was studied based on the selected Gly:lac molar ratio (1:6), having superior impact on the reduction of biodiesel CP and PP. As shown in Figure 4.16,

the CP and PP of biodiesel were decreased from 3$^{o}$C and -1.09$^{o}$C to 1$^{o}$C and -6.11$^{o}$C; -4$^{o}$C and -9.23$^{o}$C; -3$^{o}$C and 7.06$^{o}$C upon addition of the respective loading rate of 5g/l, 10g/l, and 15g/l. The maximum reduction of CP by 7$^{o}$C and PP by 8.14$^{o}$C was achieved with a loading rate of 10g/l. The CP and PP reduction effectiveness of 3-armed Gly-lac was increased with increasing loading rate up to 10g/l. However, when the loading rate was raised to 15g/l, the 3-armed Gly-lac efficiency was decreased, which might be due to a decrease in solubility of Gly-lac 3-armed within biodiesel as the loading rate increased beyond the optimal value (Pham et al., 2021). At a reduced solubility, there might be a formation of small crystal by the 3-armed Gly-lac molecules so that they could not co-crystallize with biodiesel molecules. Thus the impact of 3-armed Gly-lac on the reduction of CP and PP could become lesser (Pham et al., 2021). On the other, at lower loading rate below the optimal level, the interaction among the molecules of 3-armed Gly-lac and that of the crystal nuclei could not be sufficient to hinder the crystal growth (Pham et al., 2021). Thus, an optimum loading rate of 10 g/l is better for achieving the best efficiency of 3-armed Gly-lac as a cold flow improver to reducing the CP and PP of biodiesel.

The effects of different Gly:lac molar ratio and loading rate of 3-armed Gly-lac were also tested for other important properties of biodiesel such as viscosity, cetane number, flash point and fire point, density, and calorific value and compared with the biodiesel standard limits.

Table 4.7: Effect of Gly:lac molar ratio on biodiesel important properties

| **Properties** | Gly:lac molar ratio | | | | |
|---|---|---|---|---|---|
| | 0 Gly-lac | 1:3 | 1:6 | 1:9 | 1:12 |
| Cloud point ($^{o}$C) | 3 | -2 | -4 | -3 | -1 |
| Pour point ($^{o}$C) | -1.09 | - 6.17 | - 9.23 | - 7.30 | - 6.11 |
| Kinematic viscosity @ 25 $^{o}$C (mm$^2$/s) | 4.24 | 4.26 | 4.30 | 4.38 | 4.42 |
| Cetane number | 66.59 | 66.64 | 66.70 | 66.75 | 66.82 |
| Calorific value kJ/kg | 38970.75 | --- | 38670.576 | --- | --- |
| Density g/cm$^3$ | 0.885 | 0.887 | 0.893 | 0.897 | 0.92 |
| Flash point (℃) | 150 | 157 | 163 | 172 | 181 |
| Fire point (℃) | 165 | 172 | 180 | 187 | 192 |

As shown from Tables 4.7 and 4.8, viscosity of biodiesel was increased with increasing Gly:lac molar ratio and loading rate. However, the viscosity is within its standard limits (1.9 - 6) mm$^2$/s of viscosity standards (Astm D, 2012; ASTM D6751-02, 2002). Upon addition of 3-armed Gly-

lac with different molar ratio and different loading rate; cetane number, flash point, and density are within their standard limits (tabulated in Table 4.2), even the results show an increasing flash point, fire point and cetane number with increasing Gly**:**lac molar ratio and loading rate.

Table 4.8: Effect of loading rate of 3-armed Gly-lac on important properties of biodiesel

| **Properties** | **3-armed Gly-lac (1:6) loading rate (g/l)** | | | |
|---|---|---|---|---|
| | **0** | **5** | **10** | **15** |
| Cloud point ($^oC$) | 3 | 1 | -4 | -3 |
| Pour point ($^oC$) | -1.09 | -6.11 | -9.23 | -7.06 |
| Kinematic viscosity @ 25 $^oC$ ($mm^2/s$) | 4.24 | 4.51 | 4.70 | 4.81 |
| Cetane number | 66.59 | 66.64 | 66.70 | 66.74 |
| Calorific value (kJ/kg) | 38970.75 | --- | 38670.576 | --- |
| Density $g/cm^3$ | 0.885 | 0.889 | 0.893 | 0.895 |
| Flash point | 150 | 158 | 168 | 175 |
| Fire point | 163 | 170 | 178 | 187 |

### 4.5.3. The Effect of 3-armed Gly-lac/$Al_2O_3$-NPs on Biodiesel Cold Flow Properties

In order to the investigate effect of $Al_2O_3$-NPs dispersed 3-armed Gly-lac on the CP and PP of biodiesel was, the dispersion of 3-armed Gly-lac/$Al_2O_3$-NPs into biodiesel was performed using 1:6 molar ratio and at 10g/l based on the results from the study on effects of Gly-lac molar and loading rate. The effect of $Al_2O_3$-NPs dispersed 3-armed Gly-lac on CP and PP of biodiesel is shown in Figure 4.16, which is presented in comparison with CP and PP of pure biodiesel (i.e., with no additive condition). Upon the addition of $Al_2O_3$-NPs dispersed 3-armed Gly-lac into biodiesel, a maximum reduction of CP by 7$^oC$ and PP by 9.44$^oC$ (at 3wt% loading rate of $Al_2O_3$-NPs) was obtained as compared to that of biodiesel. The synergic effect of the $Al_2O_3$-NPs and 3-aarmed Gly-lac was better than that of 3-armed Gly-lac. This might be due to the fact that the $Al_2O_3$-NPs are capable to form emulsions capable of trapping small crystal molecules and delay the formation of large crystals to permit a better cold flow behavior of biodiesel (Fathurrahman et al., 2021). The high adsorption affinity and large surface area of the $Al_2O_3$-NPs might permit adsorption of crystal molecules in biodiesel so that it could form a needle like small crystals (Xue et al., 2022). The adsorption of crystals could result a reduction in surface energy of the crystal that decrease the interaction among crystals, thereby delaying the crystal growth so as to

improve the cold flow behavior. The $Al_2O_3$-NPs dispersed 3-armed Gly-lac might be able to form electrostatic double layer that could create electrostatic repulsion among crystal molecules adsorbed on surface of the $Al_2O_3$-NPs dispersed 3-armed Gly-lac, thereby improving the flow behavior of biodiesel at cold temperature (He et al., 2016; Sharma et al., 2019). On the other hand, variation in loading rate of $Al_2O_3$-NPs with respect to Gly-lac shows small effect on reduction of CP and PP of biodiesel.

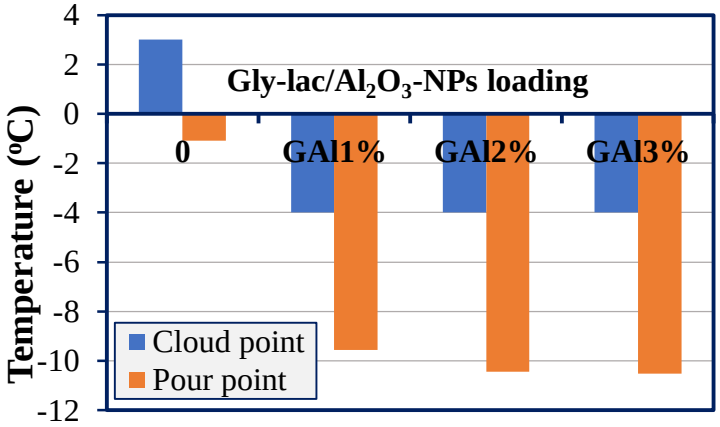


Figure 4.16: The effects of 3-armed Gly-lac/$Al_2O_3$-NPs on CP and PP of biodiesel

### 4.6. Analysis of IC Engine Performance and Emission Characteristics

#### 4.6.1. The Effect of 3-armed Gly-lac/$Al_2O_3$-NPs on Engine Performance of B20

The engine performance test for biodiesel-diesel blend (B20) was conducted by adding 3-armed Gly-lac, $Al_2O_3$-NPs and $Al_2O_3$-NPs dispersed 3-armed Gly-lac into B20 to study the effect on brake power, brake thermal efficiency (BTE), and brake specific fuel consumption (BSFC).

Figure 4.17A describes the brake (BP) for different test fuel blends with variation in engine load. BP was increased with increasing engine load for all test fuel blends. This could be due to the injection of high fuel mass and a high combustion temperature at high engine load that might facilitate the power generation (Shirneshan et al., 2014). The addition of $Al_2O_3$-NPs in to B20 increased the BP at all engine loads, which might be due to the increase in calorific value of the fuel blend upon the addition of $Al_2O_3$-NPs. And also $Al_2O_3$-NPs play a great role in the reduction of ignition delay and duration of fuel combustion, which leads to higher peak cylinder pressure and faster heat release rate (Gad & Jayaraj, 2020). $Al_2O_3$-NPs dispersed 3-armed Gly-lac brought a better increment in BP as compared to that of $Al_2O_3$-NPs alone (without Gly-lac). This might result from long ignition delay due to agglomeration while adding $Al_2O_3$-NPs alone into B20 (Soudagar et al., 2020). In average, BP was increased by 0.247 kW, 0.444 kW, 0.639

kW, and 0.843 kW for the fuel blends; B20A, B20GA1%, B20GA2%, and B20GA3% respectively as compared to that of B20. On the other hand, the addition of 3-armed Gly-lac into B20 result an average reduction of BP by 0.0213 kW, which might be due to lower heat release rate brought on by a reduction in calorific value.

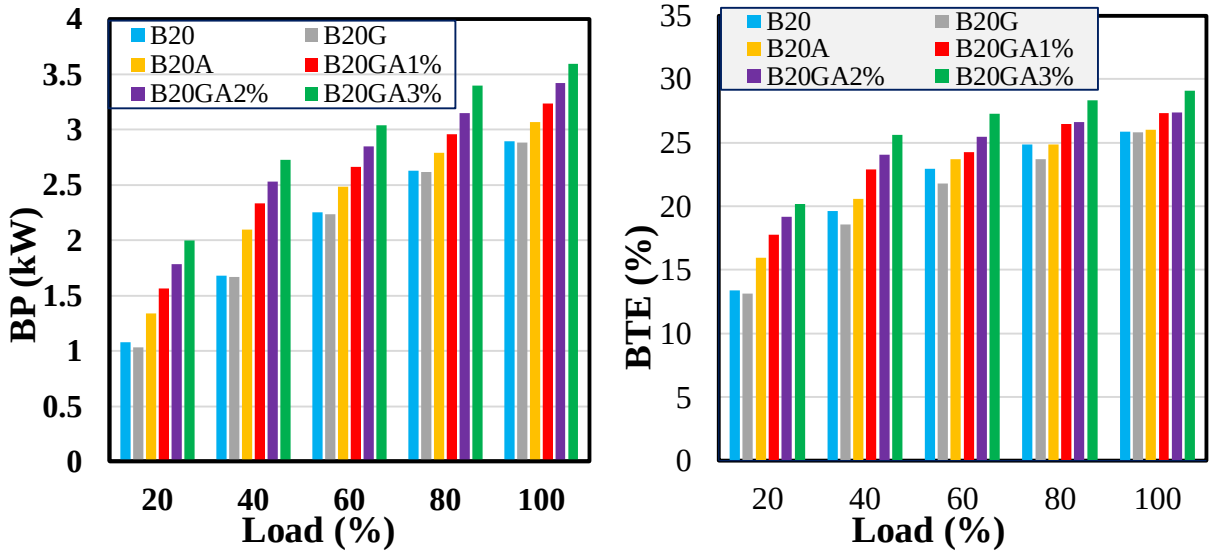


Figure 4.17: The effect 3-armed Gly-lac/$Al_2O_3$-NPs; (A) on brake power, (B) on BTE at different engine load conditions

Figure 4.17B illustrates the effect of $Al_2O_3$-NPs dispersed 3-armed Gly-lac on BTE (%) at various engine loads. BTE was increased with increasing engine load, which might be caused by high combustion temperature that aids a better fuel combustion. At all engine load conditions, BTE was found in the sequence; B20GA3%> B20GA2%> B20GA1%> B20A> B20> B20G. Addition of $Al_2O_3$-NPs into B20 brought an improvement in BTE at all engine load conditions. This might be explained by the ability of $Al_2O_3$-NPs to maintain high reactive surface so as to facilitate the fuel combustion so that the fuel's chemical energy could be converted into useful power more efficiently (Gad & Jayaraj, 2020). The increase in surface to volume ratio via the addition of $Al_2O_3$-NPs could favor generation of additional energy inside the cylinder which leads to an increase in heat transfer (Gad & Jayaraj, 2020; Shaafi & Velraj, 2015), which tends to increase the brake thermal efficiency. The reduction of BP upon the addition of 3-armed Gly-lac into B20 has brought a decrease in BTE.

Another significant finding is that the addition of $Al_2O_3$-NPs dispersed 3-armed Gly-lac brought a better improvement in BTE compared to that of ($Al_2O_3$-NPs without 3-armed Gly-lac). As

shown in Figure 4.17B, at 20% engine load, the BTE exhibits a maximum increase by 4.404%, 5.82%, and 6.837% for the blends; B20GA1%, B20GA2%, and B20GA3%, respectively compared to that of B20. In contrast, for B20A (i.e., adding $Al_2O_3$-NPs alone), the only increment in BTE was by 2.595%. When $Al_2O_3$-NPs are added without 3-armed Gly-lac, it might have a tendency to agglomerate because of their large surface area and high surface activity (Soudagar et al., 2018); this could be the main reason for the lower impact on BTE of B20 while adding $Al_2O_3$-NPs alone. On the other hand, while using $Al_2O_3$-NPs dispersed 3-armed Gly-lac, there might be lesser chance of agglomeration. In this case, 3-armed Gly-lac used as a dispersant that prevents agglomeration of $Al_2O_3$-NPs and permits a stable dispersion so as to maintain uniform distribution of $Al_2O_3$-NPs inside the fuel system. The uniform distribution of $Al_2O_3$-NPs aids a better fuel atomization by avoiding clogging problems during fuel injection (Ojha & Karmakar, 2018), that could improve the BTE. The dispersion stability of $Al_2O_3$-NPs with the help of 3-armed Gly-lac could be supported by the result of Zeta potential analysis (discussed in section 4.4.5). During the fuel combustion, an improved thermal conductivity due to stable dispersion of $Al_2O_3$-NPs could permit uniform heat distribution (Babita et al., 2016; Soudagar et al., 2018), thereby increasing the BTE.

Figure 4.18 describes the effect of $Al_2O_3$-NPs dispersed 3-armed Gly-lac on BSFC at various engine loads. The BSFC was decreased with increasing engine load, which is caused by the rise in BTE. At higher engine load, a high BTE leads to higher percentage increase in BP compared to the increase in fuel consumption, which results a lower BSFC.

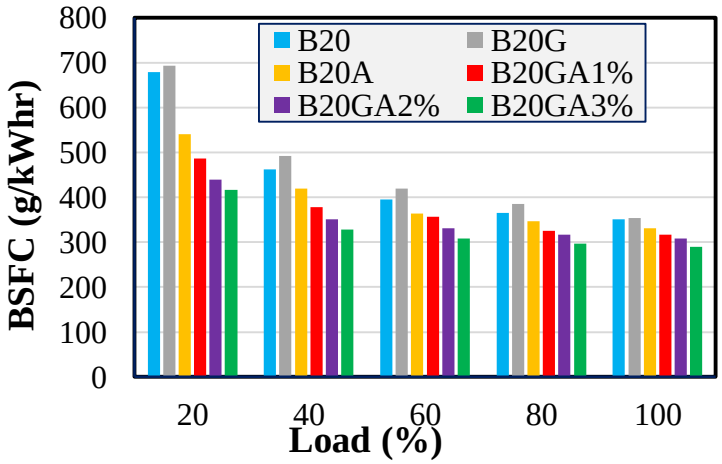


Figure 4.18: The effect of 3-armed Gly-lac/$Al_2O_3$-NPs on BSFC (g/kWhr) at different engine loads

Upon the addition of $Al_2O_3$-NPs, BSFC (g/kWhr) of B20 was reduced, which corresponds to the rise in BTE. Because the BTE and BSFC are inversely proportional i.e., when the BTE is higher, the fuel's energy is converted into useful power more efficiently, thus lowering the BSFC. In a similar circumstance with that of BTE, the BSFC of B20 was also greatly affected with the addition of $Al_2O_3$-NPs dispersed 3-armed Gly-lac (i.e. for B20GA1%, B20GA2%, and B20GA3%), as compared to the impact of $Al_2O_3$-NPs alone. Over the different engine load conditions, BSFC shows an average reduction by 15.48%, 20.22%, and 25.26% for the blends; B20GA1%, B20GA2%, and B20GA3% respectively, as compared to that of B20. Whereas only a 9.78% decline in BSFC was attained for B20A compared that of B20. The higher reduction in BSFC of B20 upon the addition $Al_2O_3$-NPs dispersed 3-armed Gly-lac might be due to enhanced fuel combustion with an improved fuel atomization as a result of uniform dispersion of $Al_2O_3$-NPs (Ojha & Karmakar, 2018).

The calorific value of the fuels is another significant factor responsible for the variation of BSFC among different fuel blends. As shown in table 4.9, the calorific value is higher for the fuel blends; B20A, B20GA1%, B20GA2%, and B20GA3%, compared to that of B20. The fuel blends with a higher calorific value have a higher heat input rate when injected into the engine, which tends to lower the mass of fuel required to generate a unit power compared to the fuel with a lower calorific value, which results lower BSFC. On the other hand B20G have lower calorific value and heat input rate than B20, which results a higher BSFC for B20G compared to that of B20.

Table 4.9: Properties of the different fuel blend used in engine tests

| **Sample fuel** | **Calorific value, CV (kJ/kg)** | **Density ($g/cm^3$)** | **Average Mass flow rate of fuel (kg/hr)** | **Average heat input rate (kJ/hr)** |
|---|---|---|---|---|
| B20 | 39645.354 | 0.847 | 0.8098 | 32104.81 |
| B20G | 39426.786 | 0.854 | 0.8125 | 32034.26 |
| B20A | 41771.772 | 0.85 | 0.816 | 34085.76 |
| B20GA1% | 41653.668 | 0.858 | 0.8275 | 34468.41 |
| B20GA2% | 42675.738 | 0.86 | 0.832 | 35506.21 |
| B20GA3% | 42804.09 | 0.865 | 0.8398 | 35946.87 |

With increasing $Al_2O_3$-NPs concentration in the fuel blends, the BP and BTE were increased whereas BSFC was decreased. This might result from a further improved combustion system as the additional $Al_2O_3$-NPs are employed to catalyze the oxidation of fuel. It might be also caused by an increase in the calorific value of the fuel blends brought on by an increase in energy density upon the addition of more $Al_2O_3$-NPs into the fuel blend (Saxena et al., 2017).

### 4.6.2. The Effect of 3-armed Gly-lac/ $Al_2O_3$-NPs on Exhaust Gas Emission of B20

**Hydrocarbon (HC) Emission** (ppm): It results from incomplete fuel combustion as a result of insufficient oxygen supply (Sunil et al., 2021) and poor fuel-air ratio (i.e. fuel-rich and fuel-lean) in which poor fuel-air ratio is caused by low injection pressure and poor fuel atomization (Hosseini et al., 2017). Figure 4.19A shows the HC emission for the test fuels under various load conditions. For all test fuels, HC emission was decreased with increasing engine load. As the engine load increases, the combustion temperature is intended to rise, which allows the available oxygen to react quickly, enabling a more thorough combustion (Prabakaran & Udhoji, 2016; Prabakaran & Vijayabalan, 2018), thereby reducing the HC emission at high engine load.

Upon the addition of 3-armed Gly-lac and $Al_2O_3$-NPs in to B20, an average decrease in HC emission by 5.4 ppm, 10 ppm, 16.8 ppm, 22.4 ppm, and 27.4 ppm were achieved for the test fuels; B20G, B20A, B20GA1%, B20GA2%, and B20GA3% respectively, compared to that of B20. This might be because the $Al_2O_3$-NPs and 3-armed Gly-lac contain chemically bonded oxygen that promotes the oxidation of the unburned hydrocarbon (Aalam & Saravanan, 2017). It could be also due to a reduction in carbon activation temperature via the addition of $Al_2O_3$-NPs, which permits an improved fuel combustion (Anchupogu, 2018; Ghanbari et al., 2021). The reduction in HC emission was higher for B20GA1%, B20GA2%, and B20GA3% when compared to B20A (i.e., $Al_2O_3$-NPs alone). In case of $Al_2O_3$-NPs dispersed 3-armed Gly-lac, the uniform dispersion of $Al_2O_3$-NPs and its smaller size helps to improve the fuel-air mixture during fuel injection as well as it prevents clogging and fuel atomization difficulties (Ojha & Karmakar, 2018). Thus, it could allow fast vaporization and enhanced combustion of the fuel that reduces HC emission.

**Nitrogen oxide ($NO_x$) Emission** (ppm): $NO_x$ is a general name for $N_2O_2$, NO, and $NO_2$ which are formed when nitrogen is oxidized at high temperature inside the engine cylinder. As shown in Figure 4.19B, the emission of $NO_x$ rises with increasing engine load for all test fuels, which

might be due to a high combustion temperature at high engine load that could breakdown strong triple bond of nitrogen molecules into reactive atomic nitrogen that reacts with oxygen to produce $NO_x$ (Varatharajan et al., 2011).

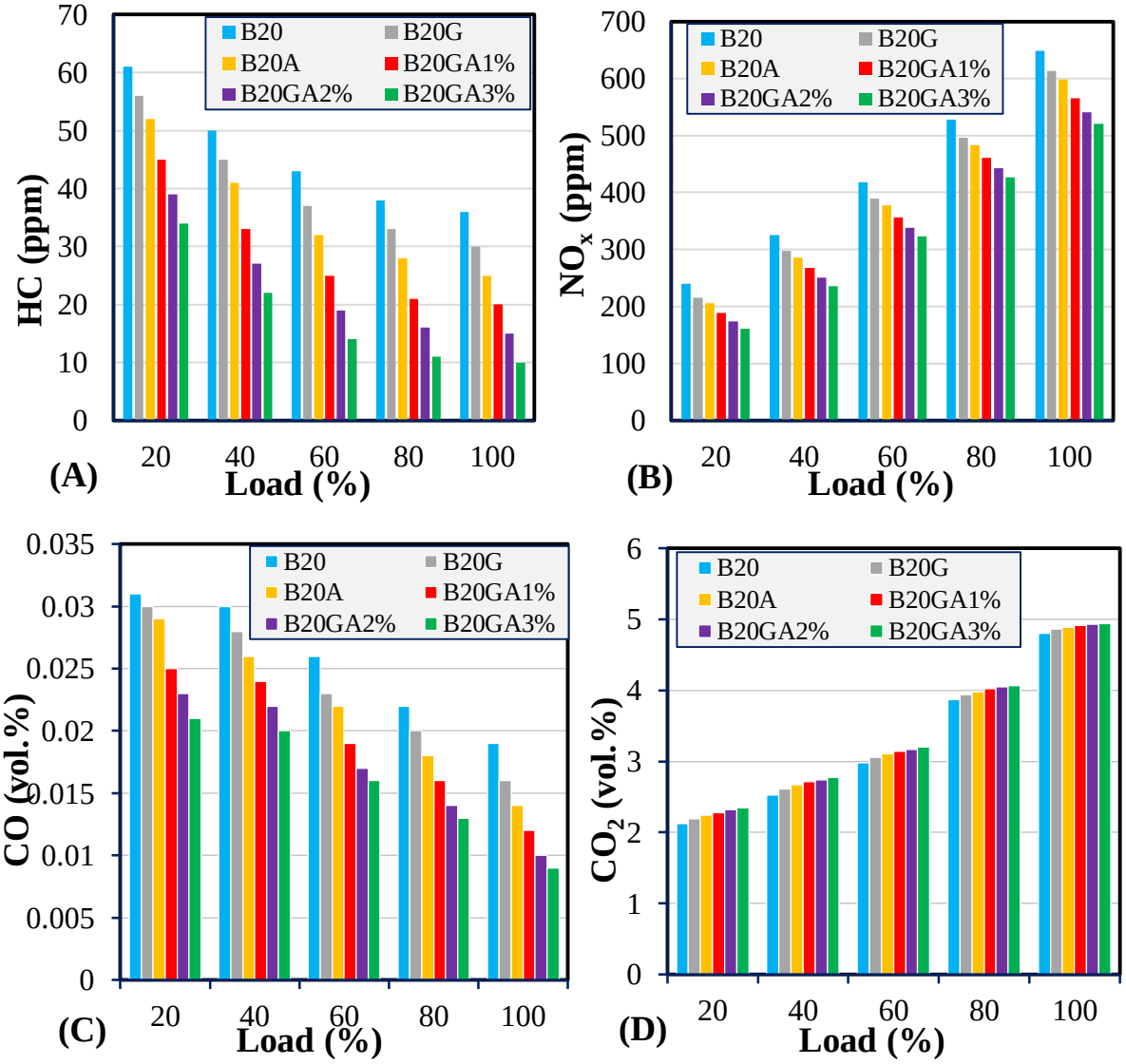


Figure 4.21: The effect of 3-armed Gly-lac/$Al_2O_3$-NPs on the exhaust gas emission; (A) HC, (B) $NO_x$, (C) CO, and (D) $CO_2$ at different engine load conditions

The addition of $Al_2O_3$-NPs into B20 reduced the $NO_x$ emission, which might due to a reduction in average temperature as a result high convective heat transfer (Anbarasu et al., 2016; Kumar et al., 2017). The ability of $Al_2O_3$-NPs to act as a catalytic convertor might cause a decrease in $NO_x$ emission, in which the $NO_x$ could be converted into $N_2$ molecule via catalytic reduction, thereby lowering the $NO_x$ emission (Aalam et al., 2015; Anchupogu, 2018). In average, the $NO_x$

emission was reduced by 41.8 ppm, 64.2 ppm, 82.8 ppm, and 98.6 ppm for the fuel blends; B20A, B20GA1%, B20GA2%, and B20GA3% respectively. The reduction in $NO_x$ emission was highly impacted with the addition of $Al_2O_3$-NPs dispersed 3-armed Gly-lac, compared that of $Al_2O_3$-NPs alone. Because, a better dispersion of $Al_2O_3$-NPs when used with 3-armed Gly-lac, permits an improved homogenization of fuel blends and a better heat transfer in the engine cylinder, thus lowering the chance to form high local temperature (Soudagar et al., 2018), which further reduce the thermal based formation of $NO_x$. The addition of 3-armed Gly-lac into B20 also reduced the $NO_x$ emission averagely by 29.8 ppm. As shown in Table 4.9, B20G has lower calorific value and heat input rate as compared that of B20 blend, thus the combustion of B20G might have lower heat release rate, which leads a reduction of $NO_x$ as a result of lower combustion temperature relative to B20 (Ağbulut et al., 2020).

**Emission of CO and $CO_2$** (vol%): CO is formed from an incomplete fuel combustion brought on by inadequate air fuel ratio, temperature fluctuation, longer ignition delay and poor carbon activation (Sunil et al., 2021). The emission of CO and $CO_2$ for test fuel blends are presented in Figures 4.19C and 4.19D respectively, with engine load variation. CO emission was decreased as engine load increases whereas that of $CO_2$ was increased that might result from the rise in average combustion temperature at higher engine load. Thus, an improved reaction among oxygen and hydrocarbon could covert CO in to $CO_2$ so as to reduce CO emission.

Upon the addition of $Al_2O_3$-NPs and 3-armed Gly-lac into B20, the emission of CO was reduced and that of $CO_2$ was increased. On average, the emission of CO was decreased by 9.26%, 15.93%, 26.078%, 34.16%, and 39.52%, and that of $CO_2$ was increased by 2.44%, 4.055%, 5.24%, 6.294%, and 7.16% for B20G, B20A, B20GA1%, B20GA2%, and B20GA3% respectively, as compared to that of B20. This is attributed to the sufficient oxygen supply from the structure of $Al_2O_3$-NPs as well as 3-armed Gly-lac that could facilitate the oxidation of CO that converts into $CO_2$. The addition of $Al_2O_3$-NPs aids a better combustion by reducing the ignition delay and by enhancing the fuel ignition probability (Tanvir & Qiao, 2012). Similar to those of $NO_x$ and HC emissions, the impact of $Al_2O_3$-NPs dispersed 3-armed Gly-lac on the reduction of CO emission for B20 was higher than that of $Al_2O_3$-NPs alone. The uniform $Al_2O_3$-NPs dispersion (when used with 3-armed Gly-lac), could enhance the heat transfer in the fuel system that advance the combustion reaction allowing the available oxygen to involve in further oxidation reaction towards converting CO into $CO_2$ that results a lower CO emission.

# 5. CONCLUSION AND RECOMMENDATION

## 5.1. Conclusion

In this study, prior to the biodiesel synthesis the physico-chemical properties soyabean oil were characterized. The %FFA and moisture content were found to be 0.495% and 1.43% respectively, so that the soyabean oil was suitable to be used for biodiesel synthesis via base catalyzed trans-esterification reaction. The functional groups of the synthesized biodiesel were confirmed by Fourier Transform Infrared (FTIR) spectroscopy analysis. Further, the chemical structure of the biodiesel was analyzed by Nuclear Magnetic Resonance (NMR) analysis. 87.55% conversion was obtained for biodiesel, which was calculated based on $^{1}$HNMR analysis result. The physico-chemical properties of biodiesel like viscosity, cetane number, flash point, fire point, and density were also tested and obtained in agreement with their standard value.

The synthesized and purified 3-armed glyceryl lactate was characterized by using FTIR, NMR, viscosity, and acid value analysis. The $Al_2O_3$-NPs was synthesized via sol-gel method using aluminum nitrate nonahydrate and citric acid and characterized using UV-vis, FTIR, PSA, and XRD analysis. The dispersion stability of $Al_2O_3$-NPs in Gly-lac and the surface charge was detected by Zeta potential analysis. Zeta potential was found +30.495 mV that indicates a positive surface charge and good dispersion stability of $Al_2O_3$-NPs with 3-armed Gly-lac.

The effect of Gly:lac molar ratio and loading rate of 3-armed Gly-lac on the biodiesel cloud point (CP) and pour point (PP) was investigated, and the results revealed that molar ratio and loading rate have significant effect on the improvement of CP and PP of biodiesel. The addition of Gly-lac with (1:6) Gly:lac molar ratio at loading rate of 10g/l brought a maximum reduction of CP by **7**$^{o}$C and PP by 8.14$^{o}$C as compared to that of pure biodiesel. The addition of $Al_2O_3$-NPs dispersed 3-armed Gly-lac into biodiesel also resulted in reduction of CP and PP up to **7**$^{o}$C and 9.44$^{o}$C respectively, at $Al_2O_3$-NPs loading rate of 3wt% of 3-armed Gly-lac.

The result of engine performance and emission test revealed that the addition of $Al_2O_3$-NPs with and without dispersant (3-armed Gly-lac) shows an improvement in engine performance and emission characteristics of biodiesel-diesel blend (B20). And the addition of 3-armed Gly-lac into B20 also brought a reduction in emission of $NO_x$, HC, and CO. As compared to the $Al_2O_3$-NPs alone, $Al_2O_3$-NPs dispersed 3-armed Gly-lac brought a better impact on the engine performance and emission characteristics of B20. The maximum impact was achieved at $Al_2O_3$-

NPs loading rate of (3wt% of 3-armed Gly-lac), which brought an increase in BTE by 6.837%, a decline in BSFC by 25.26%. In a similar condition, it was achieved a maximum reduction in emission of HC, $NO_x$, and CO by 27.4 ppm, 98.6 ppm, and 39.52%, respectively as compared to that of B20.

Generally, we can conclude that the 3-armed Gly-lac was obtained to be a dispersant for good dispersion of $Al_2O_3$-NPs. And also, $Al_2O_3$-NPs dispersed 3-armed Gly-lac was obtained a potential additive to reduce CP and PP of biodiesel, to reduce exhaust gas emission and BSFC as well as to improve the BP and BTE of the biodiesel-diesel blend.

### 5.2. Recommendations

In this study, 3-armed Gly-lac which was synthesized from glycerol and lactic acid is compatible with the biodiesel structure as well as it is biocompatible. The synthesis of $Al_2O_3$-NPs was via sol-gel method and citric acid (which was used a metal complex agent) is less toxic due to its organic nature. Therefore, the 3-armed Gly-lac and $Al_2O_3$-NPs could be employed for the biodiesel additive in real applications. Further research work should better to be done on the following cases.

- Since the structural variation of biodiesel among different feedstock have an influence on the efficacy of the different cold flow improvers, the effects of 3-armed Gly-lac (with varying molar ratio), on the cold flow properties of biodiesel obtained from feedstock (other than soyabean oil) should be studied in future works.
- Due to the surface reactive nature of $Al_2O_3$-NPs, a study on the effect of 3-armed Gly-lac/ $Al_2O_3$-NPs on engine wear and engine parts such as piston, cylinder and fuel injectors, should be focused in future work to validate the compatibility of the nano-additive in diesel engine.
- The other potential future works could be on investigation of the thermal conductivity of the $Al_2O_3$-NPs dispersed 3-armed Gly-lac with subsequent study on its possibility as potential heat transfer fluid.
- The effect of particle size of the $Al_2O_3$-NPs on biodiesel cold flow properties, IC engine performance as well as emission characteristics should be investigated in future work.

## References


Aalam, C. S., Saravanan, D. C. G., & Samath, C. M. (2015). Reduction of Diesel Engine Emissions Using Catalytic Converter with Nano Aluminium Oxide Catalyst. *International Journal for Research in Emerging Science and Technology*, *2*(7), 17–22.

Abdullah, A. Z., Razali, N., Mootabadi, H., & Salamatinia, B. (2007). Critical technical areas for future improvement in biodiesel technologies. *Environmental Research Letters*, *2*(3).

Abe M., Hirata S., Komatsu, H., Yamagiwa, K., Tajima, H. (2016). Thermodynamic selection of effective additives to improve the cloud point of biodiesel fuel. *Fuel*, *171*(December), 94-100.

Agarwal, M., Singh, K., & Chaurasia, S. P. (2010). Prediction of Biodiesel Properties from Fatty Acid Composition using Linear Regression and ANN Techniques. *Indian Chemical Engineer*, *52*(4), 347–361.

Ağbulut, Ü., Karagöz, M., Sarıdemir, S., & Öztürk, A. (2020). Impact of various metal-oxide based nanoparticles and biodiesel blends on the combustion, performance, emission, vibration and noise characteristics of a CI engine. *Fuel*, *270*(January).

Ahmadi, S., Fazilati, M., Mousavi, S. M., & Nazem, H. (2020). Anti-bacterial/fungal and anti-cancer performance of green synthesized Ag nanoparticles using summer savory extract. *Journal of Experimental Nanoscience*, *15*(1), 363–380.

Aisida, S. O., Ugwu, K., Akpa, P. A., Nwanya, A. C., Nwankwo, U., Botha, S. S., Ejikeme, P. M., Ahmad, I., Maaza, M., & Ezema, F. I. (2019). Biosynthesis of silver nanoparticles using bitter leave (Veronica amygdalina) for antibacterial activities. *Surfaces and Interfaces*, *17*(July), 100359.

Akanksha, D., Vikas, G., Neetesh, K. J., Shailendra, S., Neelam, B., & Dinesh, K. J. (2009). Formulation and Evaluation of Neomycin Sulphate Ointment containing Natural Wound Healing Agent Curcuma longa. *International Journal of Pharmaceutical Sciences and Drug Research*, *1*(2), 116–118.

Akbar, E., Yaakob, Z., Kamarudin, S. K., Ismail, M., & Salimon, J. (2009). Characteristic and composition of Jatropha curcas oil seed from Malaysia and its potential as biodiesel feedstock feedstock. *European Journal of Scientific Research*, *29*(3), 396–403.

Ali, O. M., & Mamat, R. (2013). Improving engine performance and low temperature properties of blended palm biodiesel using additive. A review. *App. Mechanic&Materia. 315*, 68-72.

Ali, O. M., Mamat, R., Najafi, G., Yusaf, T., & Ardebili, S. M. S. (2015). Optimization of biodiesel-diesel blended fuel properties and engine performance with ether additive using statistical analysis and response surface methods. *Energies*, *8*(12), 14136–14150.

Aly, A. A., Maraei, R. W., & Ali, H. G. M. (2016). Fatty Acids Profile and Chemical Composition of Egyptian Moringa oleifera Seed Oils. *JAOCS, Journal of the American Oil Chemists' Society*, *93*(3), 397–404.

Ambat, I., Srivastava, V., & Sillanpää, M. (2018). Recent advancement in biodiesel production methodologies using various feedstock: A review. *Renewable and Sustainable Energy Reviews*, *90*(March), 356–369.

Anchupogu, P. (2018). *Effect of alumina nano additives into biodiesel-diesel blends on the combustion performance and emission characteristics of a diesel engine with exhaust gas recirculation*.

Aransiola, E. F., Ojumu, T. V., Oyekola, O. O., Madzimbamuto, T. F., & Ikhu-Omoregbe, D. I. O. (2014). A review of current technology for biodiesel production: State of the art. *Biomass and Bioenergy*, *61*, 276–297.

Astm D. (2012). Standard specification for biodiesel fuel blend stock (B100) for middle distillate fuels. *ASTM International, West Conshohocken*.

ASTM D6751-02. (2002). American society for testing and materials. Standard specification for biodiesel fuel (B100) blend stock for distillate fuels, designation. *West Conshohocken, PA: ASTM International*.

ASTM, I. (1999). *ASTM D-1298-99-Standard Test Method for Density, Relative Density (Specific Gravity) or API Gravity of Crude Petroleum and Liquid Petroleum Products by Hydrometer Method. Section 5*.

ASTM, I. (2015). Standard Test Methods for Flash Point by Pensky-Martens Closed Cup Tester. *ASTM International*.

Atabani, A. E., Silitonga, A. S., Badruddin, I. A., Mahlia, T. M. I., Masjuki, H. H., & Mekhilef, S. (2012). A comprehensive review on biodiesel as an alternative energy resource and its characteristics. *Renewable and Sustainable Energy Reviews*, *16*(4), 2070–2093.

ATC Document 113. (2013). Fuel Additives: Use and Benefits. *ATC, September*, 68.

Awulu, J. O., Omale, P. A., & Ameh, J. A. (2018). Comparative analysis of calorific values of selected agricultural wastes. *Nigerian Journal of Technology*, *37*(4), 1141.

Azcan, N., & Danisman, A. (2007). Alkali catalyzed transesterification of cottonseed oil by microwave irradiation. *Fuel*, *86*(17–18), 2639–2644.

Babita, Sharma, S. K., Gupta, S. M. (2016). Preparation and evaluation of stable nanofluids for heat transfer application: A review. *Experimental Thermal and Fluid Scien. 79*, 202-12.

Baskar, G., & Aiswarya, R. (2016). Trends in catalytic production of biodiesel from various feedstocks. *Renewable and Sustainable Energy Reviews*, *57*, 496–504.

Borowicz, M., Paciorek-Sadowska, J., Isbrandt, M., Grzybowski, Ł., & Czupryński, B. (2019). Glycerolysis of poly(lactic acid) as away to extend the "life cycle" of this material. *Polymers*, *11*(12).

Bose, P. K. (2009). Empirical Approach For Predicting The Cetane Number Of Biodiesel. *International Journal of Automotive Technology*, *10*(4), 421−429.

Boshui, C., Yuqiu, S., Jianhua, F., Jiu, W., & Jiang, W. (2010). Effect of cold flow improvers on flow properties of soybean biodiesel. *Biomass and Bioenergy*, *34*(9), 1309–1313.

Canoira, L., García Galeán, J., Alcántara, R., Lapuerta, M., & García-Contreras, R. (2010). Fatty acid methyl esters (FAMEs) from castor oil: Production process assessment and synergistic effects in its properties. *Renewable Energy*, *35*(1), 208–217.

Cao, L., Wang, J., Liu, C., Chen, Y., Liu, K., & Han, S. (2014). Ethylene vinyl acetate copolymer: A bio-based cold flow improver for waste cooking oil derived biodiesel blends. *Applied Energy*, *132*, 163–167.

Chen, C., Huang, C., Tran, D., & Chang, J. (2012). Biodiesel synthesis via heterogeneous catalysis using modified strontium oxides as the catalysts. *Bioresource Tech.*, *113*, 8–13.

Cornejo, A., Barrio, I., Campoy, M., Lázaro, J., & Navarrete, B. (2017). Oxygenated fuel additives from glycerol valorization. Main production pathways and effects on fuel properties and engine performance: A critical review. *Renewable and Sustainable Energy Reviews*, *79*(November 2016), 1400–1413.

Coussirat, V., Amarilla, F., Peruzzo, P. J., & Cortizo, M. S. (2019). Dioctyl fumarate-co-vinyl benzoate copolymers preparation and their performance as flow improvers in waxy crude oils. *Journal of Petroleum Science and Engineering*, *182*(November 2018), 106290.

Dayrit, F. M. (2014). Lauric acid is a medium-chain fatty acid, coconut oil is a medium-chain triglyceride. *Philippine Journal of Science*, *143*(2), 157–166.

De Oliveira, D., Do Nascimento Filho, I., Di Luccio, M., Faccio, C., Dalla Rosa, C., Bender, J.

P., Lipke, N., Amroginski, C., Dariva, C., & De Oliveira, J. V. (2005). Kinetics of enzyme-catalyzed alcoholysis of soybean oil in n-hexane. *Applied Biochemistry and Biotechnology - Part A Enzyme Engineering and Biotechnology*, *121*(1–3), 231–241.

Demirbas, A., & Fatih Demirbas, M. (2011). Importance of algae oil as a source of biodiesel. *Energy Conversion and Management*, *52*(1), 163–170.

Djebaili, K., Mekhalif, Z., Boumaza, A., & Djelloul, A. (2013). Xps, Ftir,Edx,Xrd Analysis of Al2O3 Scales Grown on Pm2000 Alloy. *Journal of Spectroscopy*, *2015*, 1–16.

Doudin, K. I. (2021). Quantitative and qualitative analysis of biodiesel by NMR spectroscopic methods. *Fuel*, *284*(May 2020), 119114.

Dunn, R. O. (2001). Alternative jet fuels from vegetable-oils. *Trans ASAE*, *44*(6), 1751–1757.

Dwivedi, G., & Sharma, M. P. (2014). Impact of cold flow properties of biodiesel on engine performance. *Renewable and Sustainable Energy Reviews*, *31*, 650–656.

Dwivedi, G., & Sharma, M. P. (2016). Investigation of Cold Flow Properties of Waste Cooking Biodiesel. *Journal of Clean Energy Technologies*, *4*(3), 205–208.

Edith, O., Janius, R. B., & Yunus, R. (2012). Factors affecting the cold flow behaviour of biodiesel and methods for improvement—a review. *Pertanika J. Sci. Technol*, *20*(1), 1–14.

Espartero, J. L., Rashkov, I., Li, S. M., Manolova, N., & Vert, M. (1996). NMR analysis of low molecular weight poly(lactic acid)s. *Macromolecules*.

Farahmandjou, M., & Golabiyan, N. (2016). Synthesis and characterization of Alumina ($Al_2O_3$) nanoparticles prepared by simple sol-gel method. *Appl. Surface Scienc. 258*(15), 5712-15.

Fathurrahman, N. A., Wibowo, C. S., Nasikin, M., & Khalil, M. (2021). Optimization of sorbitan monooleate and γ-Al2O3 nanoparticles as cold-flow improver in B30 biodiesel blend using response surface methodology (RSM). *J. of Indust. and Engineering Chemistry*, *99*, 271–281.

Feng, L., Zhang, Z., Wang, F., Wang, T., & Yang, S. (2014). Synthesis and evaluation of alkyl acrylate-vinyl acetate-maleic anhydride terpolymers as cold flow improvers for diesel fuel. *Fuel Processing Technology*, *118*, 42–48.

Fernández, Y., Arenillas, A., Díez, M. A., Pis, J. J., & Menéndez, J. A. (2009). Pyrolysis of glycerol over activated carbons for syngas production. *Journal of Analytical and Applied Pyrolysis*, *84*(2), 145–150.

Francis, H. (2012). Developing a self-sustaining protected area system: a feasibility study of

national tourism fee and green infrastructure in the Solomon Islands. *Journal of Sustainable Finance and Investment*, *2*(3–4), 287–302.

Frusteri, F., Arena, F., Bonura, G., Cannilla, C., Spadaro, L., & Di Blasi, O. (2009). Catalytic etherification of glycerol by tert-butyl alcohol to produce oxygenated additives for diesel fuel. *Applied Catalysis A: General*, *367*(1–2), 77–83.

Fukuda, H., Kondo, A., & Noda, H. (2001). Biodiesel fuel production by transesterification of oils. *Journal of Bioscience and Bioengineering*, *92*(5), 405–416.

Gad, M. S., & Jayaraj, S. (2020). A comparative study on the effect of nano-additives on the performance and emissions of a diesel engine run on Jatropha biodiesel. *Fuel*, *267*(January), 117168.

Ghanbari, M., Mozafari-Vanani, L., Dehghani-Soufi, M., & Jahanbakhshi, A. (2021). Effect of alumina nanoparticles as additive with diesel–biodiesel blends on performance and emission characteristic of a six-cylinder diesel engine using response surface methodology (RSM). *Energy Conversion and Management: X*, *11*, 100091.

Giraldo, S. Y., Rios, L. A., & Suárez, N. (2013). Comparison of glycerol ketals, glycerol acetates and branched alcohol-derived fatty esters as cold-flow improvers for palm biodiesel. *Fuel*, *108*(x), 709–714.

Gómez-Siurana, A., Marcilla, A., Beltrán, M., Berenguer, D., Martínez-Castellanos, I., & Menargues, S. (2013). TGA/FTIR study of tobacco and glycerol-tobacco mixtures. *Thermochimica Acta*, *573*, 146–157.

Govindrao, P., Ghule, N. W., Haque, A., & Kalaskar, M. G. (2019). Journal of Drug Delivery Science and Technology Metal nanoparticles synthesis : An overview on methods of preparation , advantages and disadvantages , and applications. *Journal of Drug Delivery Science and Technology*, *53*(July), 101174.

Gross, I. P., Schneider, F. S. S., Caro, M. S. B., da Conceição, T. F., Caramori, G. F., & Pires, A. T. N. (2018). Polylactic acid, maleic anhydride and dicumyl peroxide: NMR study of the free-radical melt reaction product. *Polymer Degradation and Stability*, *155*, 1–8.

Hamada, H., Kato, H., Ito, N., Takase, Y., Nanbu, H., Mishima, S., Sakaki, H., & Sato, K. (2010). Effects of polyglycerol esters of fatty acids and ethylene-vinyl acetate co-polymer on crystallization behavior of biodiesel. *European Journal of Lipid Science and Technology*, *112*(12), 1323–1330.

He, C., Ding, Y., Chen, J., Wang, F., Gao, C., Zhang, S., & Yang, M. (2016). Influence of the nano-hybrid pour point depressant on flow properties of waxy crude oil. *Fuel*, *167*(November), 40–48.

Helwani, Z., Othman, M. R., Aziz, N., Fernando, W. J. N., & Kim, J. (2009). Technologies for production of biodiesel focusing on green catalytic techniques: A review. *Fuel Processing Technology*, *90*(12), 1502–1514.

Hong, I. K., Jeon, G. S., & Lee, S. B. (2014). Prediction of biodiesel fuel properties from fatty acid alkyl ester. *Journal of Industrial and Engineering Chemistry*, *20*(4), 2348–2353.

Hosseini, S. H., Taghizadeh-Alisaraei, A., Ghobadian, B., & Abbaszadeh-Mayvan, A. (2017). Effect of added alumina as nano-catalyst to diesel-biodiesel blends on performance and emission characteristics of CI engine. *Energy*, *124*, 543–552.

Imdadul, H. K., Masjuki, H. H., Kalam, M. A., Zulkifli, N. W. M., Alabdulkarem, A., Rashed, M. M., & Ashraful, A. M. (2016). Influences of ignition improver additive on ternary (diesel-biodiesel-higher alcohol) blends thermal stability and diesel engine performance. *Energy Conversion and Management*, *123*, 252–264.

J.E.C. Marc, V. D. M., Van Der Veen, B., Uitdehaag, J. C. M., Leemhuis, H., & Dijkhuizen, L. (2002). Properties and applications of starch-converting enzymes of the α-amylase family. *Journal of Biotechnology*, *94*(2), 137–155.

Jegannathan, K. R., Abang, S., Poncelet, D., Chan, E. S., & Ravindra, P. (2008). Production of biodiesel using immobilized lipase - A critical review. *Critical Reviews in Biotechnology*, *28*(4), 253–264.

Joshi, H., Moser, B. R., Toler, J., Smith, W. F., & Walker, T. (2011). Ethyl levulinate: A potential bio-based diluent for biodiesel which improves cold flow properties. *Biomass and Bioenergy*, *35*(7), 3262–3266.

Kaisan, M. U., Anafi, F. O., Nuszkowski, J., Kulla, D. M., & Umaru, S. (2020). Calorific value, flash point and cetane number of biodiesel from cotton, jatropha and neem binary and multi-blends with diesel. *Biofuels*, *11*(3), 321–327.

Kalaimurugan K., Karthikeyan S., Periyasamy M., Mahendran, G. (2020). Experimental investigations on the performance characteristics of CI engine fuelled with cerium oxide nanoparticle added biodiesel-diesel blends. *Materials Today Proceedings*, *33*(xxxx), 2882–85.

Kannan, G. R., Karvembu, R., & Anand, R. (2011). Effect of metal based additive on performance emission and combustion characteristics of diesel engine fuelled with biodiesel. *Applied Energy*, *88*(11), 3694–3703.

Katryniok, B., Kimura, H., Skrzyńska, E., Girardon, J. S., Fongarland, P., Capron, M., Ducoulombier, R., Mimura, N., Paul, S., Dumeignil, F. (2011). Selective catalytic oxidation of glycerol: Perspectives for high value chemicals. *Green Chemistry*, *13*(8), 1960-79.

Keera, S. T., Sabagh, S. M. El, & Taman, A. R. (2018). Castor oil biodiesel production and optimization. *Egyptian Journal of Petroleum*.

Knothe, G. (2006). Analyzing biodiesel: Standards and other methods. *JAOCS, Journal of the American Oil Chemists' Society*, *83*(10), 823–833.

Kumar S., Dinesha P., Bran, I. (2017). Influence of nanoparticles on the performance and emission characteristics of a biodiesel fuelled engine: An experimental analysis. *Energy*, *140*, 98–105.

Lawan, I., Zhou, W., Garba, Z. N., Zhang, M., Yuan, Z., & Chen, L. (2019). Critical insights into the effects of bio-based additives on biodiesels properties. *Renewable and Sustainable Energy Reviews*, *102*, 83–95.

Lee, J. H., Hwang, K. S., Jang, S. P., Lee, B. H., Kim, J. H., Choi, S. U. S., & Choi, C. J. (2008). Effective viscosities and thermal conductivities of aqueous nanofluids containing low volume concentrations of Al2O3 nanoparticles. *International Journal of Heat and Mass Transfer*, *51*(11–12), 2651–2656.

Leng, L., Li, W., Li, H., Jiang, S., & Zhou, W. (2020). Cold Flow Properties of Biodiesel and the Improvement Methods: A Review. *Energy and Fuels*, *34*(9), 10364–10383.

Leung, D. Y. C., Wu, X., & Leung, M. K. H. (2010). A review on biodiesel production using catalyzed transesterification. *Applied Energy*, *87*(4), 1083–1095.

Li, H. Z., Chen, S. C., & Wang, Y. Z. (2014). Thermoplastic PVA/PLA blends with improved processability and hydrophobicity. *Industrial and Engineering Chemistry Research*, *53*(44), 17355–17361.

Li, J., Pan, Y., Xiang, C., Ge, Q., Guo, J. (2006). Low temperature synthesis of ultrafine α-$Al_2O_3$ powder by a simple aqueous sol-gel process. *Ceramics International*, *32*(5), 587-91.

Liu, G. (2015). Development of Low-Temperature Properties on Biodiesel Fuel: A Review. *Int.*

*J. Energy Res*, *39*(10), 1295–1310.

Lotero, E., Liu, Y., Lopez, D. E., Suwannakarn, K., Bruce, D. A., & Goodwin, J. G. (2005). Synthesis of biodiesel via acid catalysis. *Industrial and Engineering Chemistry Research*, *44*(14), 5353–5363.

Lü, X. C., Yang, J. G., Zhang, W. G., & Huang, Z. (2005). Improving the combustion and emissions of direct injection compression ignition engines using oxygenated fuel additives combined with a cetane number improver. *Energy and Fuels*, *19*(5), 1879–1888.

Mat Yasin, M. H., Yusaf, T., Mamat, R., & Fitri Yusop, A. (2014). Characterization of a diesel engine operating with a small proportion of methanol as a fuel additive in biodiesel blend. *Applied Energy*, *114*, 865–873.

Meher, L. C., Dharmagadda, V. S. S., & Naik, S. N. (2006). Optimization of alkali-catalyzed transesterification of Pongamia pinnata oil for production of biodiesel. *Bioresource Technology*, *97*(12), 1392–1397.

Mirhashemi, F. S., & Sadrnia, H. (2019). NO X emissions of compression ignition engines fueled with various biodiesel blends : A review. *Journal of the Energy Institute*, *X*.

Mohammed, A. A., Khodair, Z. T., & Khadom, A. A. (2020). Preparation and investigation of the structural properties of α-Al2O3 nanoparticles using the sol-gel method. *Chemical Data Collections*, *29*, 100531.

Mohd Noor C. W., Noor M. M., Mamat R. (2018). Biodiesel as alternative fuel for marine diesel engine applications: A review. *Renewable and Sustai. Energy Revi. 94*(May), 127-42.

Morgenstern, M., Cline, J., Meyer, S., & Cataldo, S. (2006). Determination of the kinetics of biodiesel production using proton nuclear magnetic resonance spectroscopy (1H NMR). *Energy and Fuels*, *20*(4), 1350–1353.

Moser, B. R. (2009). Biodiesel production, properties, and feedstocks. *In Vitro Cellular and Developmental Biology - Plant*, *45*(3), 229–266.

Mujeeb, M. A., Vedamurthy, A. B., & T, S. C. (2016). Current strategies and prospects of biodiesel production: A review. *Pelagia Research Library Advances in Applied Science Research*, *7*(1), 120–133.

Muniz, A. S., Inoue, M. H., Oliveira, D. C., Oliveira, A. R. S., Ramos, L. P., Mittelbach, M., Aparecida, M., & Ce, F. (2020). *Bifunctional Additives To Improve the Cold Flow Properties and Oxidation Stability of Soybean Oil Biodiesel*.

Muniz, A. S., Vlnieska, V., Ferraz, F. A., Angelo, R., Oliveira, S., Ramos, L. P., & Maria, A. F. C. (2019). Polymer Additives as Cold Flow Improvers for Palm Oil Methyl Esters. *Macromol. Symp*, *1800026*, 1–7.

Nabi, M. N., Hoque, S. M. N., & Akhter, M. S. (2009). Karanja (Pongamia Pinnata) biodiesel production in Bangladesh, characterization of karanja biodiesel and its effect on diesel emissions. *Fuel Processing Technology*, *90*(9), 1080–1086.

Nakagawa, Y., Tamura, M., & Tomishige, K. (2014). Catalytic materials for the hydrogenolysis of glycerol to 1,3-propanediol. *Journal of Materials Chemistry A*, *2*(19), 6688–6702.

Nanthagopal, K., Ashok, B., Tamilarasu, A., Johny, A., & Mohan, A. (2017). Influence on the effect of zinc oxide and titanium dioxide nanoparticles as an additive with Calophyllum inophyllum methyl ester in a CI engine. *Energy Conversion and Management*, *146*, 8–19.

Nduni, M. N., Osano, A. M., & Chaka, B. (2021). Synthesis and characterization of aluminium oxide nanoparticles from waste aluminium foil and potential application in aluminium-ion cell. *Cleaner Engineering and Technology*, *3*, 100108.

Nielsen, P. M., Brask, J., & Fjerbaek, L. (2008). Enzymatic biodiesel production: Technical and economical considerations. *European J. of Lipid Science and Technology*, *110*(8), 692–700.

Nikam, A. V., Prasad, B. L. V., & Kulkarni, A. A. (2018). Wet chemical synthesis of metal oxide nanoparticles: A review. *CrystEngComm*, *20*(35), 5091–5107.

Obedi M., A., Mamat R., & C.K.M., F. (2012). Palm Biodiesel Production, Properties and Fuel Additives. *International Review of Mechanical Engineering*, *6*(7), 1573–1580.

Ojha, P. K., & Karmakar, S. (2018). Boron for liquid fuel Engines-A review on synthesis, dispersion stability in liquid fuel, and combustion aspects. *Progress in Aerospace Sciences*, *100*(December 2017), 18–45.

Ortiz L., E. G., Pinal Rosales M. A., Martínez Ortega I. A., Arévalo Niño, K. (2020). Potential use of glycerol from biodiesel industry: germination and first phase of growth evaluation of two domesticated varieties of Phaseolus vulgaris. *Biomass Conver. and Biorefinery*, *10*(1), 25–34.

Oskam, G. (2006). Metal oxide nanoparticles: Synthesis, characterization and application. *Journal of Sol-Gel Science and Technology*, *37*(3), 161–164.

Pagliaro, M., Ciriminna, R., Kimura, H., Rossi, M., & Della Pina, C. (2007). From glycerol to

value-added products. *Angewandte Chemie - International Edition*, *46*(24), 4434–4440.

Pantidos, N. (2014). Biological Synthesis of Metallic Nanoparticles by Bacteria, Fungi and Plants. *Journal of Nanomedicine & Nanotechnology*, *05*(05).

Parashar, M., Kumar, V., & Ranbir, S. (2020). Metal oxides nanoparticles via sol – gel method : a review on synthesis, characterization and applications. *Journal of Materials Science: Materials in Electronics*, *0123456789*.

Patra, A. K., Dutta, A., & Bhaumik, A. (2012). Self-assembled mesoporous γ-Al 2O 3 spherical nanoparticles and their efficiency for the removal of arsenic from water. *Journal of Hazardous Materials*, *201–202*, 170–177.

Pham, N. L., Luu, V. B., Phan, T. T. M., & Nguyen, T. S. (2021). Synthesis and characterization of alkyl-methacrylate-maleic anhydride copolymer for use as a biodiesel flow improver. *Journal of Science, Technology and Engineering, Vietnam*, *63*(3), 24–29.

Phan, M. T. T., Luu, B. Van, & Pham, L. N. (2021). Synthesis and elaboration of modified comb type (maleic anhydride-α-tetradecene) copolymers for cold flow improvers of biodiesel. *Ministry of Science and Technology, Vietnam*, *63*(2), 13–19.

Pinzi, S., Leiva, D., Arzamendi, G., Gandia, L. M., & Dorado, M. P. (2011). Multiple response optimization of vegetable oils fatty acid composition to improve biodiesel physical properties. *Bioresource Technology*, *102*(15), 7280–7288.

Prabakaran, B., & Udhoji, A. (2016). Experimental investigation into effects of addition of zinc oxide on performance, combustion and emission characteristics of diesel-biodiesel-ethanol blends in CI engine. *Alexandria Engineering Journal*, *55*(4), 3355–3362.

Prabakaran, B., & Vijayabalan, P. (2018). Influence of zinc oxide nano particles on performance, combustion and emission characteristics of butanol-diesel-ethanol blends in di CI engine. *IOP Conference Series: Materials Science and Engineering*, *377*(1).

Pullen, J., & Saeed, K. (2014). Factors affecting biodiesel engine performance and exhaust emissions - Part II: Experimental study. *Energy*, *72*, 17–34.

Rabelo, S. N., Ferraz, V. P., Oliveira, L. S., & Franca, A. S. (2015). FTIR Analysis for Quantification of Fatty Acid Methyl Esters in Biodiesel Produced by Microwave-Assisted Transesterification. *International J. of Environ'ntal Science and Develop'nt*, *6*(12), 964–69.

Ramesh, D. K., Dhananjaya Kumar, J. L., Hemanth Kumar, S. G., Namith, V., Basappa

Jambagi, P., & Sharath, S. (2018). Study on effects of Alumina nanoparticles as additive with Poultry litter biodiesel on Performance, Combustion and Emission characteristic of Diesel engine. *Materials Today: Proceedings*, *5*(1), 1114–1120.

Ranjan A., Dawn S. S., Jayaprabakar J., Nirmala N., Saikiran K., Sriram, S. S. (2018). Experimental investigation on e ff ect of MgO nanoparticles on cold fl ow properties , performance , emission and combustion characteristics of waste cooking oil biodiesel. *Fuel*, *220*(February), 780–791.

Rashed, M. M., Kalam, M. A., Masjuki, H. H., Mofijur, M., Rasul, M. G., & Zulkifli, N. W. M. (2016). Performance and emission characteristics of a diesel engine fueled with palm, jatropha, and moringa oil methyl ester. *Industrial Crops and Products*, *79*, 70–76.

Rashedul, H. K., Masjuki, H. H., Kalam, M. A., Ashraful, A. M., Ashrafur Rahman, S. M., & Shahir, S. A. (2014). The effect of additives on properties, performance and emission of biodiesel fuelled compression ignition engine. *Energy Conver. and Manage.*, *88*, 348–364.

Rashkov, I., Manolova, N., Li, S. M., Espartero, J. L., & Vert, M. (1996). Synthesis, characterization, and hydrolytic degradation of PLA/PEO/PLA triblock copolymers with short poly(L-lactic acid) chains. *Macromolecules*, *29*(1), 50–56.

Razzaq, L., Mujtaba, M. A., Soudagar, M. E. M., Ahmed, W., Fayaz, H., Bashir, S., Fattah, I. M. R., Ong, H. C., Shahapurkar, K., Afzal, A., Wageh, S., Al-Ghamdi, A., Ali, M. S., & EL-Seesy, A. I. (2021). Engine performance and emission characteristics of palm biodiesel blends with graphene oxide nanoplatelets and dimethyl carbonate additives. *Journal of Environmental Management*, *282*(December 2020), 111917.

Ribeiro, N., Pinto, A. C., Quintella, C. M., da Rocha, G. O., Teixeira, L. S. G., Guarieiro, L. L. N., Rangel, M. do C., Veloso, M. C. C., Rezende, M. J. C., da Cruz, R. S., de Oliveira, A. M., Torres, E. A., & de Andrade, J. B. (2007). The role of additives for diesel and diesel blended (ethanol or biodiesel) fuels: A review. *Energy and Fuels*, *21*(4), 2433–2445.

Ryu, K. (2013). Effects of pilot injection pressure on the combustion and emissions characteristics in a diesel engine using biodiesel-CNG dual fuel. *Energy Conver. &Manage.*, *76*, 506-16.

Sahar, Sadaf, S., Iqbal, J., Ullah, I., Bhatti, H. N., Nouren, S., Habib-ur-Rehman, Nisar, J., & Iqbal, M. (2018). Biodiesel production from waste cooking oil: An efficient technique to convert waste into biodiesel. *Sustainable Cities and Society*, *41*(December 2017), 220–26.

Sahoo, P. K., & Das, L. M. (2009). Process optimization for biodiesel production from Jatropha, Karanja and Polanga oils. *Fuel*, *88*(9), 1588–1594.

Sajjadi, B., Raman, A. A. A., & Arandiyan, H. (2016). A comprehensive review on properties of edible and non-edible vegetable oil-based biodiesel: Composition, specifications and prediction models. *Renewable and Sustainable Energy Reviews*, *63*, 62–92.

Sarin, R., Sharma, M., Sinharay, S., & Malhotra, R. K. (2007). Jatropha-Palm biodiesel blends: An optimum mix for Asia. *Fuel*, *86*(10–11), 1365–1371.

Sarkar, N., Ghosh, S. K., Bannerjee, S., & Aikat, K. (2012). Bioethanol production from agricultural wastes: An overview. *Renewable Energy*, *37*(1), 19–27.

Sarpal, A. S., Silva, S. R., Silva, P. R. M., Monteiro, T. V., Itacolomy, J., Cunha, V. S., & Daroda, R. J. (2015). Direct Method for the Determination of the Iodine Value of Biodiesel by Quantitative Nuclear Magnetic Resonance (q1H NMR) Spectroscopy. *Energy and Fuels*, *29*(12), 7956–7968.

Saxena, V., Kumar, N., & Saxena, V. K. (2017). A comprehensive review on combustion and stability aspects of metal nanoparticles and its additive effect on diesel and biodiesel fuelled C.I. engine. *Renewable and Sustainable Energy Reviews*, *70*(December 2016), 563–588.

Sekoai, P. T., Ouma, C. N. M., du Preez, S. P., Modisha, P., Engelbrecht, N., Bessarabov, D. G., & Ghimire, A. (2019). Application of nanoparticles in biofuels: An overview. *Fuel*, *237*(July 2018), 380–397.

Seneviratne, K., & Jayathilaka, N. (2020). *Coconut Oil: Chemistry and Nutrition* (Issue January 2016).

Senra, M., McCartney, S. N., & Soh, L. (2019). The effect of bio-derived additives on fatty acid methyl esters for improved biodiesel cold flow properties. *Fuel*, *242*(January), 719–727.

Shaafi, T., & Velraj, R. (2015). Influence of alumina nanoparticles, ethanol and isopropanol blend as additive with diesel-soybean biodiesel blend fuel: Combustion, engine performance and emissions. *Renewable Energy*, *80*, 655–663.

Sharma, B. K., Sharma, C. D., Tyagi, O. S., Bhagat, S. D., & Erhan, S. Z. (2007). Structural characterization of asphaltenes and ethyl acetate insoluble fractions of petroleum vacuum residues. *Petroleum Science and Technology*, *25*(1–2), 121–139.

Sharma, R., Mahto, V., & Vuthaluru, H. (2019). Synthesis of PMMA/modified graphene oxide nanocomposite pour point depressant and its effect on the flow properties of Indian waxy

crude oil. *Fuel*, *235*(August 2018), 1245–1259.

Shrivastava, N., Shrivastava, D., & Shrivastava, V. (2018). Experimental investigation of performance and emission characteristics of diesel engine using Jatropha biodiesel with alumina nanoparticles. *International Journal of Green Energy*, *15*(2), 136–143.

Sia, C. B., Kansedo, J., Tan, Y. H., & Lee, K. T. (2020). Evaluation on biodiesel cold flow properties, oxidative stability and enhancement strategies: A review. *Biocatalysis and Agricultural Biotechnology*, *24*(January), 101514.

Sierra-Cantor, J. F., & Guerrero-Fajardo, C. A. (2017). Methods for improving the cold flow properties of biodiesel with high saturated fatty acids content: A review. *Renewable and Sustainable Energy Reviews*, *72*(April 2016), 774–790.

Slivniak, R., & Domb, A. J. (2005). Lactic acid and ricinoleic acid based copolyesters. *Macromolecules*, *38*(13), 5545–5553.

Smith, P. C., Ngothai, Y., Dzuy Nguyen Q., O'Neill, B. K. (2010). Improving the low-temperature properties of biodiesel: Methods and consequences. *Renewable Energy Ener*, *35*(6), 1145–51.

Soares, S., & Rocha, F. R. P. (2018). Fast spectrophotometric determination of iodine value in biodiesel and vegetable oils. *Journal of the Brazilian Chemical Society*, *29*(8), 1701–1706.

Soudagar, M. E. M., Nik-Ghazali, N. N., Abul Kalam, M., Badruddin, I. A., Banapurmath, N. R., & Akram, N. (2018). The effect of nano-additives in diesel-biodiesel fuel blends: A comprehensive review on stability, engine performance and emission characteristics. *Energy Conversion and Management*, *178*(June), 146–177.

Soudagar, M. E. M., Nik-Ghazali, N. N., Kalam, M. A., Badruddin, I. A., Banapurmath, N. R., Bin Ali, M. A., Kamangar, S., Cho, H. M., & Akram, N. (2020). An investigation on the influence of aluminium oxide nano-additive and honge oil methyl ester on engine performance, combustion and emission characteristics. *Renewable Energy*, *146*, 2291–2307.

Suhasinee Behera, P., Bhattacharyya, S., Sarkar, R. (2017). Effect of citrate to nitrate ratio on the sol-gel synthesis of nanosized α-Al2O3 powder. *Ceramics International*, *43*(17), 15221-26.

Sundaram, D. S., Yang, V., & Zarko, V. E. (2015). Combustion of nano aluminum particles (Review). *Combustion, Explosion and Shock Waves*, *51*(2), 173–196.

Sunil, K. M., Rajasekar, R., Ganesan, S., Venkatesan, S. P., & Praveen Kumar, V. (2021). Evaluation of metal oxide nano particles in lemongrass biodiesel for engine performance, emission and combustion characteristics. *Materia. Today: Proceedings*, *44*(xxxx), 3657–65.

Tang, W., Wang, B., Li, J., Li, Y., Zhang, Y., Quan, H., & Huang, Z. (2019). Facile pyrolysis synthesis of ionic liquid capped carbon dots and subsequent application as the water-based lubricant additives. *Journal of Materials Science*, *54*(2), 1171–1183.

Tanvir, S., & Qiao, L. (2012). Surface tension of nanofluid-type fuels containing suspended nanomaterials. *Western States Section of the Combustion Institute Spring Technical Meeting 2012*, 551–573.

Tariq, M., Ali, S., Ahmad, F., Ahmad, M., Zafar, M., Khalid, N., & Khan, M. A. (2011). Identification, FT-IR, NMR (1H and 13C) and GC/MS studies of fatty acid methyl esters in biodiesel from rocket seed oil. *Fuel Processing Technology*, *92*(3), 336–341.

Tesfaye, M., & Katiyar, V. (2016). Microwave assisted synthesis of biodiesel from soybean oil: Effect of poly (lactic acid)-oligomer on cold flow properties, IC engine performance and emission characteristics. *Fuel*, *170*, 107–114.

Tomar, M., & Kumar, N. (2020). Influence of nanoadditives on the performance and emission characteristics of a CI engine fuelled with diesel, biodiesel, and blends–a review. *Energy Sources, Part A: Recovery, Utilization and Environmental Effects*, *42*(23), 2944–2961.

Tsion, S. (2021). Development of Three Armed GLY-LAC Bio-Conjugate for the Efficacy of Ointment Base Matrix and Polymer Plasticizer. *ASTU*, *March*.

Tubino, M., & Aricetti, J. A. (2013). A green potentiometric method for the determination of the iodine number of biodiesel. *Fuel*, *103*, 1158–1163.

Van Gerpen, J. (2005). Biodiesel processing and production. *Fuel Processing Technology*, *86*(10), 1097–1107.

Varatharajan K., Cheralathan M., Velraj, R. (2011). Mitigation of NOx emissions from jatropha biodiesel fuelled di diesel engine using antioxidant additive. *Fuel*, *90*(8), 2721–25.

Ved, K., & Padam, K. (2013). Study of Physical and Chemical Properties of Biodiesel from Sorghum Oil. *Research Journal of Chemical Sciences*, *3*(9), 64–68.

Velu, S., & Gangwal, S. K. (2006). Synthesis of alumina supported nickel nanoparticle catalysts and evaluation of nickel metal dispersions by temperature programmed desorption. *Solid*

*State Ionics*, *177*(7–8), 803–811.

Vicente, G., Martínez, M., & Aracil, J. (2004). Integrated biodiesel production: A comparison of different homogeneous catalysts systems. *Bioresource Technology*, *92*(3), 297–305.

Vijaya P., D., Datta J., L., & Satish D., K. (2018). Synthesis, Characterization of α-Al2O3 Nanoparticles and Its Application in Decolorization of Methyl Orange Azo Dye in the Presence of UV Light. *Journal of Nanoscience and Technology*, *5*(1), 580–83.

Wang, X., Sø, L., Su, R., Wendt, S., Hald, P., Mamakhel, A., Yang, C., Huang, Y., Iversen, B. B., & Besenbacher, F. (2014). The influence of crystallite size and crystallinity of anatase nanoparticles on the photo-degradation of phenol. *Journal of Catalysis*, *310*, 100–108.

Wang, Y., Liu, H., & Lee, C. F. F. (2016). Particulate matter emission characteristics of diesel engines with biodiesel or biodiesel blending: A review. *Renewable and Sustainable Energy Reviews*, *64*, 569–581.

Xue, J., Grift, T. E., & Hansen, A. C. (2011). Effect of biodiesel on engine performances and emissions. *Renewable and Sustainable Energy Reviews*, *15*(2), 1098–1116.

Xue, Y., Chen, F., Sun, B., Lin, H., Dai, B., & Han, S. (2022). Effect of nanocomposite as pour point depressant on the cold flow properties and crystallization behavior of diesel fuel. *Chinese Chemical Letter*, *33*(5), 2677–2680.

Xue, Y., Zhao, Z., Xu, G., Lian, X., Yang, C., Zhao, W., Ma, P., Lin, H., & Han, S. (2016). Effect of poly-alpha-olefin pour point depressant on cold flow properties of waste cooking oil biodiesel blends. *Fuel*, *184*, 110–117.

Yang, C., He, K., Xue, Y., Li, Y., Lin, H., & Sheng, H. (2018). Factors affecting the cold flow properties of biodiesel: Fatty acid esters. *Energy Sources, Part A: Recovery, Utilization and Environmental Effects*, *40*(5), 516–522.

Yang, T., Wu, J., Yuan, M., Li, X., Yin, S., Su, B., Yan, J., Lin, H., Xue, Y., & Han, S. (2021). Influence of polar groups on the depressive effects of polymethacrylate polymers as cold flow improvers for diesel fuel. *Fuel*, *290*(December 2020), 120035.

Yuan., X., Zhu, J., Tang, K., Cheng, Y., Xu, Z., & Yang, W. (2015). Formation and properties of 1-D alumina nanostructures prepared via a template-free thermal reaction. *Procedia Engineering*, *102*, 602–609.

Yuan, M., Li, X., Xue, Y., Lin, H., & Han, S. (2022). Methylcyclohexyl methacrylate–methacrylate copolymers: an effective cold flow improver for the biodiesel blends.

*Research on Chemical Intermediates*, *48*(6), 2665–2681.

Yuan, Y., Hu, Z., Fu, X., Jiang, L., Xiao, Y., Hu, K., Yan, P., & Lei, J. (2016). Poly(lactic acid) plasticized by biodegradable glyceryl lactate. *Jour. of Appl. Polymer Scienc. 133*(21), 1-9.

Zhang, P., Su, X., Yi, C., Chen, H., Xu, H., & Geng, L. (2020). Spray, atomization and combustion characteristics of oxygenated fuels in a constant volume bomb: A review. *Journal of Traffic and Transportation Engineering (English Edition)*, *7*(3), 282–297.

## Research Fund Aknowledgement

This thesis research was funded by Adama Science and Technology University under the grant number of ASTU/SM-R/583/22, Adama, Ethiopia.

# Appendix

## Appendix A: Titration Result for Oil and Biodiesel Property Test

Table A1: Results of acid value and %FFA determination via titration with 0.1N NaOH solution

| **Parameters** | **Numerical Value** | Acid value (AV) = $\frac{40\text{g/mol x } 0.1\text{N x } 2.8\text{ml}}{10.10\text{ g}}$ = 0.99 |
|---|---|---|
| $Mw_{NaOH}$ = weight of NaOH | 40 g/mol | |
| N = normality of NaOH | 0.1N | %FFA = $\frac{AV}{2}$ = 0.495 % |
| $V_T$ = volume of titrant solution | 2.9 – 0.1 = 2.8 ml | |
| $W_S$ = weight of sample oil | 10.10 g | |

Table A2: Oil moisture content determination results

| **Measurement trial (within 10 min)** | **Initially** | **1st trial** | **2nd trial** | **3rd** | **4th** | **5th** |
|---|---|---|---|---|---|---|
| Mas of oil (g) | 10 | 9.982 | 9.941 | 9.874 | 9.857 | 9.857 |
| Moisture content (%) = $\frac{\textbf{(initial mass – final mass)}}{\textbf{initial mass}}$ **x** 100 = $\frac{\textbf{(10 – 9.857)}}{\textbf{10}}$ $\boldsymbol{x}$ 100 = 1.43% | | | | | | |

Table A3: Results for Iodine value determination for soyabean oil

| **Weight of oil sample (g)** | **B (ml)** | **S (ml)** | **N** |
|---|---|---|---|
| 0.15 | 18.6 | 3.7 | 0.1 |
| Iodine value = $\frac{\textbf{12.69 (B−S)N}}{\boldsymbol{W_S}}$ = $\frac{\textbf{(18.7 − 3.7) x 0.1 x 12.69}}{\textbf{0.15}}$ = 126.054 g $I_2$/100 g | | | |

Table A3: Results of Iodine value determination for the biodiesel

| **Weight of sample (g)** | **B (ml)** | **S (ml)** | **N** |
|---|---|---|---|
| 0.15 | 9.4 | 0.7 | 0.1 |
| Iodine value = $\frac{\textbf{12.69 (B−S)N}}{\boldsymbol{W_S}}$ = $\frac{\textbf{(9.4 − 0.7) x 0.1 x 12.69}}{\textbf{0.15}}$ = 73.602 g $I_2$/100 g | | | |

Table A4: Results of saponification value determination for the biodiesel

| **Weight of sample (g)** | **B (ml)** | **S (ml)** | **N** |
|---|---|---|---|
| 5 | 10.2 | 1.4 | 1.5 |
| Saponification value = $\frac{\textbf{(10.2−1.4) x 1.5 x 56.1}}{\textbf{5.48}}$ = 148.104 mg of KOH/g | | | |

Where, 'B' and 'S' are Titrate value for blank and sample respectively, 'N' normality of (sodium thiosulfate solution for iodine value test) and normality of (HCl for saponification value test).

## Appendix B: Particle Size and Zeta Potential Analysis Result for $Al_2O_3$-NPs

**Size Distribution Report by Intensity**
*v2.2*

Malvern

**Sample Details**

| | | | |
|---|---|---|---|
| **Sample Name:** | Al2O3 1 | | |
| **SOP Name:** | mansettings.nano | | |
| **General Notes:** | | | |
| **File Name:** | Nano material.dts | **Dispersant Name:** | Propan-2-ol |
| **Record Number:** | 452 | **Dispersant RI:** | 1.390 |
| **Material RI:** | 1.59 | **Viscosity (cP):** | 2.3200 |
| **Material Absorbtion:** | 0.010 | **Measurement Date and Time:** | Monday, April 18, 2022 6:03:... |

**System**

| | | | |
|---|---|---|---|
| **Temperature (°C):** | 25.0 | **Duration Used (s):** | 4 |
| **Count Rate (kcps):** | 14.2 | **Measurement Position (mm):** | 4.65 |
| **Cell Description:** | Clear disposable zeta cell | **Attenuator:** | 11 |

**Results**

| | | | **Size (d.nm):** | **% Intensity:** | **St Dev (d.n...** |
|---|---|---|---|---|---|
| **Z-Average (d.nm):** | 3060 | **Peak 1:** | 91.28 | 100.0 | 0.000 |
| **PdI:** | 1.000 | **Peak 2:** | 0.000 | 0.0 | 0.000 |
| **Intercept:** | 1.28 | **Peak 3:** | 0.000 | 0.0 | 0.000 |

**Result quality :** Refer to quality report

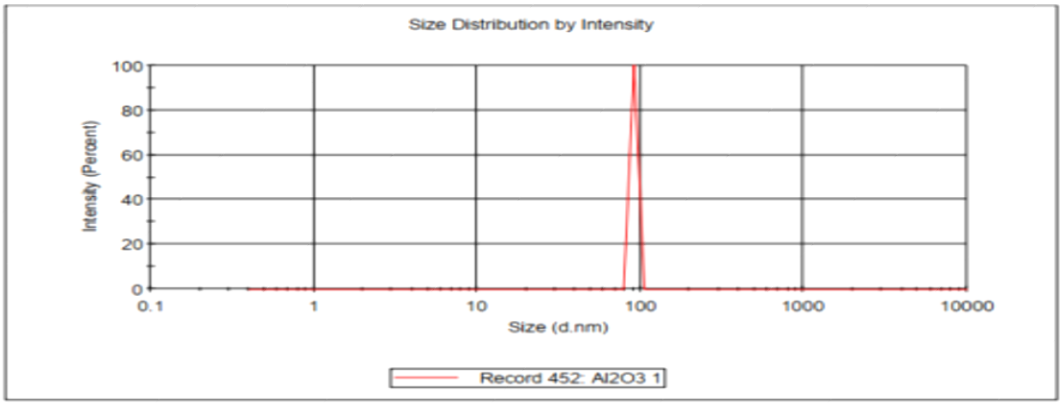


Figure B1: Analysis result of size distribution by intensity for $Al_2O_3$ nanoparticle (Propan-2-ol used as a dispersant)

## Size Distribution Report by Intensity

v2.2

Malvern

**Sample Details**

| | | | |
|---|---|---|---|
| **Sample Name:** | Al2O3 - NP 1 | | |
| **SOP Name:** | CNC.sop | | |
| **General Notes:** | | | |
| **File Name:** | Nano material.dts | **Dispersant Name:** | Water |
| **Record Number:** | 491 | **Dispersant RI:** | 1.330 |
| **Material RI:** | 1.59 | **Viscosity (cP):** | 0.8872 |
| **Material Absorbtion:** | 0.010 | **Measurement Date and Time:** | Tuesday, April 19, 2022 3:49:... |

**System**

| | | | |
|---|---|---|---|
| **Temperature (°C):** | 25.0 | **Duration Used (s):** | 40 |
| **Count Rate (kcps):** | 41.7 | **Measurement Position (mm):** | 0.45 |
| **Cell Description:** | Disposable sizing cuvette | **Attenuator:** | 11 |

**Results**

| | | | **Size (d.nm):** | **% Intensity:** | **St Dev (d.n...** |
|---|---|---|---|---|---|
| **Z-Average (d.nm):** | 6915 | **Peak 1:** | 71.24 | 100.0 | 5.596 |
| **PdI:** | 1.000 | **Peak 2:** | 0.000 | 0.0 | 0.000 |
| **Intercept:** | 0.387 | **Peak 3:** | 0.000 | 0.0 | 0.000 |

**Result quality :** Refer to quality report

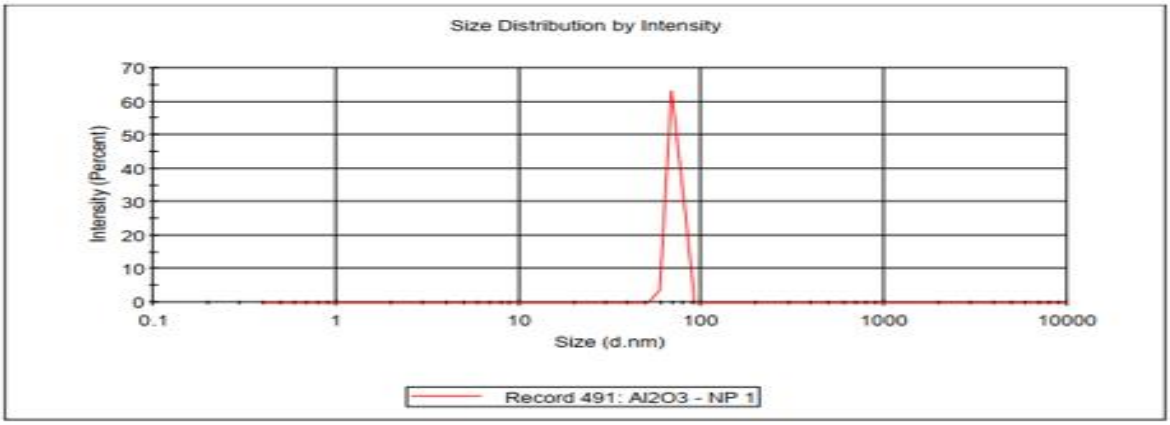


Figure B2: Analysis result of size distribution by intensity for $Al_2O_3$ nanoparticle (Water used as a dispersant)

**Zeta Potential Report**
*v2.3*

Malvern Instruments Ltd · © Copyright 2008

Malvern

**Sample Details**

| | | | |
|---|---|---|---|
| **Sample Name:** | G-Al 1 | | |
| **SOP Name:** | Zeta potential test sample v2 DTS1070.sop | | |
| **General Notes:** | This SOP is also suitable for most samples of conductivity less than 5 mS. | | |
| **File Name:** | Nano material.dts | **Dispersant Name:** | Water |
| **Record Number:** | 760 | **Dispersant RI:** | 1.330 |
| **Date and Time:** | Thursday, July 7, 2022 4:43:03 AM | **Viscosity (cP):** | 0.8872 |
| | | **Dispersant Dielectric Constant:** | 78.5 |

**System**

| | | | |
|---|---|---|---|
| **Temperature (°C):** | 25.0 | **Zeta Runs:** | 100 |
| **Count Rate (kcps):** | 48.9 | **Measurement Position (mm):** | 2.00 |
| **Cell Description:** | Clear disposable zeta cell | **Attenuator:** | 7 |

**Results**

| | | Mean (mV) | Area (%) | St Dev (mV) |
|---|---|---|---|---|
| **Zeta Potential (mV):** 30.495 | **Peak 1:** | 30.495 | 100.0 | 5.45 |
| **Zeta Deviation (mV):** 5.45 | **Peak 2:** | 0.00 | 0.0 | 0.00 |
| **Conductivity (mS/cm):** 2.42e-4 | **Peak 3:** | 0.00 | 0.0 | 0.00 |
| **Result quality :** See result quality report | | | | |

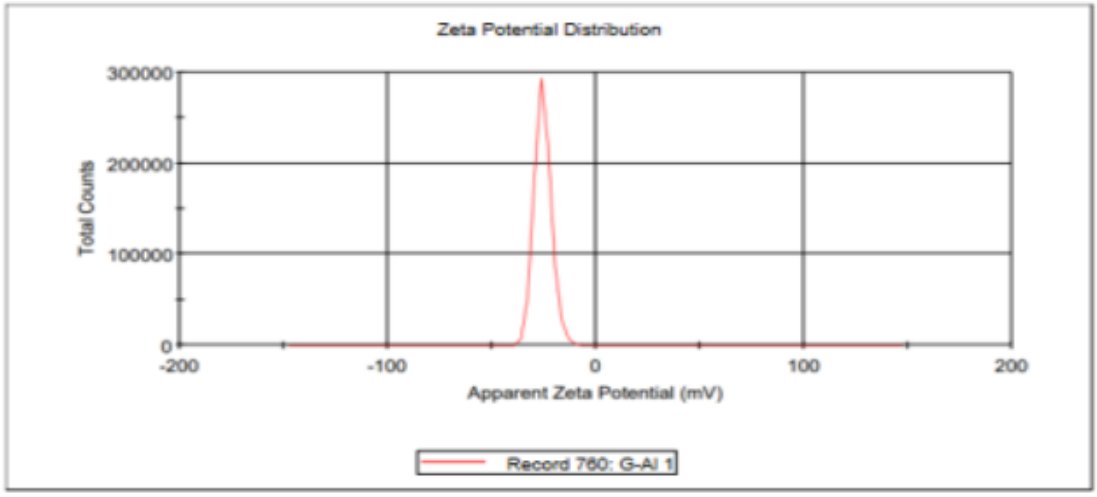


Figure B3: Analysis result of Zeta potential for $Al_2O_3$ nanoparticle dispersed in Gly-lac

## Appendix C: Cold Flow Property Analysis Results

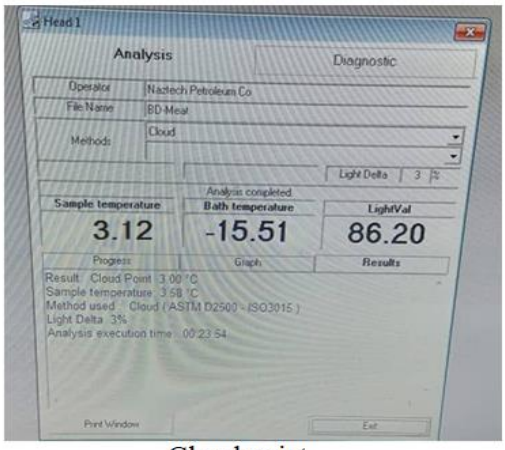


Cloud point

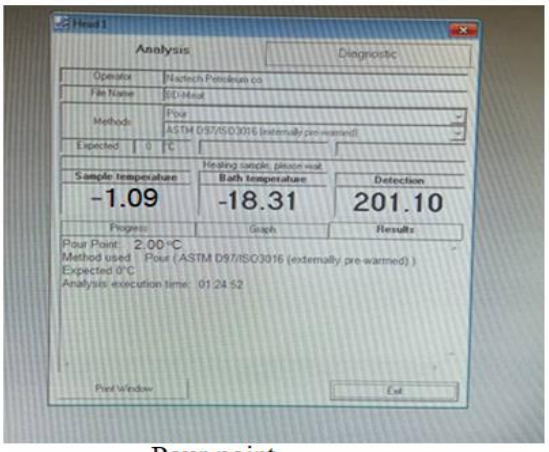


Pour point

1. **Pure biodiesel**

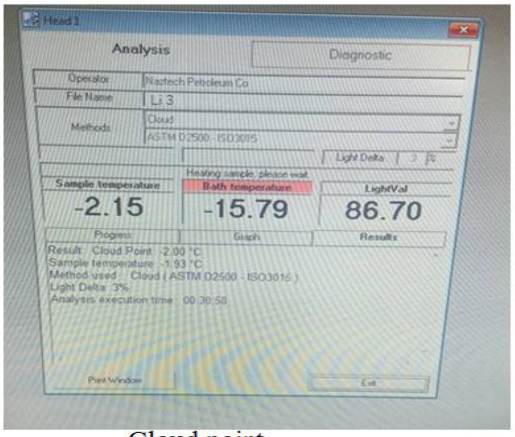


Cloud point

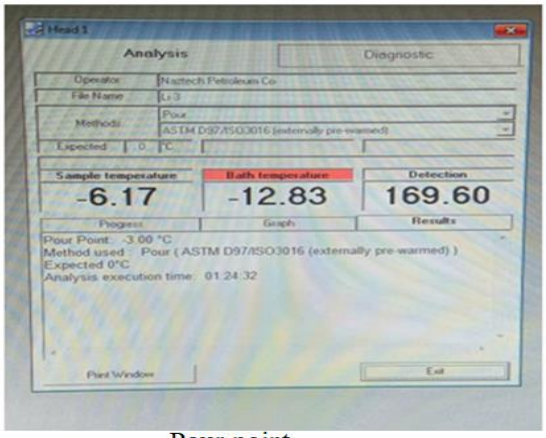


Pour point

2. **Gly-lac (1:3)**

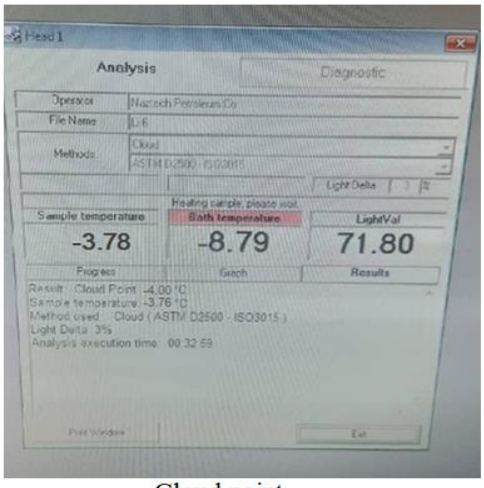


Cloud point

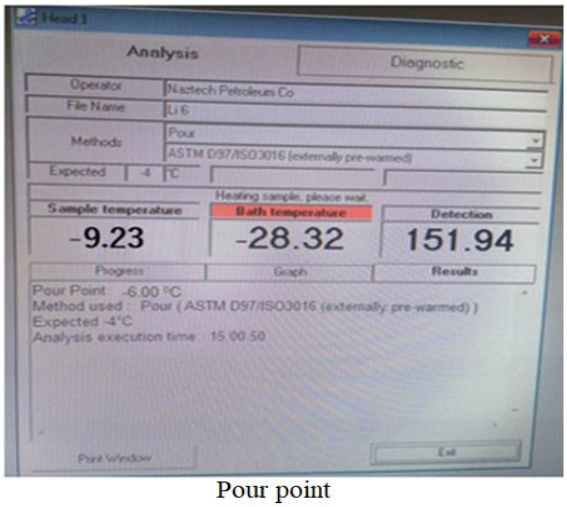


Pour point

3. **Gly-lac (1:6)**

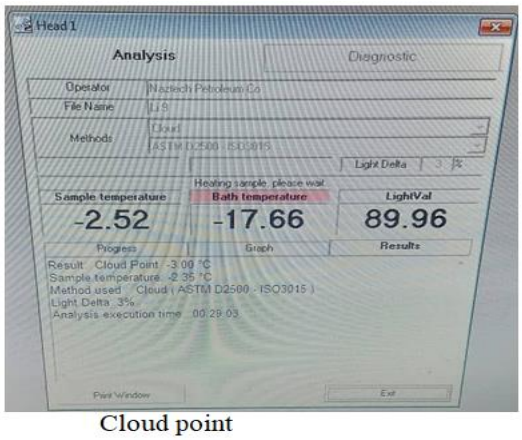


Cloud point

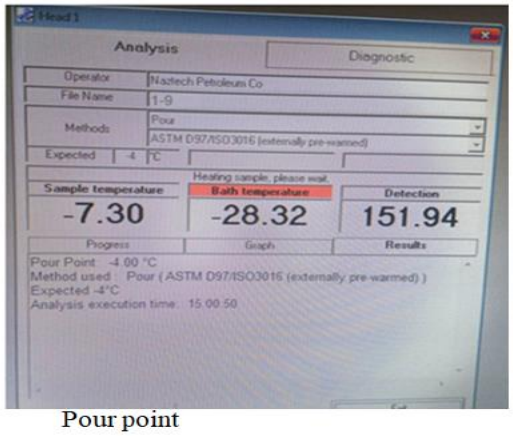


Pour point

4. **Gly-lac (1:9)**

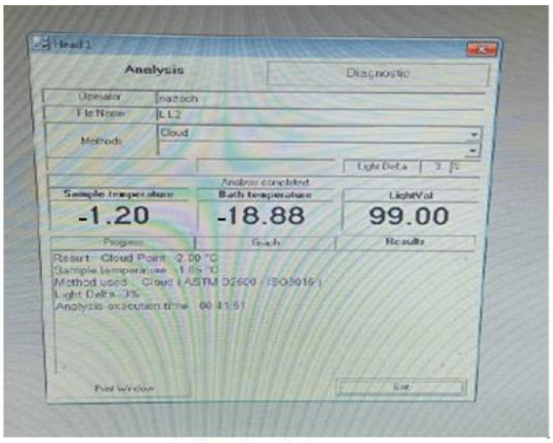


Cloud point

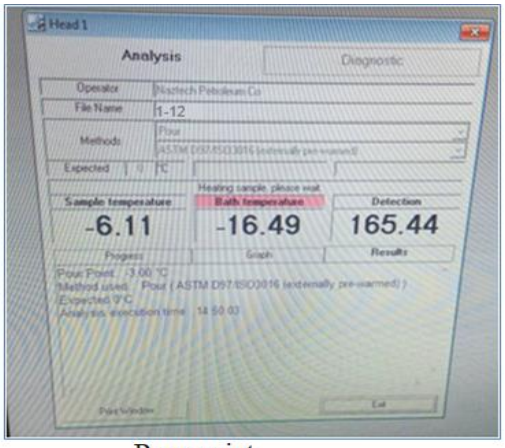


Pour point

5. **Gly-lac (1-12)**

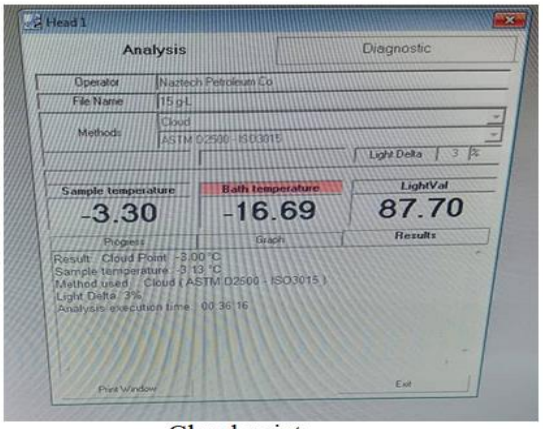


Cloud point

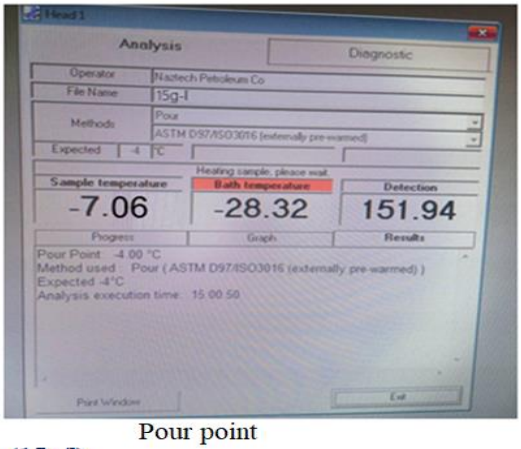


Pour point

6. **Gly-lac (15g/l)**

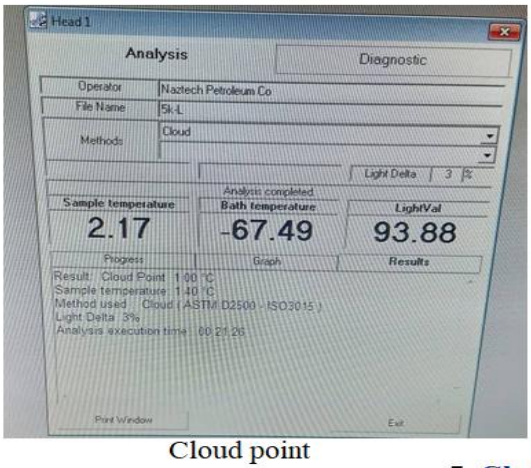


Cloud point

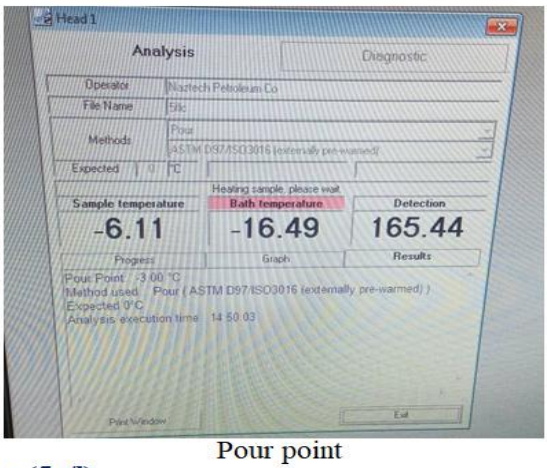


Pour point

7. **Gly-lac (5g/l)**

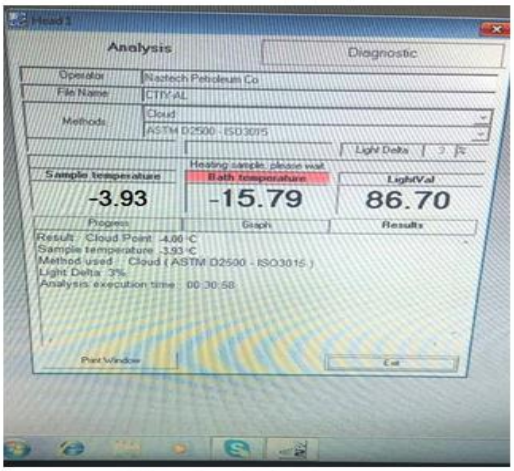


Cloud point

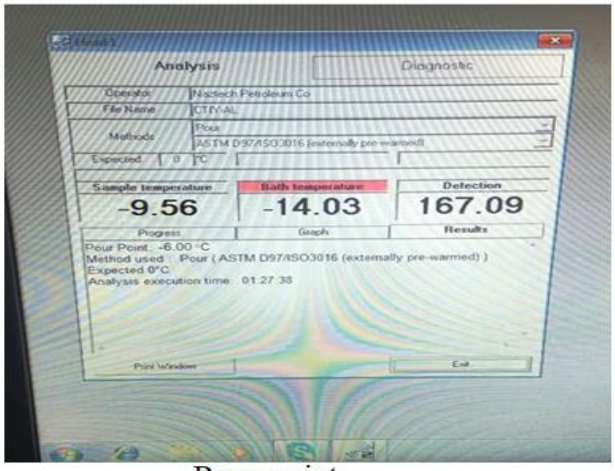


Pour point

8. **Gly-lac+Al1%**

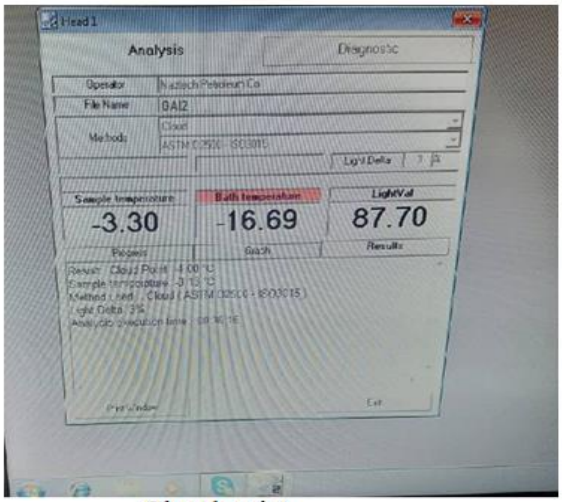


Cloud point

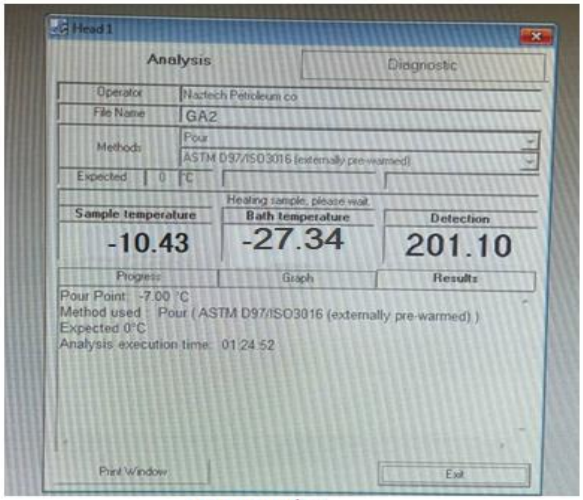


Pour point

9. **GAl2%**

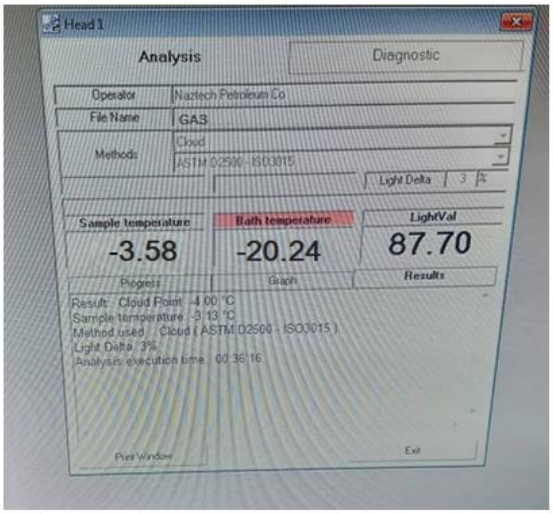


Cloud point

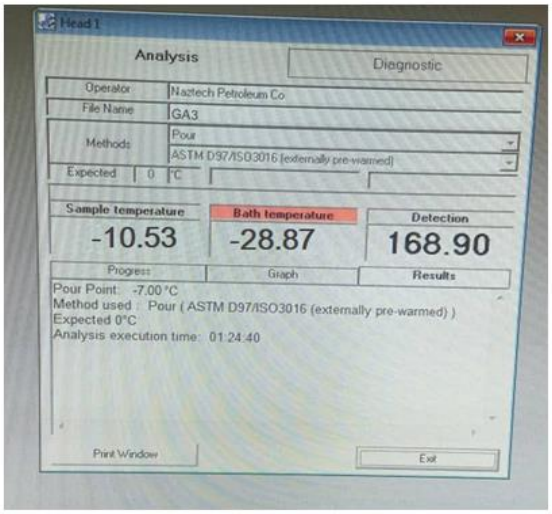


Pour point

10. **GAI3%**

## Appendix D: Calorific Value Test Result

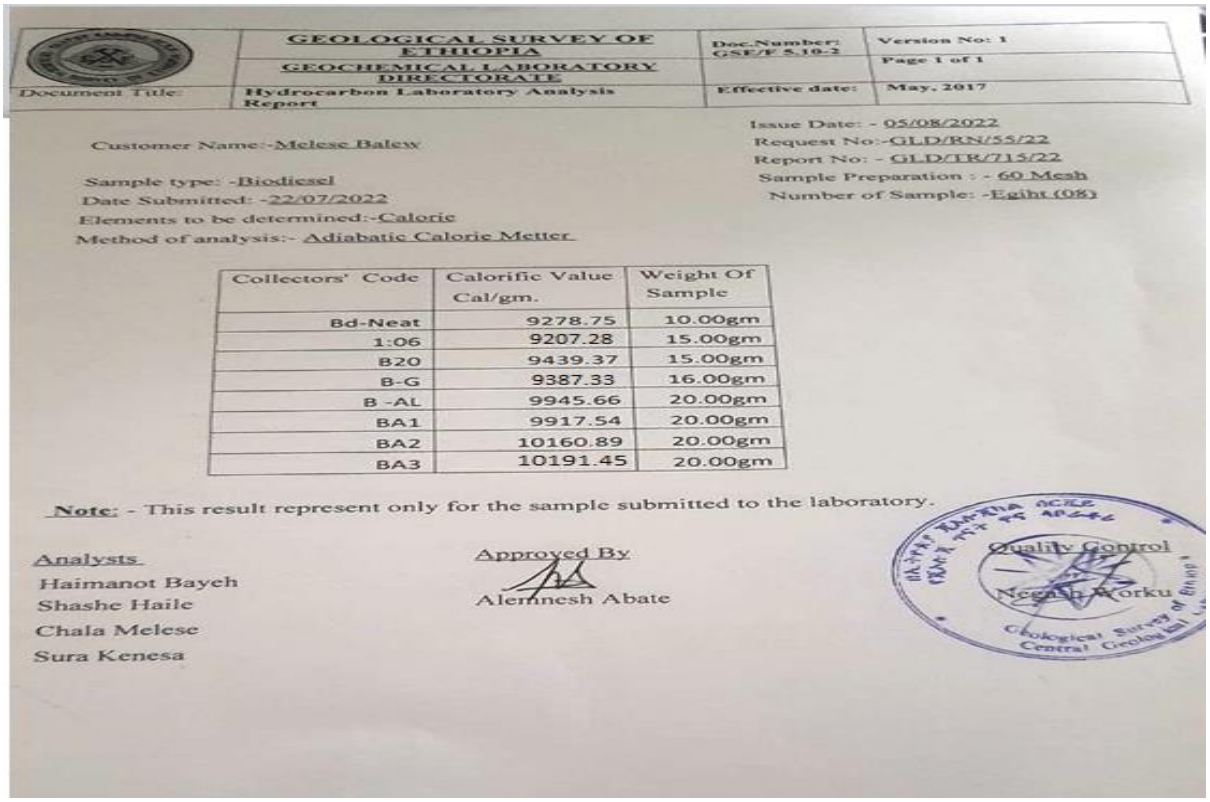

GEOLOGICAL SURVEY OF ETHIOPIA
GEOCHEMICAL LABORATORY DIRECTORATE

| Document Title: | Hydrocarbon Laboratory Analysis Report | Doc.Number: GSE/F 5.10-2 | Version No: 1 |
|---|---|---|---|
| | | | Page 1 of 1 |
| | | Effective date: | May, 2017 |

Customer Name:-Melese Balew

Sample type: -Biodiesel
Date Submitted: -22/07/2022
Elements to be determined:-Caloric
Method of analysis:- Adiabatic Caloric Metter

Issue Date: - 05/08/2022
Request No:-GLD/RN/55/22
Report No: - GLD/TR/715/22
Sample Preparation : - 60 Mesh
Number of Sample: -Eight (08)

| Collectors' Code | Calorific Value Cal/gm. | Weight Of Sample |
|---|---|---|
| Bd-Neat | 9278.75 | 10.00gm |
| 1:06 | 9207.28 | 15.00gm |
| B20 | 9439.37 | 15.00gm |
| B-G | 9387.33 | 16.00gm |
| B -AL | 9945.66 | 20.00gm |
| BA1 | 9917.54 | 20.00gm |
| BA2 | 10160.89 | 20.00gm |
| BA3 | 10191.45 | 20.00gm |

Note: - This result represent only for the sample submitted to the laboratory.

Analysts
Haimanot Bayeh
Shashe Haile
Chala Melese
Sura Kenesa

Approved By
Alemnesh Abate

Quality Control
Negash Worku

## Appendix E: Analysis Results for Engine Performance and Emission Test

Table D1: Engine performance test results

| Load (%) | Measured Variables | Sample | | | | | |
|---|---|---|---|---|---|---|---|
| | | B20 | B20G | B20A | B20GA1 % | B20GA2 % | B20GA3 % |
| 20 | Volume flow rate (ml/hr) | 803.57 | 798.226 | 808.98 | 813.56 | 817.25 | 820.045 |
| | Torque (N.m) | 6.38 | 6.26 | 8.11 | 9.14 | 10.18 | 12.74 |
| 40 | Volume flow rate (ml/hr) | 867.47 | 862.27 | 870.61 | 875.91 | 879.12 | 882.35 |
| | Torque (N.m) | 10.12 | 9.53 | 11.25 | 12.67 | 13.73 | 17.38 |
| 60 | Volume flow rate (ml/hr) | 953.65 | 948.61 | 957.44 | 962.567 | 966.44 | 970.35 |
| | Torque (N.m) | 13.01 | 12.31 | 14.27 | 14.76 | 15.98 | 19.35 |
| 80 | Volume flow rate (ml/hr) | 1025.65 | 1021.28 | 1028.57 | 1034.48 | 1035.97 | 1040.46 |
| | Torque (N.m) | 15.14 | 14.42 | 16.06 | 17.35 | 17.89 | 22.89 |
| 100 | Volume flow rate (ml/hr) | 1130.3 | 1126.76 | 1133.86 | 1135.64 | 1139.24 | 1141.046 |
| | Torque (N.m) | 17.56 | 17.35 | 18.54 | 19.63 | 20.24 | 21.63 |

Table D2: Exhaust gas emission test results

| **Load** (%) | **Exhaust gas emission** | **Sample** | | | | | |
|---|---|---|---|---|---|---|---|
| | | **B20** | **B20G** | **B20A** | **B20GA1%** | **B20GA2%** | **B20GA3%** |
| 20 | HC (ppm) | 61 | 56 | 52 | 45 | 39 | 34 |
| | $NO_x$ (ppm) | 240 | 215 | 206 | 189 | 174 | 161 |
| | CO (vol%) | 0.031 | 0.030 | 0.029 | 0.025 | 0.023 | 0.021 |
| | $CO_2$ (vol%) | 2.12 | 2.19 | 2.24 | 2.28 | 2.32 | 2.35 |
| 40 | HC (ppm) | 50 | 45 | 41 | 33 | 27 | 22 |
| | $NO_x$ (ppm) | 325 | 297 | 286 | 267 | 250 | 236 |
| | CO (vol%) | 0.030 | 0.028 | 0.026 | 0.024 | 0.022 | 0.020 |
| | $CO_2$ (vol%) | 2.53 | 2.61 | 2.67 | 2.71 | 2.74 | 2.77 |
| 60 | HC (ppm) | 43 | 37 | 32 | 25 | 19 | 14 |
| | $NO_x$ (ppm) | 418 | 389 | 377 | 356 | 338 | 323 |
| | CO (vol%) | 0.026 | 0.023 | 0.022 | 0.019 | 0.017 | 0.016 |
| | $CO_2$ (vol%) | 2.98 | 3.06 | 3.11 | 3.14 | 3.17 | 3.20 |
| 80 | HC (ppm) | 38 | 33 | 28 | 21 | 16 | 11 |
| | $NO_x$ (ppm) | 528 | 496 | 483 | 461 | 442 | 426 |
| | CO (vol%) | 0.022 | 0.020 | 0.018 | 0.016 | 0.014 | 0.013 |
| | $CO_2$ (vol%) | 3.87 | 3.94 | 3.98 | 4.02 | 4.05 | 4.07 |
| 100 | HC (ppm) | 36 | 30 | 25 | 20 | 15 | 10 |
| | $NO_x$ (ppm) | 648 | 613 | 598 | 565 | 541 | 520 |
| | CO (vol%) | 0.019 | 0.016 | 0.014 | 0.012 | 0.01 | 0.009 |
| | $CO_2$ (vol%) | 4.80 | 4.86 | 4.89 | 4.91 | 4.93 | 4.94 |
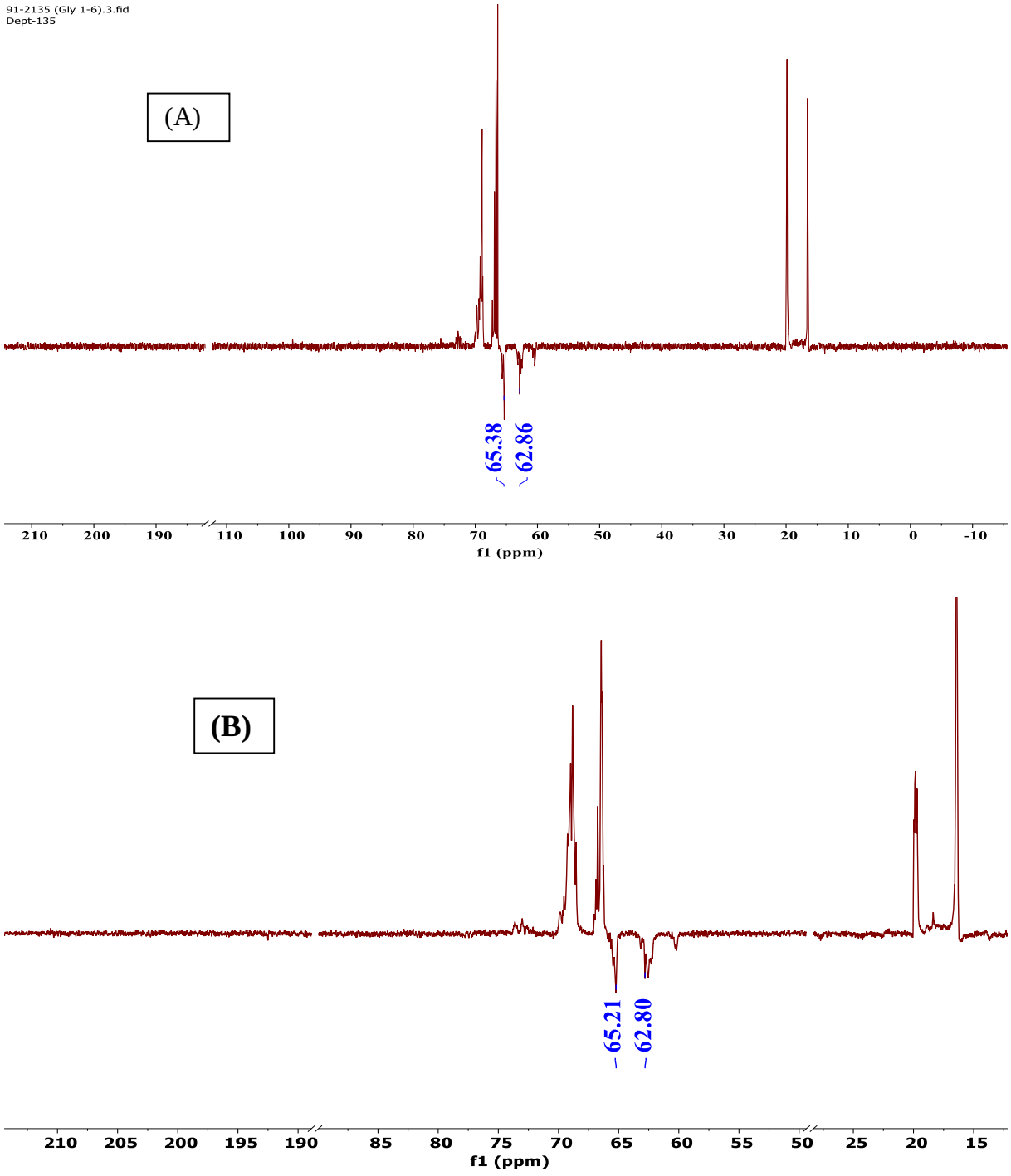
**Appendix F: Dept -135 for 3-armed Gly-lac (A) non-purified, (B) purified**